ASPECTS OF SOLAR CORONAL STABILITY THEORY

Peter J. J. De Bruyne

A Thesis Submitted for the Degree of PhD
at the
University of St Andrews

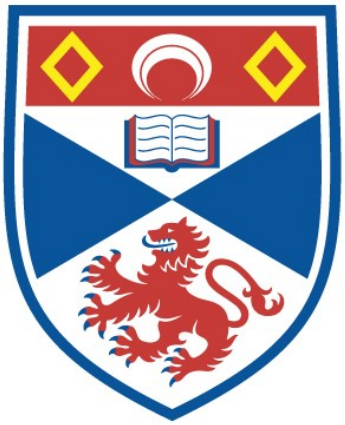

1991

Aspects of
Solar Coronal Stability Theory

PETER J. J. DE BRUYNE

Thesis submitted for the Degree of Doctor of Philosophy
of the University of St. Andrews
27th August 1990

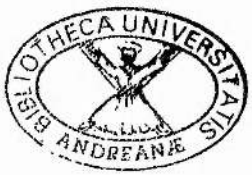

ProQuest LLC.
789 East Eisenhower Parkway
P.O. Box 1346
Ann Arbor, MI 48106 – 1346

Abstract

Solar coronal stability theory is a powerful tool for understanding the complex behaviour of the Sun's atmosphere. It enables one to discover the driving forces behind some intriguing phenomena and to gauge the soundness of theoretical models for observed structures. In this thesis, the linear stability analysis of line-tied symmetric magnetohydrostatic equilibria is studied within the framework of ideal MHD, aimed at its application to the solar corona.

Firstly, a tractable stability procedure based on a variational method is devised. It provides a necessary condition for stability to disturbances localised about a particular flux surface, and a sufficient condition for stability to all accessible perturbations that vanish at the photosphere. The tests require the minimisation of a line integral along the magnetic field lines. For 1-D equilibria, this can be performed analytically, and simple stability criteria are obtained. The necessary condition then serves as an extended Suydam criterion, incorporating the stabilising effect of line-tying. For 2-D equilibria, the minimisation requires the integration of a system of ordinary differential equations along the field lines. This stability technique is applied to arcade, loop, and prominence models, yielding tight bounds on the equilibrium parameters.

Secondly, global modes in 1-D coronal loops are investigated using a normal mode method, in order to clarify their link with localised interchange modes. For nearly force-free fields it is shown that instability to localised modes implies the existence of a fast growing global kink mode driven in the neighbourhood of the radius predicted by the local analysis. This confers a new significance on the study of localised interchange modes and the associated extended Suydam criterion.

Declarations

I, Peter Jules Johan De Bruyne, hereby certify that this thesis has been composed by myself, that it is a record of my own work, and that it has not been accepted in partial or complete fulfilment of any other degree or professional qualification.

Signed . .. Date 27/8/90.....

I was admitted to the Faculty of Science of the University of St. Andrews under Ordinance General No. 12 in October 1987 and as a candidate for the degree of Ph.D. on 29th September 1988.

Signed . Date 27/8/90.....

I hereby certify that the candidate has fulfilled the conditions of the Resolution and Regulations appropriate to the Degree of Ph.D.

Signature of Supervisor . Date 27/8/90.....

In submitting this thesis to the University of St. Andrews I understand that I am giving permission for it to be made available for use in accordance with the regulations of the University Library for the time being in force, subject to any copyright vested in the work not being affected thereby. I also understand that the title and abstract will be published, and that a copy of the work may be made and supplied to any *bona fide* library or research worker.

Acknowledgements

To leave family and friends, and embark upon a three-years' adventure in a country that is said to be chilly and wet, is a choice that is not made lightly, especially if it is to be one's honeymoon. I would therefore like to thank all who contributed to the quality of life during our stay in St. Andrews, including the Sun.

My parents' encouragement has been unfaltering throughout my studies. Without them, none of this would have been possible. The staff of the 'Astronomisch Instituut' of the 'Katholieke Universiteit Leuven' laid the solid foundation on which this work could be built. Eric Priest made sure we had a roof over our head, against all odds. Alan Hood, my supervisor, carefully initiated me into the secrets of stability research and five-a-side (Fife aside?) football. I have yet to meet the person who tops his enthusiasm and inspiration. Bernie Roberts offered me a glimpse of the other side of the $\omega^2 = 0$ fence. I am much obliged to all of them, as I am to Hania Allen, David Evans, Alan Miles, Marco Velli, and the whole Department of Mathematical and Computational Sciences.

I am very grateful to the University of St. Andrews for awarding me a Research Studentship and for financially supporting my attendance at various conferences, meetings and workshops, to the staff of the Computing Laboratory for logistic assistance, and to Sheena Stewart and Alasdair Macdonald for proofreading.

Finally I would like to thank my wife Mariska : "We did it!". To her I dedicate this thesis.

Contents

1

Introduction

> "Yet not every solution of the equations of motion, even if it is exact, can actually occur in Nature. The flows that occur in Nature must not only obey the equations of fluid dynamics, but also be stable. For the flow to be stable it is necessary that small perturbations, if they arise, should decrease with time. If, on the contrary, the small perturbations which inevitably occur in the flow tend to increase with time, then the flow is absolutely unstable. Such a flow unstable with respect to infinitely small perturbations cannot exist."
>
> L. D. Landau and E. M. Lifshitz, *Fluid Mechanics*, p. 102 (1959)

1.1. The Role of Stability Theory in Solar Coronal Physics

The Sun is the Rosetta stone of astrophysics. Satellite borne X-ray observations and groundbased studies of radio emission verify the existence of solar phenomena on various types of other stars (see, for instance, Uchida, 1986). Stellar magnetic fields and activity cycles, stellar winds, coronae and chromospheres, and the occurrence of starspots and flares have been confirmed. This provides an important feedback to theorists in the form of a test for their models : do these allow for, and explain, the observed features? A sound physical understanding of their solar counterparts thus seems a prerequisite for every astrophysicist. Conversely the solar community can benefit from a broadening of horizons : it invites them to seek physical explanations that are not just tailored to fit the Sun but are valid in a general stellar context.

The Sun is also a giant plasma physics laboratory. Although the respective parameters, configurations and boundary conditions can be widely different, there is scope for a fruitful cross-fertilisation between solar and nuclear fusion research (see, for instance, Browning, 1988). Early coronal modelling was largely based on well-established equilibrium and stability results obtained in the quest for parameter regimes suitable for energy generation. Insight into the way cool prominence material is stably supported in, and insulated from, the surrounding hot corona might shed new light on the problem of fusion plasma containment.

A stability theory forms the testbench for its underlying frame of precepts, or Model. The theory of stellar oscillations has proved a powerful tool in the study of stellar structure and evolution (Cox, 1980). Similarly, many macroscopic instabilities in fusion devices are predicted by the magnetohydrodynamic Model (Bateman, 1978). The role of solar coronal stability theory is twofold. Firstly, it should account for both the long quasi-static lifespan of coronal structures such as loops, arcades or filaments, and the sudden transition to dynamic behaviour as in the triggering of a flare or the eruption of a prominence. Secondly, but closely related to the above, it should allow discrimination against those theoretical models that cannot be reconciled with the observations, and provide quantitative bounds on the physical parameters that cannot be measured accurately at present.

1.2. Basic Equations and Definitions

The Model adopted in this thesis is that of ideal (i.e., non-dissipative) magnetohydrodynamics (MHD). It is the simplest working Model that adequately describes the long wavelength–low frequency interaction between a plasma and a permeating magnetic field. Its governing equations, stemming from pre-Maxwell electromagnetism and continuum mechanics, are

$$\rho\frac{d\mathbf{v}}{dt} = -\nabla p + \mathbf{j}\times\mathbf{B} - \rho\nabla\phi, \tag{1.2.1}$$

$$\frac{\partial\rho}{\partial t} = -\nabla\cdot(\rho\mathbf{v}), \tag{1.2.2}$$

$$\frac{\partial p}{\partial t} = -(\mathbf{v}\cdot\nabla p + \gamma p\nabla\cdot\mathbf{v}), \tag{1.2.3}$$

$$\frac{\partial\mathbf{B}}{\partial t} = \nabla\times(\mathbf{v}\times\mathbf{B}), \tag{1.2.4}$$

$$\mathbf{j} = \frac{1}{\mu}\nabla\times\mathbf{B}, \tag{1.2.5}$$

$$\nabla\cdot\mathbf{B} = 0, \tag{1.2.6}$$

$$p = \frac{\mathcal{R}}{\tilde{\mu}}\rho T. \tag{1.2.7}$$

A derivation of the MHD equations and a discussion of the underlying assumptions can be found in, for example, Boyd and Sanderson (1969). Here, SI units are used throughout and symbols have their conventional meaning, i.e., t is time, ρ is the mass density, $\mathbf{v}$ is the plasma velocity, p is the plasma pressure, $\mathbf{j}$ is the electric current density, $\mathbf{B}$ is the magnetic induction (often referred to as the magnetic field), ϕ is the prescribed external gravitational potential, and T is the temperature. The constants $\gamma = c_p/c_v, \mu, \mathcal{R}$ and $\tilde{\mu} = m/m_p$ are the adiabatic index (ratio of specific heats),

the (vacuum) magnetic permeability, the ideal gas constant and the mean molecular weight, respectively. d/dt is the convective (Lagrangian) derivative, defined as

$$\frac{d}{dt} = \frac{\partial}{\partial t} + \mathbf{v} \cdot \nabla,$$

representing the time rate of change as one follows the plasma in its motion. Equation (1.2.1) is the momentum equation when viscosity is assumed negligible. Equation (1.2.2) is the continuity equation, expressing conservation of mass. Equation (1.2.3) is a form of the adiabatic energy equation; the most important physical effect neglected here is parallel heat conduction. Combining Ohm's law for a medium of zero electrical resistivity with Faraday's law eliminates an explicit reference to the electric field $\mathbf{E}$ and yields the induction equation (1.2.4). Equations (1.2.5) and (1.2.6) are Ampere's law and Gauss's law, respectively. Finally, Equation (1.2.7) is the ideal gas law. Mathematically, Equations (1.2.1)–(1.2.4) form a closed system of 8 evolution equations for eight macroscopic variables $(\mathbf{v}, \rho, p, \mathbf{B})$. Equations (1.2.5) and (1.2.7) are auxiliary equations defining $\mathbf{j}$ and T, respectively. Faraday's law ensures that the initial condition (1.2.6) on $\mathbf{B}$ remains satisfied for all times. The assumption that the gravitational field is externally applied removes the condition that ϕ has to satisfy Poisson's equation. In the case of a static equilibrium, i.e., no time dependence or basic flows, the momentum equation (1.2.1) reduces to the magnetohydrostatic equation

$$-\nabla p + \mathbf{j} \times \mathbf{B} - \rho \nabla \phi = \mathbf{0}, \tag{1.2.8}$$

while the evolution equations for ρ, p, and $\mathbf{B}$ (1.2.2)–(1.2.4) are trivially satisfied. When pressure and gravity forces are much weaker than magnetic forces, the equilibrium is said to be *force-free*.

The following definitions will also be used :

$$v_A = \frac{B}{\sqrt{\mu\rho}} \tag{1.2.9}$$

is the Alfvén speed;

$$c_s = \sqrt{\frac{\gamma p}{\rho}} \tag{1.2.10}$$

is the isentropic sound speed;

$$\hat{\beta} = \frac{\gamma \mu p}{B^2} = \frac{c_s^2}{v_A^2} = \frac{\gamma}{2}\frac{2\mu p}{B^2} \tag{1.2.11}$$

is the square of the ratio of sound speed to Alfvén speed, which is approximately equal to the ratio of plasma pressure to magnetic pressure; and

$$g = \|\nabla \phi\| \tag{1.2.12}$$

is the magnitude of the gravitational acceleration.

Although it is clear from Equations (1.2.1)–(1.2.8) that many physical processes

are not included in the ideal MHD Model (see, for instance, Freidberg, 1987), it is well established as an adequate framework for investigating the macroscopic stability of coronal configurations.

1.3. A Brief Review of Ideal MHD Stability Theory

1.3.1. Linearised Ideal MHD Equations

To study the linear stability of an equilibrium satisfying Equations (1.2.5)–(1.2.8), all variables are expressed as the sum of their equilibrium value and a small (infinitesimal) Eulerian perturbation, for example,

$$\mathbf{B} = \mathbf{B}^0(\mathbf{r}) + \mathbf{B}^1(\mathbf{r}, t).$$

Substitution into Equations (1.2.1)–(1.2.7), neglecting products of small quantities, then yields the system of linearised equations :

$$\rho \frac{\partial \mathbf{v}^1}{\partial t} = -\nabla p^1 + \mathbf{j}^1 \times \mathbf{B} + \mathbf{j} \times \mathbf{B}^1 - \rho^1 \nabla \phi, \tag{1.3.1}$$

$$\frac{\partial \rho^1}{\partial t} = -\nabla \cdot (\rho \mathbf{v}^1), \tag{1.3.2}$$

$$\frac{\partial p^1}{\partial t} = -(\mathbf{v}^1 \cdot \nabla p + \gamma p \nabla \cdot \mathbf{v}^1), \tag{1.3.3}$$

$$\frac{\partial \mathbf{B}^1}{\partial t} = \nabla \times (\mathbf{v}^1 \times \mathbf{B}), \tag{1.3.4}$$

$$\mathbf{j}^1 = \frac{1}{\mu} \nabla \times \mathbf{B}^1, \tag{1.3.5}$$

$$\nabla \cdot \mathbf{B}^1 = 0, \tag{1.3.6}$$

$$\frac{p^1}{p} = \frac{\rho^1}{\rho} + \frac{T^1}{T}, \tag{1.3.7}$$

where the superscript ^{0} has been omitted for ease of notation.

Introducing a Lagrangian displacement $\boldsymbol{\xi}$ as

$$\mathbf{v}^1 = \frac{\partial \boldsymbol{\xi}}{\partial t}, \tag{1.3.8}$$

the system (1.3.1)–(1.3.4) can be reduced to a single vector equation in $\boldsymbol{\xi}$, namely

$$\rho \frac{\partial^2 \boldsymbol{\xi}}{\partial t^2} = \mathbf{F}(\boldsymbol{\xi}), \tag{1.3.9}$$

where the force operator is defined as

$$\begin{aligned} \mathbf{F}(\boldsymbol{\xi}) = \nabla(\boldsymbol{\xi} \cdot \nabla p + \gamma p \nabla \cdot \boldsymbol{\xi}) + \frac{1}{\mu}[\nabla \times (\nabla \times (\boldsymbol{\xi} \times \mathbf{B}))] \times \mathbf{B} + \\ + \frac{1}{\mu}(\nabla \times \mathbf{B}) \times \nabla \times (\boldsymbol{\xi} \times \mathbf{B}) + \nabla \cdot (\rho \boldsymbol{\xi}) \nabla \phi. \end{aligned} \tag{1.3.10}$$

The linearised momentum equation (1.3.9) forms the starting point for the ideal MHD stability analysis.

1.3.2. Methods of Stability Analysis

The two main approaches to a stability investigation are the *normal mode analysis* and the *energy method.* In a normal mode analysis an exponential time dependence is assumed, i.e.,

$$\boldsymbol{\xi}(\mathbf{r},t) = \boldsymbol{\xi}(\mathbf{r})\, \mathrm{e}^{-\mathrm{i}\omega t}. \tag{1.3.11}$$

The linearised momentum equation (1.3.9) then reads

$$-\rho\omega^2\boldsymbol{\xi} = \mathbf{F}(\boldsymbol{\xi}). \tag{1.3.12}$$

Together with the appropriate boundary conditions, say, the vanishing of the perturbation at the edge of the system, this forms an eigenvalue problem for the displacement $\boldsymbol{\xi}$ with eigenvalues ω^2. Self-adjointness of the force operator $\mathbf{F}$ (see, for instance, Kovetz, 1966) implies that all square-integrable eigenvectors and all eigenvalues are real. From expression (1.3.11) for $\boldsymbol{\xi}$ it is clear that one negative eigenvalue ensures instablity of the equilibrium. Only if all eigenvalues are positive is the equilibrium linearly stable to ideal modes. Transition from stability to instability occurs at $\omega^2 = 0$, the point of *marginal stability.*

The basic philosophy behind the energy principle is quite straightforward : since the total energy of a system is conserved in time in ideal MHD when no flows penetrate its edges, a rise in kinetic energy, which is the hallmark of an instability, must be accompanied by a drop in potential energy. Investigating stability then boils down to finding out whether there exists a disturbance that lowers the potential energy of the system from its equilibrium value.

The kinetic energy, K, of the system due to a perturbation $\boldsymbol{\xi}$ is

$$K = \frac{1}{2}\int \rho\, \dot{\boldsymbol{\xi}}^2\, d\mathcal{V},$$

with an upper dot denoting a time derivative. Hence, using the linearised momentum equation (1.3.9),

$$\frac{\partial K}{\partial t} = \int \rho\, \dot{\boldsymbol{\xi}}\cdot\ddot{\boldsymbol{\xi}}\, d\mathcal{V} = \int \dot{\boldsymbol{\xi}}\cdot\mathbf{F}(\boldsymbol{\xi})\, d\mathcal{V}.$$

The conservation of energy in time then implies that the change in potential energy, δW, satisfies

$$\frac{\partial \delta W}{\partial t} = -\frac{\partial K}{\partial t} = -\int \dot{\boldsymbol{\xi}}\cdot\mathbf{F}(\boldsymbol{\xi})\, d\mathcal{V},$$

or, making use of the self-adjointness of the force operator $\mathbf{F}$,

$$\frac{\partial \delta W}{\partial t} = -\frac{1}{2}\frac{\partial}{\partial t}\int \boldsymbol{\xi}\cdot\mathbf{F}(\boldsymbol{\xi})\, d\mathcal{V}.$$

So, the change in potential energy of the system from its equilibrium value due to an adiabatic perturbation $\boldsymbol{\xi}$ is

$$\delta W = -\frac{1}{2}\int \boldsymbol{\xi}\cdot\mathbf{F}(\boldsymbol{\xi})\, d\mathcal{V}, \tag{1.3.13}$$

where the integration is taken over the coronal volume of the plasma. If δW is positive for all $\boldsymbol{\xi}$ satisfying the boundary conditions, the equilibrium is stable; otherwise it is linearly unstable. Marginal stability corresponds to $\delta W = 0$. A detailed derivation of the energy integral can be found in, for example, Chapter 8 of Roberts (1967).

The potential energy integral (1.3.13) offers three lines of approach (Hood, 1983a). One can use trial perturbations in an attempt to show $\delta W < 0$, leading to necessary conditions for stability (sufficient for instability). These trial functions only need to satisfy the appropriate boundary conditions, not the linearised equation of motion (1.3.9), as was demonstrated by Laval, Mercier, and Pellat (1965). Alternatively one can carry out a partial minimisation by neglecting some positive terms in the energy integral and derive sufficient conditions for stability (necessary for instability) by showing δW is positive. Finally one can perform a complete minimisation of the energy integral, subject to any convenient normalising constraint that excludes the trivial solution $\boldsymbol{\xi} = \mathbf{0}$. If the constraint is chosen to be

$$\frac{1}{2}\int \rho\, \boldsymbol{\xi}^2 \, d\mathcal{V} = 1, \tag{1.3.14}$$

solving the full Euler-Lagrange equations becomes equivalent to performing a normal mode analysis. Although the third approach results in necessary and sufficient conditions for stability, it also involves tackling a system of three coupled partial differential equations, a non-trivial problem.

1.3.3. Some Basic Papers

As was mentioned before, the foundations of solar and stellar coronal stability research were laid during the early stages of the nuclear fusion programme. Many of the key results are therefore to be found in the plasma physics literature rather than in astrophysical journals.

The normal mode analysis has mainly been used to study one-dimensional (1-D) equilibria, i.e., those whose physical quantities only depend on one space variable. Hain and Lüst (1958) reduced the stability investigation of an infinite plasma cylinder to one of solving a single eigenvalue differential equation of second order. A similar result for a plane plasma layer was obtained by Goedbloed (1971a). Appert, Gruber, and Vaclavik (1974) showed that the ideal eigenspectrum of 1-D equilibria can have at most two continua. Normal mode analyses in a solar context have been performed by, for example, Migliuolo and Cargill (1983) who examined arcades, and Velli, Einaudi, and Hood (1990b) who looked into coronal loop stability.

The energy principle was first put into practice by Lundquist (1951), Hain, Lüst, and Schlüter (1957), and Bernstein *et al.* (1958) for nuclear fusion purposes. It was

extended by Anzer (1969) to include configurations where magnetic fields penetrate through discontinuity surfaces, as in (current sheet) models of prominences. Laval, Mercier, and Pellat (1965) proved that the normal mode method and the energy method lead to identical stability verdicts. An excellent physical analysis of the different terms in the energy integral can be found in Greene and Johnson (1968), while its application to magnetohydrostatic coronal atmospheres was discussed by Zweibel (1985).

Suydam (1958) utilised the energy method to derive an analytic criterion for stability of 1-D plasma columns to localised perturbations. This was generalised by Mercier (1960) to cover all axisymmetric equilibria. Newcomb (1960) reduced the global stability investigation of an infinite cylinder to finding the roots of the solution of a second order ordinary differential equation.

Anzer (1968) found all force-free infinite loops unstable to global disturbances, a somewhat worrying result at the time. However, Raadu (1972) pointed out that coronal fields are anchored in the dense photosphere, which provides a strong stabilising effect known as *line-tying*. This was incorporated by, for example, Hood and Priest (1979, 1981) and Einaudi and Van Hoven (1981, 1983) in 1-D stability studies, and Schindler, Birn, and Janicke (1983) exploring 2-D equilibria. Hood (1986b) demonstrated that the correct modelling of ideal modes requires the complete vanishing of coronal perturbations at the corona-photospheric interface, known as the *rigid plate* boundary conditions.

A special class of disturbances, playing a prominent role in this thesis, are the localised interchange modes. They are the counterpart of the *ballooning modes* in fusion research, driven by the interplay of outward pressure gradients and unfavourable field line curvature. The basic theory was developed by Conner, Hastie, and Taylor (1979), while a more rigorous mathematical treatment for toroidal systems was given by Dewar and Glasser (1983). Hood (1986a) adopted this method to fit coronal situations by including the effect of line-tying.

Far more extensive reviews of MHD stability are presented in, for example, Kadomtsev (1966), Wesson (1978), and Freidberg (1982) for laboratory plasmas, and Van Hoven (1981), Birn and Schindler (1981), and Hood (1990), dealing with coronal configurations. A selection of reprints of papers on MHD stability can be found in Jeffrey and Taniuti (1966). The standard textbook on MHD instabilities is Bateman (1978). For a superb 15-page overview of the relative merits of different instability mechanisms in explaining coronal behaviour, see Sakurai (1989).

1.4. Aims and Outline of the Thesis

Two incentives lie behind this thesis. Firstly, we wanted to devise easy-to-use stability procedures and employ them to test coronal magnetohydrostatic equilibria. Therefore, the energy integral is rearranged in the form

$$\delta W = \frac{1}{2\mu}(\mathcal{I} + \mathcal{J}), \tag{1.4.1}$$

where $\mathcal{I}$ does not contain derivatives of the plasma displacement across the magnetic field, and $\mathcal{J} \geq 0$. Then two tests for stability are derived. They are purely analytic in the case of 1-D equilibria, and only demand the integration of a set of *ordinary* differential equations along field lines for 2-D structures. Using localised perturbations as trial functions, δW can be shown to be negative in a certain region of parameter space. This produces a *necessary condition for stability* (sufficient for instability). A partial minimisation by neglecting $\mathcal{J}$ in δW determines a parameter region of definite stability to all coronal disturbances satisfying the rigid plate boundary conditions :

$$\boldsymbol{\xi} = \mathbf{0} \quad \text{on the photosphere.} \tag{1.4.2}$$

This represents a *sufficient condition for stability* (necessary for instability). Combining both conditions yields a stability verdict whose usefulness comes close to that obtained by a complete minimisation of δW, at a fraction of the effort required.

Chapter 2 deals with 1-D equilibria, both cylindrically symmetric arcades and loops, and plane plasma layers in a perpendicular gravitational field. In Chapter 3 the stability theory of 2-D translationally invariant configurations is developed and applied to coronal arcades. It is used to study prominence stability in Chapter 4. An ideal MHD stability procedure for general line-tied symmetric equilibria is then presented in Chapter 5.

Secondly, we wanted to discover the relationship between the global modes, which perturb the entire coronal structure envisaged, and the localised interchange modes, which are concentrated near a particular flux surface. Therefore, in Chapter 6 a normal mode analysis is performed on 1-D coronal loops and the results are compared with those of Chapter 2. The principal effect of this juxtaposition is a revaluation of the localised stability criterion. Finally, Chapter 7 presents conclusions and suggestions for future work.

2

Stability of Line-Tied 1-D Coronal Equilibria

2.1. Introduction

The stability analysis of coronal fields has traditionally been divided into two main areas, namely coronal loops and coronal arcades. Coronal loop stability has been studied by Raadu (1972) and Hood and Priest (1979) for a force-free field, using trial functions in the energy method. Hood and Priest (1981) performed a complete minimisation of the perturbed potential energy for the same field and solved the resulting partial differential equations by a finite difference scheme. They found that a constant twist force-free loop becomes unstable if it is twisted by 2.5π, just over one revolution. The same critical condition was obtained by Einaudi and Van Hoven (1983) using a truncated Fourier series. A similar technique, applied to a normal mode analysis, was employed by Velli, Einaudi, and Hood (1990b) investigating growth rates and geometrical properties of ideal kink modes. Goedbloed (1990) included the stabilising effect of neighbouring flux tubes in his analysis.

The stability of coronal arcades has been studied by several authors. Hood and Priest (1980) investigated cylindrically symmetric force-free arcades using trial functions in the energy method and found that all the arcades tested are stable to a wide class of displacements when the axis of symmetry lies on or below the photosphere. To produce an instability, they found that the axis of symmetry must exceed a critical height above the photosphere. This means that magnetic islands or helical fields must be present. Thus, a flux tube embedded inside an arcade structure is necessary for an instability to occur. The stability of cylindrically symmetric arcades has also been investigated by Ray and Van Hoven (1982), Migliuolo and Cargill (1983), Hood (1983a), and Migliuolo, Cargill, and Hood (1984). In a later paper, Cargill, Hood, and Migliuolo (1986) used the numerical scheme of Hood and Priest (1981) to study the influence of pressure gradients on the stability of arcades. When the axis of symmetry lies on the photosphere, substantial pressure gradients are required for an instability. Normally, equipartition of energy is necessary. This

technique verified the results from trial functions of Hood and Priest (1980) that certain force-free arcades are stable.

Cargill, Hood, and Migliuolo (1986) and Hood and Anzer (1987) considered a wide class of force-free equilibria and found that they are stable. This led them to conjecture that all force-free arcades are indeed stable and that a necessary requirement for a two-ribbon flare is the existence of an active region filament. It may drive a thermal instability because its helical field lines exceed a critical length, or it may generate the substantial pressure gradients needed for an ideal instability.

Gravity has a destabilising effect on equilibria with an unfavourable density stratification. They are susceptible to Rayleigh-Taylor instabilities, which lower the gravitational potential energy by interchanging heavier and lighter plasma elements (Rayleigh, 1883; Taylor, 1950; see also Chandrasekhar, 1961, Chapter 10). A disadvantage of 1-D cylindrical geometry is the inability to study the effect this class of instabilities has on arcades and loops. To bypass this obstacle, the coronal structures are approximated by a plane plasma layer in a perpendicular gravitational field. Kruskal and Schwarzschild (1954) and Newcomb (1961) studied the convective instability in an infinite uni-directional magnetic field. Hughes and Cattaneo (1987) looked at the physical mechanisms behind this instability, while Gratton, Gratton, and González (1988) considered the influence of shear and compressibility on the instability threshold and growth rates. Gravitational instabilities in finite systems have been investigated by Roberts and Taylor (1965), but without incorporating the stabilising effect of line-tying.

In this Chapter we want to extend the ideas of Hood (1986a) and Hood and Anzer (1987) to more general equilibria. Section 2.2 deals with arcades and loops, while Section 2.3 is devoted to plane plasma layers. In both cases the energy integral is rewritten in a form that allows the extraction of necessary conditions and sufficient conditions for stability. These are then applied to specific equilibrium profiles. The results are summarised in Section 2.4.

2.2. Cylindrically Symmetric Arcades and Loops

2.2.1. Energy Integral

Consider cylindrically symmetric equilibria

$$\begin{aligned} \mathbf{B} &= (0, B_\theta(r), B_z(r)), \\ p &= p(r), \end{aligned} \tag{2.2.1}$$

that satisfy the magnetostatic equation

$$\frac{d}{dr}\left(p+\frac{B^2}{2\mu}\right)=-\frac{B_\theta^2}{\mu r}\,, \tag{2.2.2}$$

where $B^2=B_\theta^2+B_z^2$, and gravity is assumed negligible. The line-tying effect of the dense photosphere, located at

$$y=-\frac{1}{2} \quad \text{and} \quad y=\frac{1}{2}\,, \tag{2.2.3}$$

where

$$y=\frac{\theta}{\pi} \quad \text{for arcades,} \tag{2.2.4a}$$

or

$$y=\frac{z}{L} \quad \text{for loops,} \tag{2.2.4b}$$

a dimensionless coordinate, is modelled by the rigid plate boundary conditions (1.4.2). This is equivalent to assuming that the photosphere is energetically decoupled from the corona (Zweibel, 1985).

If the equilibrium is perturbed, the subsequent motions satisfy the linearised momentum equation (1.3.9) with $\nabla\phi=\mathbf{0}$. The corresponding change in potential energy, (1.3.13), may be rearranged, by integration by parts and using boundary conditions (1.4.2), to give

$$\begin{aligned}\delta W=\frac{1}{2\mu}\int\Big\{&|\nabla\times(\boldsymbol{\xi}\times\mathbf{B})|^2+(\nabla\times\mathbf{B})\cdot(\boldsymbol{\xi}\times\nabla\times(\boldsymbol{\xi}\times\mathbf{B}))+\\&+(\boldsymbol{\xi}\cdot\nabla\mu p)(\nabla\cdot\boldsymbol{\xi})+\gamma\mu p(\nabla\cdot\boldsymbol{\xi})^2\Big\}\,d\mathcal{V},\end{aligned} \tag{2.2.5}$$

the form normally used in stability analysis.

To manipulate δW it is convenient to use a set of variables and derivatives compatible with the equilibrium magnetic field. The perturbation $\boldsymbol{\xi}$ is decomposed into a component perpendicular to the flux surface (ξ_r in this geometry), a component parallel to the equilibrium magnetic field ($\xi_\parallel$), and a third component in the flux surface and perpendicular to the field (ζ in this geometry). Similarly three differential operators are defined ($\partial/\partial r, \partial/\partial s$, and $\partial/\partial n$ in this geometry). Definitions are stated in Appendix A.1. As shown in Appendix B, the change in potential energy (2.2.5) may then be written as

$$\delta W=\frac{1}{2\mu}(\mathcal{I}+\mathcal{J}), \tag{2.2.6}$$

where

$$\begin{aligned}\mathcal{I}=\int\Bigg\{&B^2\left[\frac{\partial\xi_r}{\partial s}\right]^2-\frac{2B_\theta}{r^2}(rB_\theta)'\xi_r^2+\frac{\gamma\mu p}{B^2+\gamma\mu p}\left[\frac{\partial\xi_\parallel}{\partial s}+\frac{2B_\theta^2}{rB}\xi_r\right]^2+\\&+\left[\frac{\partial\zeta}{\partial s}-\frac{2B_\theta B_z}{rB}\xi_r\right]^2\Bigg\}\,r\,dr\,d\theta\,dz\end{aligned} \tag{2.2.7}$$

and

$$\mathcal{J} = \int \left\{ \frac{B^2 + \gamma\mu p}{B^2} \left[rB \frac{\partial}{\partial r}\left(\frac{\xi_r}{r}\right) + \frac{\partial \zeta}{\partial n} + \frac{\gamma\mu p}{B^2 + \gamma\mu p} \frac{\partial \xi_\parallel}{\partial s} + \right.\right. \\ \left.\left. + 2\frac{B_z^2 + \gamma\mu p}{B^2 + \gamma\mu p} B \frac{\xi_r}{r} \right]^2 \right\} r\, dr\, d\theta\, dz. \tag{2.2.8}$$

Primes denote derivatives with respect to r. This form of δW reduces to Equations (2.4) and (2.5) of Hood (1986a) in the case of shearless arcades and to Equation (4.2) of Hood and Anzer (1987) in the case of force-free arcades, and so represents a generalisation of these particular cases.

2.2.2. Necessary Conditions and Sufficient Conditions for Stability

The complete minimisation of δW to all allowable displacements requires solving a system of partial differential equations, for which no general analytical method is known at present. Since the aim is to produce simple tests for (in-)stability a different line of approach is used. First δW is shown to be negative to a particular family of localised perturbations when critical parameter values are exceeded. This provides necessary conditions for stability (sufficient for instability). Then a partial minimisation of δW, by neglecting its $\mathcal{J}$-contribution, yields a sufficient condition for stability if $\mathcal{I}$ is positive.

A. NECESSARY CONDITIONS FOR STABILITY : THE BALLOONING APPROXIMATION

Following Hood (1986a), consider perturbations that vary across the field on a short scale $1/m$, where $1/m \ll a$, the equilibrium length scale. Hence take

$$\boldsymbol{\xi}(r, \theta, z) = \boldsymbol{\xi}(r, y) \cos mS, \tag{2.2.9}$$

where the wave vector $\mathbf{k} \equiv \nabla S$ and

$$\mathbf{B} \cdot \nabla S = 0. \tag{2.2.10}$$

The amplitude factor $\boldsymbol{\xi}(r, y)$, that satisfies the line-tying conditions (1.4.2), describes slow variations of the perturbation along the field, so that the stabilising effect of magnetic tension is reduced. If one is interested in the least stable mode, Equation (2.2.10) has the simple solution

$$S = z - q\theta \qquad \text{for arcades,} \tag{2.2.11a}$$

or

$$S = \theta - z/q \qquad \text{for loops,} \tag{2.2.11b}$$

where the safety factor q is defined as

$$q(r) = \frac{rB_z(r)}{B_\theta(r)}\,. \tag{2.2.12}$$

Periodicity in the z-direction for arcades and in the θ-direction for loops was imposed. Expanding the variables in inverse powers of m, for example

$$\xi_r = \xi_{r_0} + \frac{1}{m}\xi_{r_1} + \frac{1}{m^2}\xi_{r_2} + \cdots,$$

the leading order contribution to the $\mathcal{J}$-part of δW vanishes if

$$\zeta_0 = \alpha B_\theta q' y \xi_{r_0}, \tag{2.2.13}$$

where $\alpha = (lB_\theta/rB)$, the angle over which the field line is twisted in going from one footpoint to the other, and l is the length of the field line, namely

$$l = r\pi B/B_\theta \qquad \text{for arcades,} \tag{2.2.14a}$$

or

$$l = LB/B_z \qquad \text{for loops.} \tag{2.2.14b}$$

Substituting (2.2.13) into (2.2.6), the leading order, $O(1)$, is

$$\delta W_{\text{ball}} = \mathcal{A}^2(r_0)\int_{-1/2}^{1/2}\left\{\left[(q'B_\theta y)^2 + \left(\frac{B}{\alpha}\right)^2\right]\left[\frac{\partial \xi_r}{\partial y}\right]^2 + 2r\mu p'\xi_r^2 + \right.$$
$$\left. + \frac{\gamma\mu p}{B^2+\gamma\mu p}\left[\frac{1}{\alpha}\frac{\partial \xi_\parallel}{\partial y} + 2B_\theta \xi_r\right]^2\right\} dy, \tag{2.2.15}$$

where integration over one period in z for arcades and in θ for loops has been performed, and a δ-function behaviour in r for ξ_r^2 and $\xi_\parallel^2$ is assumed to isolate any particular radius r_0, giving rise to the arbitrary amplitude $\mathcal{A}^2(r_0)$. The subscripts $_0$ in ξ_{r_0} and $\xi_{\parallel_0}$ have been suppressed for ease of notation.

To minimise the change in potential energy it is necessary to solve the Euler-Lagrange equations of the integral (2.2.15). This can be done numerically (see, for instance, Hood, 1986a) or analytically for the constant twist field (see Subsection 2.2.3). However, to obtain an analytical and easy-to-use instability criterion applicable to any cylindrically symmetric equilibrium, it is preferable to select trial functions for ξ_r and $\xi_\parallel$ and check the sign of δW. There is no need for $\boldsymbol{\xi}$ to satisfy the momentum equation (1.3.9) (Laval, Mercier, and Pellat, 1965), so the only constraint for the trial functions is that they vanish at the photosphere.

Consider two different choices of trial functions. Firstly, take

$$\xi_r = \cos^n \pi y, \tag{2.2.16}$$

where n is a positive integer and $\xi_\parallel$ is selected to minimise the third term in the integrand of (2.2.15). The necessary condition for stability then becomes (cf. Hood, 1986a)

$$a_1\left(\frac{\pi B}{\alpha r}\right)^2 + a_2\frac{B_z^2}{4}\left(\frac{q'}{q}\right)^2 + a_3\frac{2\mu p'}{r} + a_4\left(\frac{2B_\theta}{r}\right)^2\frac{c_s^2}{v_A^2+c_s^2} > 0, \tag{2.2.17}$$

where

$$a_1 = \frac{n^2}{2n-1}\,, \tag{2.2.18a}$$

$$a_2 = \begin{cases} \frac{4n^2}{2n-1}\left[\frac{\pi^2}{12} - \frac{1}{2}\left(\frac{1}{(n-1)^2} + \cdots + \frac{1}{1^2}\right)\right] + 2 & (n \neq 1), \\ \frac{\pi^2+6}{3} & (n = 1), \end{cases} \tag{2.2.18b}$$

$$a_3 = 1, \tag{2.2.18c}$$

$$a_4 = \begin{cases} \frac{(2n)!!}{(2n-1)!!}\left[\frac{(n-1)!!}{(n)!!}\right]^2 \frac{4}{\pi^2} & (n \text{ odd}), \\ \frac{(2n)!!}{(2n-1)!!}\left[\frac{(n-1)!!}{(n)!!}\right]^2 & (n \text{ even}). \end{cases} \tag{2.2.18d}$$

Neglecting the first and last terms we recover a form of Suydam's criterion (Suydam, 1958), with the stabilising effect due to shear and the destabilising effect due to an outward pressure force. The first and last terms are two extra stabilising terms due to line-tying, representing the effect of tension and compression, respectively. When $n \to \infty$, a_1 increases as $n/2$ while a_2 decreases towards $3/4$ and a_4 towards 0. So, if there is one value of n and r for which the inequality (2.2.17) does not hold, the equilibrium is definitely unstable.

Secondly, take

$$\xi_r = \cos xy - \cos x/2, \tag{2.2.19}$$

where x is any positive constant, or even a positive function of r or an equilibrium parameter, and $\xi_\parallel$ is again selected to minimise the third term in the integrand of (2.2.15). One then finds another Suydam-like necessary condition for stability, where this time

$$a_1 = \frac{x^2}{\pi^2}(x - \sin x), \tag{2.2.20a}$$

$$a_2 = \frac{x^3}{3} - (x^2 - 2)\sin x + 2x\cos x, \tag{2.2.20b}$$

$$a_3 = 2x - 3\sin x + x\cos x, \tag{2.2.20c}$$

$$a_4 = \frac{1}{x}[x^2 + 4 + (x^2 - 4)\cos x - 4x\sin x]. \tag{2.2.20d}$$

Again, if there is one value of x and r such that the inequality (2.2.17) does not hold, the equilibrium is definitely unstable. Note that $x = \pi$ recovers the $n = 1$ case of (2.2.16) while $x = 2\pi$ yields results of $n = 2$.

B. SUFFICIENT CONDITIONS FOR STABILITY

Since $\mathcal{J} \geq 0$ in (2.2.6) this contribution to δW can be neglected and the remaining part of δW can be minimised to obtain a sufficient condition for stability. The Euler-

Lagrange equations for the integral (2.2.7) are

$$B^2\frac{\partial^2\xi_r}{\partial s^2} = \Big(-\Lambda\frac{B^2}{l^2} - \frac{2B_\theta}{r^2}(rB_\theta)'\Big)\xi_r + \frac{\gamma\mu p}{B^2+\gamma\mu p}\frac{2B_\theta^2}{rB}\Big(\frac{\partial\xi_\parallel}{\partial s} + \frac{2B_\theta^2}{rB}\xi_r\Big) - \\ - \frac{2B_\theta B_z}{rB}\Big(\frac{\partial\zeta}{\partial s} - \frac{2B_\theta B_z}{rB}\xi_r\Big),$$

$$\frac{\partial}{\partial s}\Big(\frac{\partial\xi_\parallel}{\partial s} + \frac{2B_\theta^2}{rB}\xi_r\Big) = 0, \qquad (2.2.21)$$

$$\frac{\partial}{\partial s}\Big(\frac{\partial\zeta}{\partial s} - \frac{2B_\theta B_z}{rB}\xi_r\Big) = 0,$$

where Λ is a Lagrange multiplier, obtained from the normalising condition

$$\int \frac{B^2}{l^2}\xi_r^2\, r\, dr\, d\theta\, dz = \text{constant}, \qquad (2.2.22)$$

and Λ has the same sign as $\mathcal{I}$. Since these equations have constant coefficients with respect to s, we look for solutions of the form

$$\exp\Big(i\frac{xs}{l}\Big), \qquad (2.2.23)$$

where $\xi_r = \xi_\parallel = \zeta = 0$ at $s = \pm l/2$ $(y = \pm\frac{1}{2})$ to satisfy line-tying, and

$$\Lambda = x^2 - \alpha^2\frac{2(rB_\theta)'}{B_\theta} \qquad (2.2.24)$$

from Equations (2.2.21), with $\alpha = (lB_\theta/rB)$ as before. For ξ_r odd about $s = 0$,

$$\xi_r = \sin\frac{xs}{l}\,, \qquad (2.2.25)$$

where

$$x = 2n\pi, \qquad n = 1, 2, 3, \ldots. \qquad (2.2.26)$$

For ξ_r even about $s = 0$,

$$\xi_r = \cos\frac{xs}{l} - \cos\frac{x}{2}\,, \qquad (2.2.27)$$

where

$$\tan\frac{x}{2} = \frac{x}{2}\Big(1 - \frac{x^2}{4\alpha^2}\frac{B^2+\gamma\mu p}{B_z^2+\gamma\mu p}\Big). \qquad (2.2.28)$$

Equations (2.2.24) and (2.2.28) reduce to Equations (2.7) and (2.9a) of Hood (1986a) in the case of shearless arcades and to Equations (4.4) and (4.7) of Hood and Anzer (1987) in the case of force-free arcades, and so represent a generalisation of these particular cases.

2.2.3. Application to Equilibria in Arcade and Loop Geometry

A. FOUR CLASSES OF EQUILIBRIA

To illustrate the use of the method developed in the previous Subsection, four classes of cylindrically symmetric magnetostatic equilibria are investigated. Using the dimensionless variables $\bar{r} = r/a, \bar{L} = L/a, \bar{\lambda} = \lambda/a, \bar{B}_\theta = B_\theta/B_0, \bar{B}_z = B_z/B_0, \bar{p} = \mu p/B_0^2$,

where a and B_0 are the characteristic equilibrium length scale and magnetic field strength, respectively, and suppressing the bars for simplicity, these are

$$B_\theta = \frac{r}{1+r^2}\,, \qquad B_z = \frac{\lambda}{1+r^2}\,, \qquad p = \frac{1-\lambda^2}{2(1+r^2)^2}\,; \tag{E1}$$

$$B_\theta = \sqrt{r}\mathrm{e}^{-r/2}, \qquad B_z = \lambda[\sigma + (2-r)\mathrm{e}^{-r}]^{1/2},$$
$$p = \frac{1-\lambda^2}{2}[\sigma + (2-r)\mathrm{e}^{-r}]; \tag{E2}$$

$$B_\theta = r\mathrm{e}^{-r/2}, \qquad B_z = \lambda[\sigma + (2+2r-r^2)\mathrm{e}^{-r}]^{1/2},$$
$$p = \frac{1-\lambda^2}{2}[\sigma + (2+2r-r^2)\mathrm{e}^{-r}]; \tag{E3}$$

$$B_\theta = \frac{r}{1+r^2}\,, \qquad B_z = \lambda\,, \qquad p = \frac{1}{2(1+r^2)^2}\,. \tag{E4}$$

E1 is the constant twist field of Gold and Hoyle (1960), E2 and E3 are generalisations of the equilibria proposed by Anzer (1968), and E4 is a constant B_z field (see, for instance, Priest, 1982, p. 130). A description of the global stability of the first three arcade equilibria is given by Cargill, Hood, and Migliuolo (1986).

λ is a measure for the shear of the magnetic field while σ represents the constant component of the z-field. Increasing λ or σ are both stabilising effects. In the former case the shear is increased and in the latter energy is needed to deform the constant axial field. A background uniform plasma pressure P_0, also a stabilising effect, is neglected. If P_0 is included, λ can exceed the maximum value of 1 for the first three equilibria. For these fields $\lambda = 1$ corresponds to a force-free magnetic field, while in all four cases $\lambda = 0$ yields a shearless field. For E2 and E3 both B_z and p become negative at a certain radius $r = r^*$ when σ is less then e^{-3} and $6\,\mathrm{e}^{-4}$, respectively. In that case we modify the equilibrium by attaching a potential field outside $r = r^*$. E2 is also somewhat unphysical in that the axial current density is infinite on the axis $r = 0$.

As was mentioned in Subsection 2.2.2, the potential energy (2.2.15) can be minimised analytically in the case of the constant twist field E1. The Euler-Lagrange equations then are

$$B^2\frac{\partial^2\xi_r}{\partial y^2} = (-\Lambda B^2 + 2\alpha^2 r\mu p')\xi_r + \frac{2\alpha^2\gamma\mu p B_\theta}{B^2+\gamma\mu p}\Big(\frac{1}{\alpha}\frac{\partial\xi_\parallel}{\partial y} + 2B_\theta\xi_r\Big),$$
$$\frac{\partial}{\partial y}\Big(\frac{1}{\alpha}\frac{\partial\xi_\parallel}{\partial y} + 2B_\theta\xi_r\Big) = 0, \tag{2.2.29}$$

where Λ is a Lagrange multiplier, obtained from the normalising condition

$$\mathcal{A}^2(r_0)\int_{-1/2}^{1/2}\frac{B^2}{\alpha^2}\xi_r^2\,dy = \text{constant}, \tag{2.2.30}$$

and Λ has the same sign as δW_{ball}. As before, the solutions are of the form $\exp(ixy)$,

line-tying is assumed at $y = \pm\frac{1}{2}$, and

$$\Lambda = x^2 + \alpha^2 \frac{2r\mu p'}{B^2} \tag{2.2.31}$$

from Equations (2.2.29). For ξ_r odd about $y = 0$,

$$\xi_r = \sin xy, \tag{2.2.32}$$

where

$$x = 2n\pi, \qquad n = 1, 2, 3, \ldots, \tag{2.2.33}$$

and for ξ_r even about $y = 0$,

$$\xi_r = \cos xy - \cos x/2, \tag{2.2.34}$$

where

$$\tan \frac{x}{2} = \frac{x}{2}\left(1 - \frac{x^2}{4\alpha^2}\frac{B^2}{B_\theta^2}\frac{B^2 + \gamma\mu p}{\gamma\mu p}\right). \tag{2.2.35}$$

Note that for B_z=0 (i.e., $\lambda = 0$) Equations (2.2.31) and (2.2.35) are identical to Equations (2.2.24) and (2.2.28), showing that the sufficient condition for stability is identical to the necessary condition in the case of shearless arcades.

First of all, marginal stability with $\delta W = 0$ is studied. For fixed parameters r, n or x, σ in the case of E2 and E3, and L in the case of loops, Equation (2.2.17) is a function of λ alone. The largest λ that makes this function vanish separates the instability region from the 'stability' region. Plotting that value of λ against r in a $\lambda(r)$ diagram, an *instability curve* is obtained. Below that curve the equilibrium is unstable, above that curve it may be either stable or unstable. The maximum of that curve gives the value λ_1 below which the field is definitely unstable and the radius at which these localised modes are situated.

In Equation (2.2.24) marginal stability corresponds to $\Lambda = 0$. Substituting the resulting expression for x into Equation (2.2.28) yields, for fixed parameters r, σ in the case of E2 and E3, and L in the case of loops, a function of λ alone. The largest λ that makes this function vanish separates the stability region from the 'instability' region. Again, plotting that value of λ against r in a $\lambda(r)$ diagram, a *stability curve* is obtained. Above that curve the equilibrium is stable, below that curve it may be either stable or unstable. Its maximum gives the value λ_2 above which the field is definitely stable. The smaller the difference between λ_1 and λ_2, the smaller the *uncertainty interval*, i.e., the range in λ for which the developed method is unable to distinguish between stability and instability.

B. RESULTS FOR THE EQUILIBRIA IN ARCADE GEOMETRY

Figure 2.1 shows the instability curves for the constant twist field E1, using Equations (2.2.17) and (2.2.18). There is no curve if $n \geq 3$. The outer curve defined by the

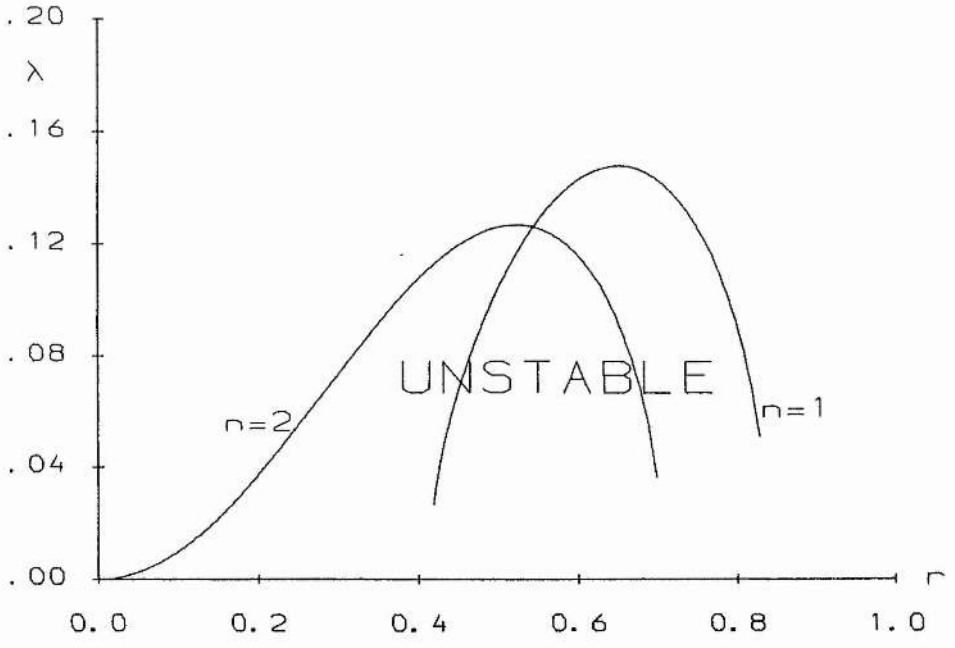

Fig. 2.1. Instability curves $\lambda(r)$ for the constant twist field E1 ($\gamma = 1$) in arcade geometry, resulting from the inequality (2.2.17) using (2.2.18). The left curve is for $n = 2$ while the right curve originates from choosing $n = 1$. The region below the envelope of both curves is definitely unstable.

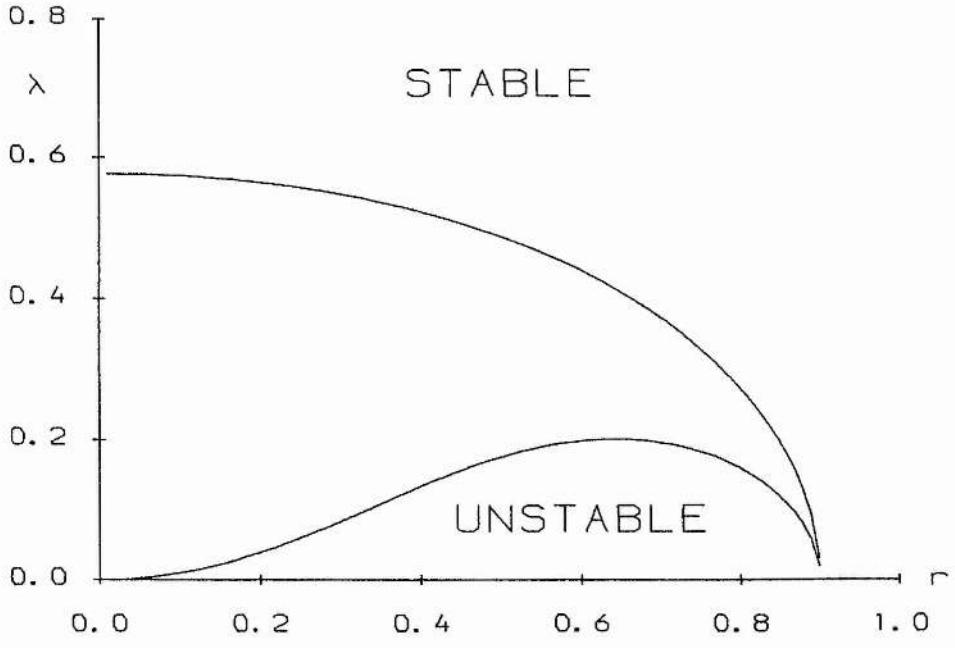

Fig. 2.2. Stability (upper) and instability (lower) curve $\lambda(r)$ for E1 ($\gamma = 1$) in arcade geometry. Stable and unstable regions are indicated.

envelope of these two curves gives the best instability curve for this choice of perturbations. In Figure 2.2 the stability curve $\lambda(r)$ using Equations (2.2.24) and (2.2.28) and the instability curve $\lambda(r)$ using Equations (2.2.17) and (2.2.20) are plotted, where x was taken as

$$x = \pi\left(\frac{-2r\mu p'}{B^2}\right)^{1/2} \tag{2.2.36}$$

from (2.2.31). This yields the exact instability curve. There is a broad region in r where instabilities can occur. Comparing Figures 2.1 and 2.2 it can be seen that the curve $\lambda(r)$ generated by choosing perturbations of the form (2.2.19) rather than (2.2.16) results in a smaller uncertainty interval. This is the case for all investigated equilibria. The uncertainty interval in λ for this equilibrium is $[0.201, 0.577]$. Figures 2.1 and 2.2 depict the situation when $\gamma = 1$. Taking the physically more relevant case $\gamma = 5/3$, the constant twist field turns out to be completely stable for all λ and, in fact, it is stable for $\gamma > 4/3$ (cf. Schindler, Birn, and Janicke, 1983).

Figure 2.3 displays stability and instability curves $\lambda(r)$ for the equilibrium E3, where x is given by the same expression (2.2.36), $\gamma = 1$ and $\sigma = 6\,\mathrm{e}^{-4}$. When $\lambda(r)$ is obtained by numerically solving the Euler-Lagrange equations of the integral (2.2.15) (see Hood, 1986a), there is no difference with the results obtained by applying the inequality (2.2.17) using (2.2.20), up to three significant figures. Obviously the latter approach is easier than solving the differential equations. The uncertainty interval in λ is $[0.309, 0.555]$. Plotting the maximum values of both curves $\lambda(r)$ against σ, as shown in Figure 2.4 for E3 with $\gamma = 1$, shows how the uncertainty interval varies with σ. Comparing this with Velli and Hood (1986), who solved the Euler-Lagrange equations for the integral (2.2.15) numerically, it can be seen that there is very little difference between both instability curves. Note that the uncertainty interval for λ shrinks as σ increases. When $\gamma = 5/3$ equilibrium E3 is stable for $\sigma \geq 0.053$.

Equilibrium E2 has similar $\lambda(r)$ curves to those of E3, but the instability region in r is much narrower (for instance, for $\gamma = 1$ and $\sigma = 0.01$ the instabilities are located within the r interval $[1.36, 1.67]$, see Figure 2.5). E2 is stable for $\sigma \geq 0.012$ when $\gamma = 1$ (Figure 2.6) and is completely stable if $\gamma \geq 1.3$. Equilibrium E4 has similar $\lambda(r)$ curves to those of E1, with uncertainty interval in λ being $[0.194, 0.409]$ if $\gamma = 1$ (Figure 2.7). It is also completely stable for $\gamma \geq 4/3$.

For all four classes of equilibria investigated, the instability curves obtained by applying the inequality (2.2.17) using (2.2.20) are almost indistinguishable from those resulting from numerically integrating the Euler-Lagrange equations of the integral (2.2.15).

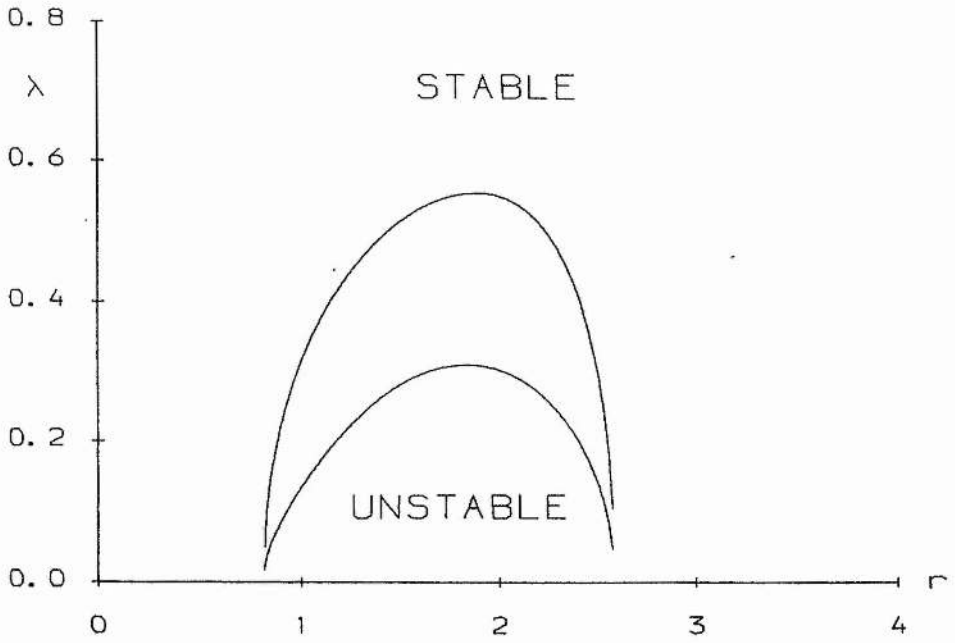

Fig. 2.3. Stability (upper) and instability (lower) curve $\lambda(r)$ for E3 ($\gamma = 1, \sigma = 6\,e^{-4}$) in arcade geometry. Stable and unstable regions are indicated.

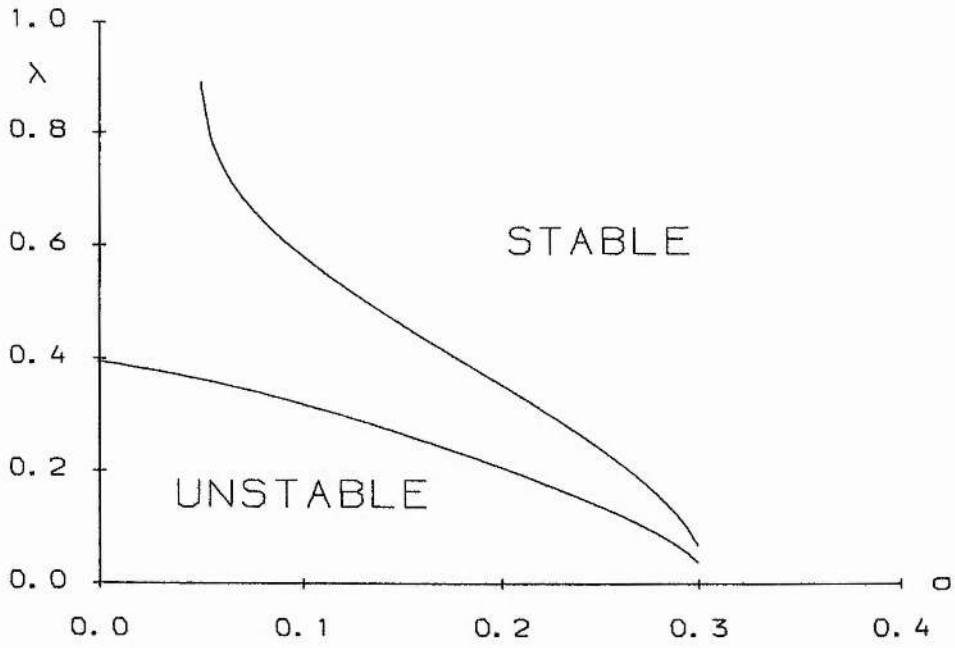

Fig. 2.4. Stability (upper) and instability (lower) curve $\lambda(\sigma)$ for E3 ($\gamma = 1$) in arcade geometry. The equilibria below the lower curve are unstable, those above the upper curve are stable.

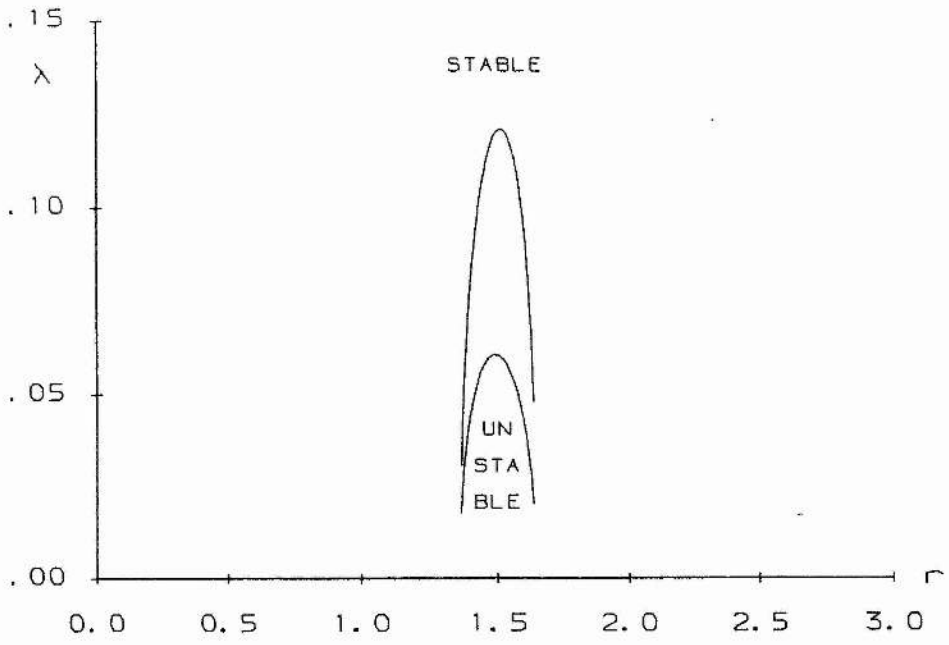

Fig. 2.5. Stability (upper) and instability (lower) curve $\lambda(r)$ for E2 ($\gamma = 1, \sigma = 0.01$) in arcade geometry. Stable and unstable regions are indicated.

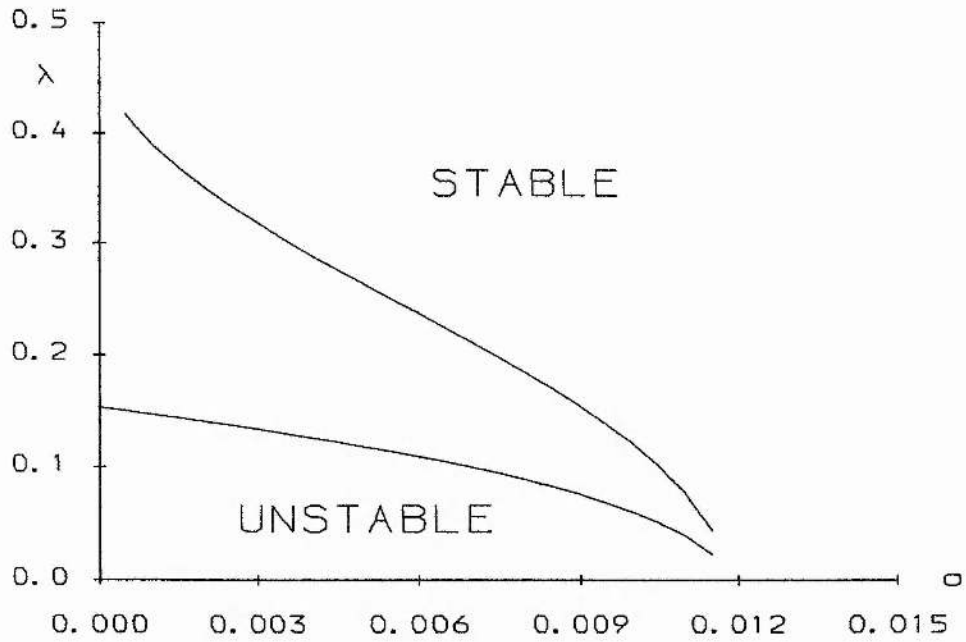

Fig. 2.6. Stability (upper) and instability (lower) curve $\lambda(\sigma)$ for E2 ($\gamma = 1$) in arcade geometry. The equilibria below the lower curve are unstable, those above the upper curve are stable.

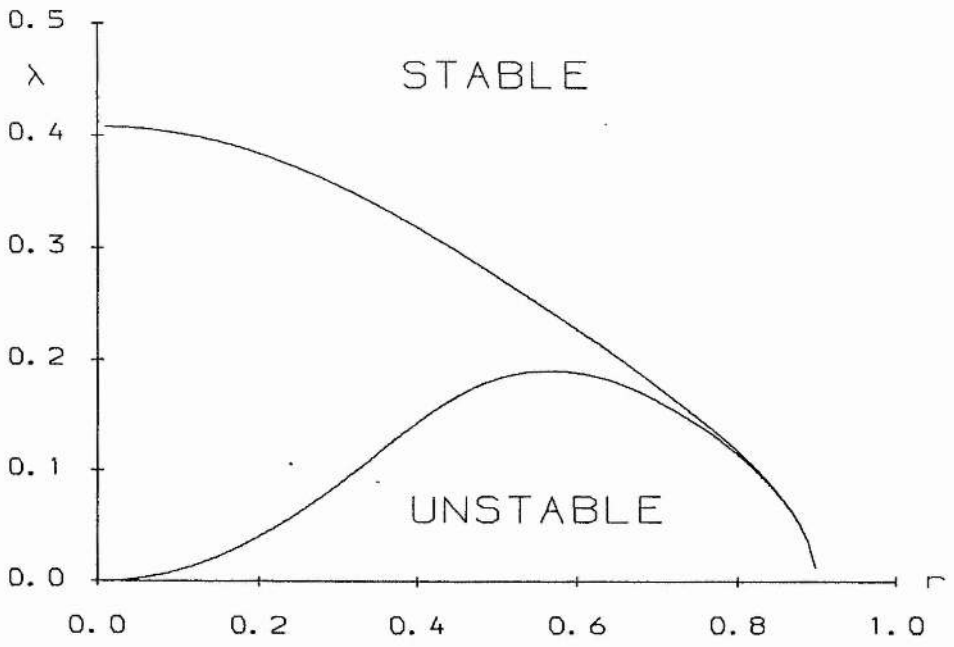

Fig. 2.7. Stability (upper) and instability (lower) curve $\lambda(r)$ for E4 ($\gamma = 1$) in arcade geometry. Stable and unstable regions are indicated.

C. RESULTS FOR THE EQUILIBRIA IN LOOP GEOMETRY

Considering a coronal loop geometry, Figure 2.8 shows, for the equilibrium E1, the stability curve $\lambda(L)$ for $\gamma = 1$ using Equations (2.2.24) and (2.2.28) and the instability curves $\lambda(L)$ for $\gamma = 1$ and $\gamma = 5/3$ using Equations (2.2.17) and (2.2.20). Here

$$x = \Phi\left(\frac{-2r\mu p'}{B^2}\right)^{1/2} \tag{2.2.37}$$

from Equation (2.2.31), and Φ is the twist of the magnetic field, i.e., the angle over which a field line is twisted in going from one footpoint to the other, given by

$$\Phi(r) = \frac{L}{q(r)} \, . \tag{2.2.38}$$

This yields the exact instability curves. It can be seen that for large loop lengths L a slight departure from the force-free state makes the equilibrium unstable to ballooning modes. If the critical twist Φ is plotted as a function of the loop length L, as in Figure 2.9, it is obvious that the uncertainty region is very narrow. The part of the diagram below the line $\Phi = L$ is physically irrelevant, since λ cannot be greater than 1 for positive gas pressures.

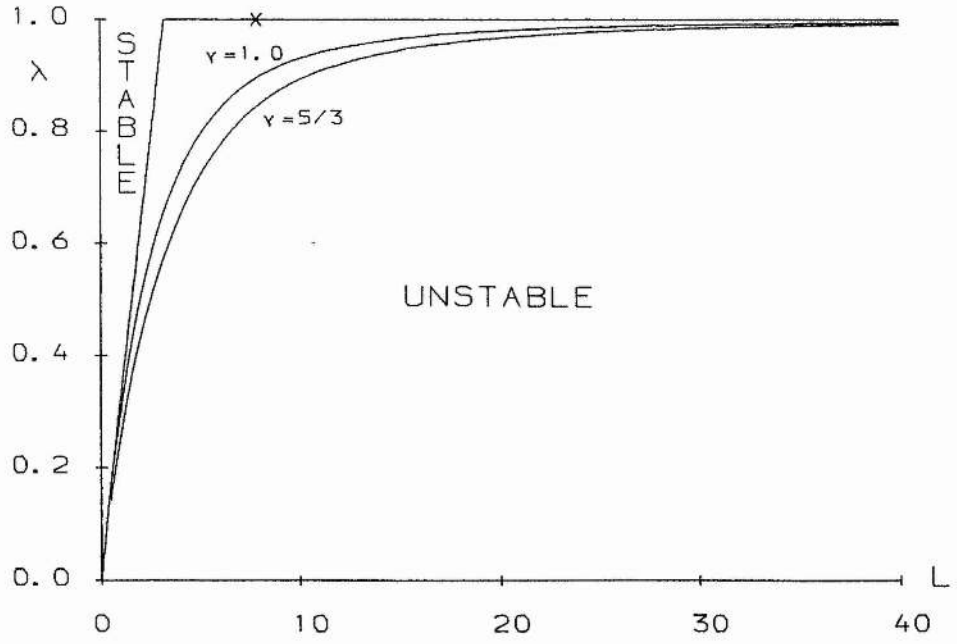

Fig. 2.8. Stability (upper) curve $\lambda(L)$ for $\gamma = 1$ and instability curves $\lambda(L)$ when $\gamma = 1$ and $\gamma = 5/3$, for E1 in loop geometry. Stable and unstable regions are indicated. The 'X' denotes the position where the force-free field becomes unstable to kink modes (see Section 6.3).

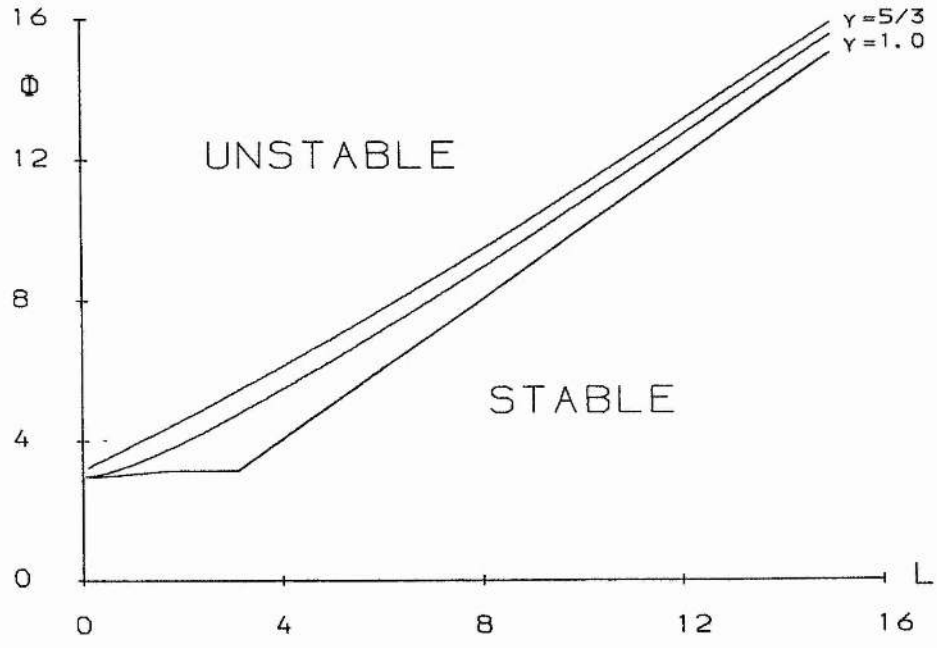

Fig. 2.9. Stability (lower) curve $\Phi(L)$ for $\gamma = 1$ and instability curves $\Phi(L)$ when $\gamma = 1$ and $\gamma = 5/3$, for E1 in loop geometry. Stable and unstable regions are indicated. The region below the bisector $\Phi = L$ is physically irrelevant.

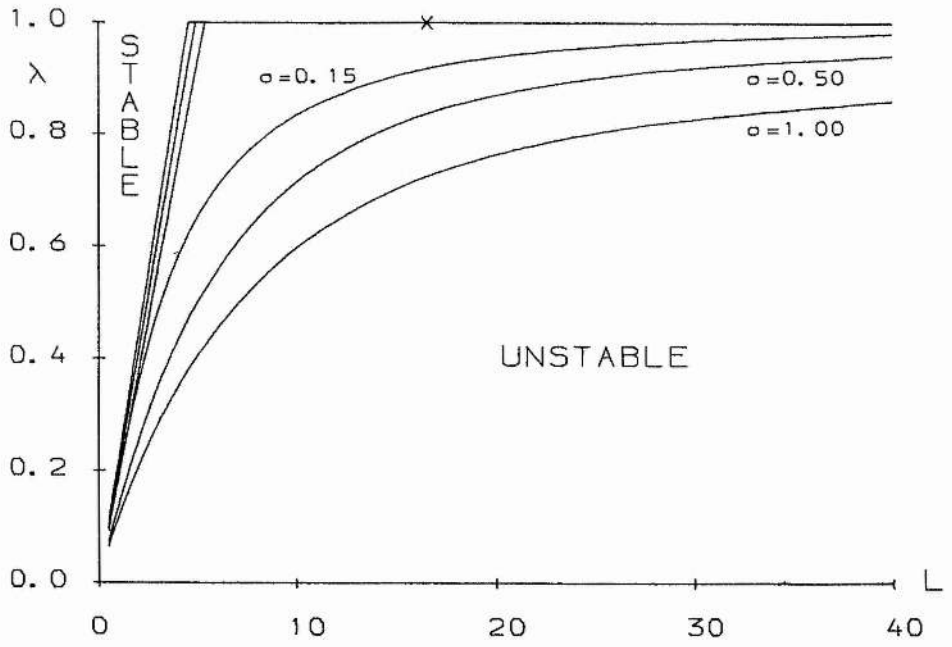

Fig. 2.10. Stability (upper) and instability (lower) curves $\lambda(L)$ for E3 ($\gamma = 1$) in loop geometry. In both cases the highest curve corresponds to $\sigma = 0.15$, the middle curve to $\sigma = 0.50$, and the lowest curve to $\sigma = 1.00$. Stable and unstable regions are indicated. The 'X' denotes the position where the force-free field becomes unstable to kink modes (see Section 6.3).

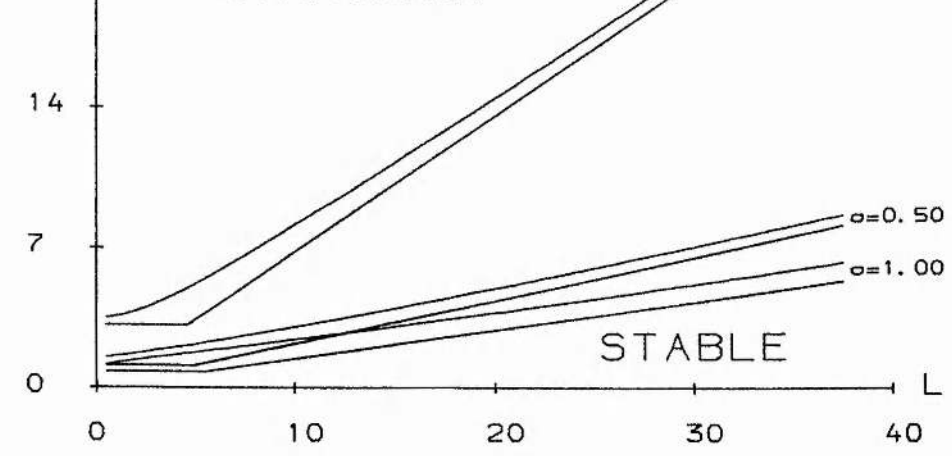

Fig. 2.11. Stability (lower) and instability (upper) curves $\Phi(L)$ for E3 ($\gamma = 1$) in loop geometry. The upper two curves correspond to $\sigma = 0.15$, the middle two curves to $\sigma = 0.50$, and the lower two curves to $\sigma = 1.00$. Stable and unstable regions are indicated.

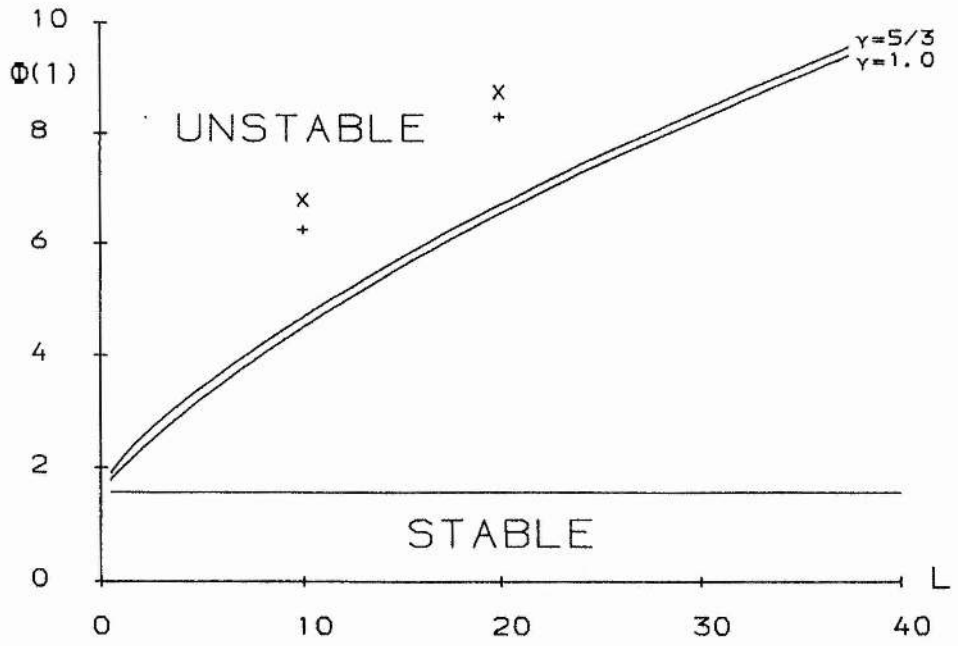

Fig. 2.12. Stability (lower) curve $\Phi(L)$ and instability curves $\Phi(L)$ when $\gamma = 1$ and $\gamma = 5/3$, for E4 in loop geometry. Stable and unstable regions are indicated. The 'X's denote the instability thresholds for incompressible kink modes ($\gamma = 2$) calculated by Hood and Priest (1979) while the '+'s mark those found by An (1984) for the compressible modes.

Figures 2.10 and 2.11 for equilibrium E3 are the counterparts of Figures 2.8 and 2.9, for three values of the parameter σ ($\gamma = 1$). It is clear that increasing σ has a stabilising effect. On the other hand, when $\sigma \leq 6\,e^{-4}$, there is a radius r for which $B_z = 0$. When this occurs the equilibrium is unstable for all loop lengths L. For $\sigma \geq 0.15$ the stability curve has equation

$$\lambda = \frac{L}{\pi(\sigma+2)^{1/2}}\,, \tag{2.2.39}$$

which implies that a force-free loop E3 of length L can be made stable by putting

$$\sigma \geq \frac{L^2}{\pi^2} - 2. \tag{2.2.40}$$

The results for E2 and E4 are similar. In the case of E4, the critical twist for instability, derived using Equations (2.2.17) and (2.2.20) with (2.2.37), is smaller than that found by Hood and Priest (1979) and An (1984) (see Figure 2.12). It may be noted that, as opposed to arcades, increasing γ from 1 to 5/3 does not greatly change the position of the marginal curves in loop geometry. For example, for E4 it reduces λ_1 from 1.11 to 1.07 for $L = 10$.

2.3. Plane Plasma Layers in a Perpendicular Gravitational Field

2.3.1. Energy Integral

Consider slab equilibria

$$\begin{aligned} \mathbf{B} &= (B_x(z), B_y(z), 0), \qquad \phi = gz, \\ p &= p(z), \qquad \rho = \rho(z), \end{aligned} \tag{2.3.1}$$

satisfying the magnetohydrostatic equation

$$\frac{d}{dz}\Big(p + \frac{B^2}{2\mu}\Big) = -\rho g, \tag{2.3.2}$$

where $B^2 = B_x^2 + B_y^2$. The line-tying effect of the dense photosphere, located at

$$x = -\frac{L}{2} \qquad \text{and} \qquad x = \frac{L}{2}\,, \tag{2.3.3}$$

where L is the dimension in the direction of line-tying of the coronal structure envisaged, is again modelled by the rigid plate boundary conditions (1.4.2). The change in potential energy due to a coronal disturbance then takes the form

$$\begin{aligned} \delta W = \frac{1}{2\mu}\int \Big\{ &|\nabla\times(\boldsymbol{\xi}\times\mathbf{B})|^2 + (\nabla\times\mathbf{B})\cdot(\boldsymbol{\xi}\times\nabla\times(\boldsymbol{\xi}\times\mathbf{B})) + \\ &+(\boldsymbol{\xi}\cdot\nabla\mu p)(\nabla\cdot\boldsymbol{\xi}) + \gamma\mu p(\nabla\cdot\boldsymbol{\xi})^2 - (\boldsymbol{\xi}\cdot\nabla\phi)\nabla\cdot(\mu\rho\boldsymbol{\xi})\Big\}\, d\mathcal{V}. \end{aligned} \tag{2.3.4}$$

Using an appropriate set of variables and derivatives (see Appendix A.2) this can be rewritten as (see Appendix C)

$$\delta W = \frac{1}{2\mu}(\mathcal{I} + \mathcal{J}), \tag{2.3.5}$$

where

$$\mathcal{I} = \int\left\{ B^2\left[\frac{\partial\xi_z}{\partial s}\right]^2 + \mu\rho N^2\xi_z^2 + \frac{\gamma\mu p}{B^2+\gamma\mu p}\left[\frac{\partial\xi_\parallel}{\partial s} - \frac{g}{c_s^2}B\xi_z\right]^2 + \left[\frac{\partial\zeta}{\partial s}\right]^2\right\} dx\,dy\,dz \tag{2.3.6}$$

and

$$\mathcal{J} = \int\left\{ \frac{B^2+\gamma\mu p}{B^2}\left[B\xi_z' + \frac{\partial\zeta}{\partial n} + \frac{\gamma\mu p}{B^2+\gamma\mu p}\Big(\frac{\partial\xi_\parallel}{\partial s} - \frac{g}{c_s^2}B\xi_z\Big)\right]^2\right\} dx\,dy\,dz. \tag{2.3.7}$$

Primes denote derivatives with respect to z, and

$$N^2 = -g\Big(\frac{g}{c_s^2} + \frac{\rho'}{\rho}\Big) \tag{2.3.8}$$

is the square of the Brunt-Väisälä or buoyancy frequency. Note that

$$\frac{\gamma\mu p}{B^2+\gamma\mu p} = \frac{c_s^2}{v_A^2+c_s^2} = \frac{c_T^2}{v_A^2} \tag{2.3.9}$$

is the square of the ratio of tube (or cusp) speed to Alfvén speed.

2.3.2. Necessary Conditions and Sufficient Conditions for Stability

The same approach is taken as in Subsection 2.2.2. First a necessary condition for stability is derived, using localised interchange modes as trial function in δW. Then

a sufficient condition for stability is obtained by minimising the $\mathcal{I}$-contribution to the energy integral.

A. NECESSARY CONDITIONS FOR STABILITY : THE BALLOONING APPROXIMATION

Consider perturbations of the form

$$\boldsymbol{\xi}(x,y,z) = \boldsymbol{\xi}(x,z)\cos mS, \tag{2.3.10}$$

where the wave vector $\mathbf{k} \equiv \nabla S$ and $\mathbf{B}\cdot\nabla S = 0$ by choosing

$$S = y - \frac{B_y}{B_x}x, \tag{2.3.11}$$

imposing periodicity in the y-direction. Expanding the variables in inverse powers of m, for example

$$\xi_z = \xi_{z_0} + \frac{1}{m}\xi_{z_1} + \frac{1}{m^2}\xi_{z_2} + \cdots,$$

the leading order contribution to the $\mathcal{J}$-part of δW vanishes if

$$\zeta_0 = B_x\left(\frac{B_y}{B_x}\right)' x\xi_{z_0}. \tag{2.3.12}$$

Substituting (2.3.12) into (2.3.5), the leading order, $O(1)$, is

$$\begin{aligned}\delta W_{\text{ball}} = \mathcal{A}^2(z_0)\int_{-L/2}^{L/2}\Bigg\{\left[\left(B_x\left(\frac{B_y}{B_x}\right)' x\right)^2 + B^2\right]\left[\frac{\partial\xi_z}{\partial x}\right]^2 + \mu\rho N^2\frac{B^2}{B_x^2}\xi_z^2 + \\ + \frac{\gamma\mu p}{B^2+\gamma\mu p}\left[\frac{\partial\xi_\parallel}{\partial x} - \frac{g}{c_s^2}\frac{B^2}{B_x}\xi_z\right]^2\Bigg\}dx,\end{aligned} \tag{2.3.13}$$

where integration over one period in y has been performed, and a δ-function behaviour in z for ξ_z^2 and $\xi_\parallel^2$ is assumed to isolate any particular radius z_0, giving rise to the arbitrary amplitude $\mathcal{A}^2(z_0)$. Here too, the subscripts $_0$ in ξ_{z_0} and $\xi_{\parallel_0}$ have been suppressed for convenience.

A complete minimisation of the ballooning integral (2.3.13) requires the solution of its Euler-Lagrange equations. This can be done analytically for a shearless field, i.e., when $(B_y/B_x)' = 0$, or numerically for sheared equilibria. Alternatively, one can select trial functions for ξ_z and $\xi_\parallel$ and check the sign of δW.

Firstly, consider the case of a shearless field. The Euler-Lagrange equations then are

$$\begin{aligned}B^2\frac{\partial^2\xi_z}{\partial x^2} &= \left(-\Lambda\frac{B^2}{L^2} + \mu\rho N^2\frac{B^2}{B_x^2}\right)\xi_z - \frac{\mu\rho g}{B^2+\gamma\mu p}\frac{B^2}{B_x}\left(\frac{\partial\xi_\parallel}{\partial x} - \frac{g}{c_s^2}\frac{B^2}{B_x}\xi_z\right), \\ \frac{\partial}{\partial x}\left(\frac{\partial\xi_\parallel}{\partial x} - \frac{g}{c_s^2}\frac{B^2}{B_x}\xi_z\right) &= 0,\end{aligned} \tag{2.3.14}$$

where Λ is a Lagrange multiplier, obtained from the normalising condition

$$\mathcal{A}^2(z_0)\int_{-L/2}^{L/2}\frac{B^2}{L^2}\xi_z^2\,dx = \text{constant}, \tag{2.3.15}$$

and Λ has the same sign as δW_{ball}. Hence the solutions are of the form $\exp(irx/L)$, line-tying is assumed at $x = \pm L/2$, and

$$\Lambda = r^2 + l^2 \frac{N^2}{v_A^2} \tag{2.3.16}$$

from Equation (2.3.14), with $l = LB/B_x$, the length of a field line. For ξ_z odd about $x = 0$,

$$\xi_z = \sin \frac{rx}{L} , \tag{2.3.17}$$

where

$$r = 2n\pi, \qquad n = 1, 2, 3, \ldots , \tag{2.3.18}$$

and for ξ_z even about $x = 0$,

$$\xi_z = \cos \frac{rx}{L} - \cos \frac{r}{2} , \tag{2.3.19}$$

where

$$\tan \frac{r}{2} = \frac{r}{2}\left(1 - \frac{r^2}{l^2}\frac{c_s^2}{g}\frac{v_A^2 + c_s^2}{g}\right). \tag{2.3.20}$$

Secondly, for a sheared equilibrium, take a trial function suggested by the above analysis, namely

$$\xi_z = \cos \frac{rx}{L} - \cos \frac{r}{2} , \tag{2.3.21}$$

where r is any positive constant, or even a positive function of z or an equilibrium parameter, and $\xi_\parallel$ is selected to minimise the third term in the integrand of (2.3.13). The necessary condition for stability then becomes

$$a_1 + a_2 \frac{1}{4}\frac{B_x^4}{B^4}\left(\frac{B_y}{B_x}\right)'^2 + a_3 \frac{N^2}{v_A^2} + a_4 \frac{g}{c_s^2}\frac{g}{v_A^2 + c_s^2} > 0, \tag{2.3.22}$$

where

$$a_1 = \frac{r^2}{l^2}(r - \sin r), \tag{2.3.23a}$$

$$a_2 = \frac{r^3}{3} - (r^2 - 2)\sin r + 2r \cos r, \tag{2.3.23b}$$

$$a_3 = 2r - 3 \sin r + r \cos r, \tag{2.3.23c}$$

$$a_4 = \frac{1}{r}[r^2 + 4 + (r^2 - 4)\cos r - 4r \sin r]. \tag{2.3.23d}$$

Compare this with Equations (2.2.17) and (2.2.20) for cylindrical symmetry. Neglecting the first and last terms we recover the form of Suydam's criterion in slab geometry (see, for instance, Goedbloed, 1971a), with the stabilising effect due to shear and the destabilising effect due to buoyancy. As before, the first and last terms are two extra stabilising terms due to line-tying, representing the effect of tension and compression, respectively. If there is one value of r and z for which the inequality (2.3.22) does not hold, the equilibrium is definitely unstable.

B. SUFFICIENT CONDITIONS FOR STABILITY

Discarding the $\mathcal{J}$-contribution to δW, one can obtain a sufficient condition for stability by minimising $\mathcal{I}$. The Euler-Lagrange equations for that integral, (2.3.6), are

$$\begin{aligned} B^2\frac{\partial^2\xi_z}{\partial s^2} &= \Big(-\Lambda\frac{B^2}{l^2}+\mu\rho N^2\Big)\xi_z - \frac{\mu\rho g B}{B^2+\gamma\mu p}\Big(\frac{\partial\xi_\parallel}{\partial s}-\frac{g}{c_s^2}B\xi_z\Big), \\ \frac{\partial}{\partial s}\Big(\frac{\partial\xi_\parallel}{\partial s}-\frac{g}{c_s^2}B\xi_z\Big) &= 0, \\ \frac{\partial^2\zeta}{\partial s^2} &= 0, \end{aligned} \tag{2.3.24}$$

where Λ is a Lagrange multiplier, obtained from the normalising condition

$$\int \frac{B^2}{l^2}\xi_z^2\,dx\,dy\,dz = \text{constant}, \tag{2.3.25}$$

and Λ has the same sign as $\mathcal{I}$. As before, we look for solutions of the form

$$\exp\Big(i\frac{rs}{l}\Big), \tag{2.3.26}$$

where $\xi_z = \xi_\parallel = \zeta = 0$ at $s = \pm l/2$ $(x = \pm L/2)$ to satisfy line-tying, and

$$\Lambda = r^2 + l^2\frac{N^2}{v_A^2} \tag{2.3.27}$$

from Equations (2.3.24). For ξ_z odd about $s = 0$,

$$\xi_z = \sin\frac{rs}{l}\,, \tag{2.3.28}$$

where

$$r = 2n\pi, \qquad n = 1, 2, 3, \ldots. \tag{2.3.29}$$

For ξ_z even about $s = 0$,

$$\xi_z = \cos\frac{rs}{l} - \cos\frac{r}{2}\,, \tag{2.3.30}$$

where

$$\tan\frac{r}{2} = \frac{r}{2}\Big(1 - \frac{r^2}{l^2}\frac{c_s^2}{g}\frac{v_A^2+c_s^2}{g}\Big). \tag{2.3.31}$$

Note that for shearless equilibria $((B_y/B_x)' = 0)$ Equations (2.3.30) and (2.3.31) are identical to Equations (2.3.19) and (2.3.20), showing that in that case the sufficient condition for stability is identical to the necessary condition.

2.3.3. Application to a Force-Free Equilibrium

The stability criteria developed in the previous Subsection are applied to the situation of a slab with adverse density gradient (i.e., a heavier plasma on top of a lighter one), permeated by a force-free magnetic field. This is a crude model for the lower half of a coronal loop, where Rayleigh-Taylor instabilities might be expected to occur. The equilibrium profiles are

$$\rho = \rho_c\left[1 + (R_d - 1)\left(-\frac{z^3}{4\epsilon^3} + \frac{3z}{4\epsilon} + \frac{1}{2}\right)\right] \qquad \text{when } |z| < \epsilon, \tag{2.3.32a}$$

$$p = P_0 - g\int_{\epsilon}^{z} \rho dz, \tag{2.3.32b}$$

$$B = B_0. \tag{2.3.32c}$$

Here ρ_c is the constant coronal ($z < -\epsilon$) plasma density, R_d is the ratio of loop to coronal density, ϵ is a quarter of the loop diameter, P_0 is the plasma pressure at the loop center, and B_0 is the magnetic field strength. Assume the field rotates over an angle α in going from $z = -\epsilon$ to $z = \epsilon$. For coronal values of plasma beta $2\mu p/B^2$, Alfvén speed, and gravitational acceleration, say $2\mu p/B^2 = 10^{-2}$, $v_{A_c} = 10^6$ m/s, and $g = 274$ m/s^2, the necessary condition for stability (2.3.22)–(2.3.23) reduces to

$$\alpha > 3\sqrt{\frac{6}{2\pi^2 - 3}}\frac{\sqrt{g}\sqrt{\epsilon}}{v_{A_c}}\sqrt{R_d - 1} \tag{2.3.33}$$

in the case of very long structures ($l \to \infty$), while the sufficient condition for stability derived from Equations (2.3.27) and (2.3.31) can be written as

$$l < \frac{2\pi}{\sqrt{3}}\frac{v_{A_c}\sqrt{\epsilon}}{\sqrt{g}\sqrt{R_d - 1}}\,. \tag{2.3.34}$$

Note that the latter criterion is independent of the shear angle α. For typical values of density ratio and loop diameter, say $R_d = 3$–5, $\epsilon = 1000$–2500 km, this implies that very small shear angles ($\alpha = 3°$–$5°$) are required to produce instabilities, even in infinitely long structures, while stability is ensured for solar dimensions ($l = 100$–250 Mm).

2.4. Summary

Calculating the necessary and sufficient condition for stability of line-tied 1-D equilibria normally involves a complicated numerical study. Here a different approach was taken by rewriting the expression for the perturbed potential energy in a form suitable for manipulation.

To derive a necessary condition for stability (sufficient for instability) we concentrated on a particular class of perturbations, namely the solar equivalent of the laboratory ballooning modes. These perturbations have a slow variation along the magnetic field, hence reducing the stabilising effect of magnetic tension, and a fast variation across the field lines. Any instability is driven by outward gas pressure gradients and unfavourable field line curvature, or adverse density gradients. Minimising the corresponding expression for δW requires the solution of a system of two ordinary differential equations. This was done analytically for a constant twist cylindrical equilibrium and a shearless plasma layer. Alternatively, aiming for simple tests, trial functions were selected for the slow variation of the perturbation along the field, resulting in Suydam-like instability criteria.

To derive a sufficient condition for stability, we neglected a positive contribution to δW and solved the Euler-Lagrange equations for the remaining part analytically. It turns out that necessary conditions and sufficient conditions coincide when the equilibrium is shearless, implying that in that case the localised interchange modes are the most unstable perturbations in the sense of yielding the lowest threshold for instability. For sheared equilibria, the combination of the stability and the instability curves provides an uncertainty interval in the parameter space scanned that needs further investigation.

The test were applied to a variety of equilibria. The stability of arcades tends to be very sensitive to the value of the adiabatic index γ, and for coronal values they are largely stable. Applying the developed method to equilibria in loop geometry shows that, for large values of the loop length L, a small departure from the force-free state rapidly results in an equilibrium that is unstable to ballooning modes. Finally, the investigation of a crude model for coronal loops suggests that they are stable to gravity-driven Rayleigh-Taylor instabilities.

3

Stability of Line-Tied 2-D Coronal Arcades

3.1. Introduction

The stability of two-dimensional equilibrium arcades is considerably more difficult to study than its one-dimensional counterpart. Straightforward universal analytical tests like a Suydam criterion (Suydam, 1958) are unavailable, and one often has to resort to advanced numerical techniques. In addition there are relatively few analytical profiles.

Low (1977a) and Birn, Goldstein, and Schindler (1978) obtained a family of equilibrium magnetic fields that exhibit a catastrophe point at some critical value of a parameter, say $\lambda_{\rm crit}$, such that no neighbouring equilibria exist when $\lambda > \lambda_{\rm crit}$. The suggestion was that this lack of equilibrium is associated with the eruption of a prominence or the onset of a solar flare. This view, however, is not shared by all (see, for instance, Jockers, 1976, 1978; Klimchuk and Sturrock, 1989; Finn and Chen, 1990). The lower energy solutions were shown to be stable to 2-D disturbances (Low, 1977b; Birn and Schindler, 1981) but the question of the stability to more general displacements is still unanswered. Melville, Hood, and Priest (1983) extended the equilibrium solutions of Birn, Goldstein, and Schindler (1978) to include gravity, while later on they constructed a class of sheared equilibria, i.e., where the magnetic field also has a component in the ignorable direction, simulating photospheric footpoint displacements (Melville, Hood, and Priest, 1984)

Schindler, Birn, and Janicke (1983) and Hood (1984) derived a form of the energy integral that allows gravitational effects, for general 2-D arcades, to be included in the stability investigation. Zweibel and Hundhausen (1982) constructed a series of shearless linear magnetohydrostatic equilibria including gravity. Zweibel (1981) found that these fields are unstable, in the absence of line-tying, to localised modes that have a very short axial wavelength compared to the equilibrium length scale. Hood (1983b) and Melville, Hood, and Priest (1986) included the effect of photospheric line-tying and showed that a localised instability occurs at the appearance of the first magnetic

island. Su Qing-rui (1984) generalised the equilibria of Zweibel and Hundhausen (1982) to incorporate the effect of shear. Low (1982a) and Melville, Hood, and Priest (1987) produced models for isothermal, magnetohydrostatic atmospheres and the latter authors investigated the stability of these shearless arcades. In some cases, the field becomes unstable to localised modes before a catastrophe point is reached. A different family of shearless isothermal atmospheres was introduced and analysed by Webb and Ko (1989), but they failed to obtain necessary and sufficient conditions for stability.

Zwingmann (1987) numerically derived equilibrium magnetic arcades with a prescribed photospheric footpoint displacement and pressure gradient. For shearless arcades he found that catastrophe points occur when the pressure is varied through a parameter, λ_p. He also investigated the 2-D stability of these arcades and showed that they are stable up to the catastrophe point. On the other hand, increasing the shear, through λ_s, of a force-free arcade did not produce a catastrophe point and the field remains stable to 2-D disturbances. This indirectly backs up the conjecture of Hood and Anzer (1987) that force-free arcades without a magnetic island are stable. Other numerical studies of coronal arcade stability were performed by, for example, Mikić, Barnes, and Schnack (1988) and An, Suess, and Wu (1989).

In this Chapter we want to extend the procedure developed in the previous Chapter to 2-D coronal arcades with a translational invariance, taking into account the effect of line-tying, gravity and shear. The main advantage of this method over others is that it does not require the solution of a system of coupled partial differential Euler-Lagrange equations, as is normally the case (see, for instance, Galindo Trejo, 1987). Instead there are two sets of ordinary differential equations to be integrated along the field lines. In Section 3.2 a suitable form for the perturbed potential energy integral is presented. The derivation of both necessary conditions and sufficient conditions for stability is contained in Section 3.3. In Section 3.4 two classes of isothermal arcades are introduced and their ideal MHD stability is analysed numerically by means of the developed tests. The results are discussed in the final Section.

3.2. Energy Integral

Assume the atmosphere has a planar lower boundary with gravity acting downwards and consider 2-D equilibria with a straight magnetic axis. Introduce a Cartesian coordinate system x, y, z with the z-axis pointing upwards and y being the ignorable

coordinate. The equilibrium magnetic field $\mathbf{B}(x,z)$ then has the form

$$\begin{aligned}\mathbf{B} &= \mathbf{B}_p + B_y\mathbf{e}_y,\\ \mathbf{B}_p &= \nabla A \times \mathbf{e}_y,\end{aligned} \tag{3.2.1}$$

where $\mathbf{B}_p$ denotes the projection of $\mathbf{B}$ on the x,z-plane and is derived from a vector potential $\mathbf{A}_p = A\mathbf{e}_y$, and $\mathbf{B}_y = B_y\mathbf{e}_y$ is the longitudinal field. A static equilibrium, including the action of pressure, magnetic, and gravitational forces, is described by the magnetohydrostatic equation (1.2.8), with $\phi = gz$. The plasma is assumed to obey the ideal gas law (1.2.7) where T is an arbitrary prescribed temperature that need not be uniform at present. Substituting for the magnetic field by making use of Equation (3.2.1), the three components of the force balance equation (1.2.8) are (Low, 1975a; Schindler, Birn, and Janicke, 1983)

$$B_y = B_y(A), \tag{3.2.2a}$$

$$\frac{\partial p}{\partial \phi} + \rho = 0, \tag{3.2.2b}$$

$$\nabla^2 A + J(A,\phi) = 0, \tag{3.2.2c}$$

where

$$J(A,\phi) = \frac{\partial}{\partial A}\left(\mu p + \frac{1}{2}B_y^2(A)\right) = \mu j_y, \tag{3.2.3}$$

and A,ϕ are used as coordinates instead of x,z. Equation (3.2.2a) states that the equilibrium longitudinal field depends on x and z through A only, while Equation (3.2.2b) expresses hydrostatic equilibrium along a field line. Equation (3.2.2c) determines the flux function A once p and B_y are prescribed.

Choosing an appropriate set of variables and derivatives (see Appendix A.3) and applying the rigid plate boundary conditions (1.4.2), the change in potential energy, δW, takes the form (see Appendix D)

$$\delta W = \frac{1}{2\mu}(\mathcal{I} + \mathcal{J}), \tag{3.2.4}$$

where

$$\begin{aligned}\mathcal{I} = \int\Bigg\{ &\frac{B^2}{B_p^2}\left[\frac{\partial}{\partial s}(B_p\xi_A)\right]^2 - \left(2J\left(J + \frac{\partial B_p}{\partial a}\right) - B_p\frac{\partial\phi}{\partial a}\frac{\partial J}{\partial\phi}\right)\xi_A^2 - \mu\rho\tilde{A}\tilde{\xi}_\phi^2 + \\ &+ \frac{\gamma\mu p}{B^2+\gamma\mu p}\left[B\left(B\frac{\partial\tilde{\xi}_\parallel}{\partial s} - \frac{\tilde{\xi}_\phi}{c_s^2}\right) - 2\frac{B_p}{B}\left(\left(J + \frac{\partial B_p}{\partial a}\right)\xi_A + \frac{\partial B_p}{\partial n}\xi_n\right)\right]^2 + \\ &+ \left[B\frac{\partial\xi_n}{\partial s} - \frac{B_y}{B}\left(2\left(J + \frac{\partial B_p}{\partial a}\right)\xi_A + \frac{\partial B_p}{\partial n}\xi_n\right)\right]^2\Bigg\}\, d\mathcal{V}\end{aligned} \tag{3.2.5}$$

and

$$\begin{aligned}\mathcal{J} = \int\Bigg\{ &(B^2+\gamma\mu p)\left[B_p\frac{\partial\tilde{\xi}_A}{\partial a} + BB_p\frac{\partial\tilde{\xi}_n}{\partial n} - J\tilde{\xi}_A + \frac{\gamma\mu p}{B^2+\gamma\mu p}\left(B\frac{\partial\tilde{\xi}_\parallel}{\partial s} - \frac{\tilde{\xi}_\phi}{c_s^2}\right) + \right. \\ &\left. + \frac{2B_p}{B^2+\gamma\mu p}\left(\left(J + \frac{\partial B_p}{\partial a}\right)\xi_A + \frac{\partial B_p}{\partial n}\xi_n\right)\right]^2\Bigg\}\, d\mathcal{V}.\end{aligned} \tag{3.2.6}$$

The integration is taken over the coronal volume of the plasma, and the following notations have been used :

$$\tilde{A} = \left(\frac{\rho}{\gamma p} + \frac{1}{\rho} \frac{\partial \rho}{\partial \phi} \right) \tag{3.2.7}$$

is related to the modified Brunt-Väisälä (buoyancy) frequency N by $N^2 = -g^2 \tilde{A}$ when g is constant;

$$\tilde{\xi}_\phi = \nabla \phi \cdot \boldsymbol{\xi} \tag{3.2.8}$$

is related to ξ_z by $\tilde{\xi}_\phi = g \xi_z$ when g is constant.

This new expression for δW has been derived from and is physically equivalent to Equation (31) in Schindler, Birn, and Janicke (1983). It reduces to Equation (2.32) in Hood (1984) for isothermal equilibria, to Equation (2.10) in Melville, Hood, and Priest (1986) for shearless (i.e., $B_y = 0$) isothermal equilibria, to Equations (2.2.6)–(2.2.8) for cylindrically symmetric equilibria, and to Equations (2.3.5)–(2.3.7) for plane plasma layers. As before, note that $\mathcal{J}$ is non-negative and $\mathcal{I}$ contains no derivatives of the plasma displacement across the magnetic field. These are two main points in the procedure developed in the next Section. The energy integral δW has only two potentially negative (i.e., destabilising) terms. The first accounts for both current-driven and pressure-driven instabilities while the second can drive Rayleigh-Taylor instabilities.

3.3. Necessary Conditions and Sufficient Conditions for Stability

The complete minimisation of δW would result in necessary and sufficient conditions for stability. This requires solving a system of three coupled partial differential equations. No general analytic method is known for this kind of problem at present, so one has to resort to numerical techniques (such as finite difference, finite element, or spectral methods). These however have some serious drawbacks. It is for instance doubtful whether such numerical codes can easily pick up very localised modes (see, for instance, Cargill, Hood, and Migliuolo, 1986). This might lead to an overestimation of the stability of the equilibrium. The question of the boundary conditions on the 'edges' of the system other than the photosphere is a sensitive issue too (see, for instance, Galindo Trejo, 1987). How far out must one put these boundaries to make sure that taking the plasma displacements to vanish there does not risk the same trap as mentioned above? In what follows a procedure is worked out which does not suffer from either of these shortcomings and is easier to implement than a code for solving partial differential equations. Unfortunately a price must be paid for this convenience. Instead of a necessary and sufficient condition for stability, the method

provides a necessary condition for stability and a sufficient condition for stability which blend together only in the case of shearless (i.e., $B_y = 0$) fields.

As in Chapter 2, localised modes are selected as trial functions in δW, yielding a necessary condition for stability. A sufficient condition is obtained by neglecting $\mathcal{J}$ in the energy integral (3.2.4). Combining these two approaches yields a parameter region of instability to localised modes, a parameter region of definite stability to all modes, and a parameter region in which the actual marginal stability threshold is located. In this Chapter the procedure is developed assuming the temperature and the gravitational acceleration to be uniform such that the pressure scale height

$$H = \frac{\mathcal{R}T}{\tilde{\mu}g}$$

is a constant. Note that for such an atmosphere the third term of the integrand of $\mathcal{I}$ in Equation (3.2.5) cannot be negative, and hence is not destabilising. The method is easily extendable to non-isothermal and non-constant gravity situations (see Chapters 4 and 5).

3.3.1 Necessary Conditions for Stability

The choice of trial function is determined by the heuristic principle of minimal bending (see, for instance, Suydam, 1958). Consider perturbations that vary rapidly across the field and slowly along it, hence reducing the stabilising effect of magnetic tension. Thus, following Hood (1986a), take $\boldsymbol{\xi}$ of the form

$$\boldsymbol{\xi}(x, y, z) = \boldsymbol{\xi}(x, z) \cos mS, \tag{3.3.1}$$

where $1/m$, the perturbation length scale, is assumed to be much smaller than the equilibrium length scales. The amplitude factor $\boldsymbol{\xi}(x, z)$, describing the slow variations, must vanish at the photosphere to satisfy the boundary conditions (1.4.2), and S is chosen such that $\mathbf{B} \cdot \nabla S = 0$, while $\cos mS$ is periodic in y. If one is only interested in the least stable mode a simple solution for S is

$$S = y - \int_0^s \left(\frac{B_y}{B}\right)_{A=\text{const.}} ds, \tag{3.3.2}$$

where s is the distance along a field line, measured from the top. The lower boundary of the integral in Equation (3.3.2) is positioned such that it minimises the potential energy. Normally its location will be obvious from the symmetry of the configuration (Conner, Hastie, and Taylor, 1979). These perturbations tend to be highly localised about the flux surface where the interplay between a strong outward pressure gradient and an unfavourable field line curvature is most pronounced, hence reducing the stabilising effect of the neighbouring plasma.

Expanding the displacement in inverse powers of m,

$$\boldsymbol{\xi} = \boldsymbol{\xi}_0 + \frac{1}{m}\boldsymbol{\xi}_1 + \frac{1}{m^2}\boldsymbol{\xi}_2 + \cdots,$$

it follows that the leading order, $O(m)$, contribution to the $\mathcal{J}$-part of δW, which comes from

$$B_p \frac{\partial \tilde{\xi}_{A_0}}{\partial a} + B B_p \frac{\partial \tilde{\xi}_{n_0}}{\partial n} = \frac{\partial \xi_{A_0}}{\partial a} - \frac{B}{B_p}\frac{\partial \xi_{n_0}}{\partial y} + O(1),$$

vanishes if

$$\xi_{n_0} = \frac{B_p}{B}\frac{\partial S}{\partial a}\xi_{A_0}. \tag{3.3.3}$$

Substituting this into the expression (3.2.4) for δW and choosing $\boldsymbol{\xi}_1$ such that there is no $O(1)$ contribution from $\mathcal{J}$, one gets, to leading order, the ballooning integral

$$\begin{aligned}\delta W_{\text{ball}} = \frac{1}{2\mu}\int\Bigg\{ & \frac{B^2}{B_p^2}\left[\frac{\partial}{\partial s}(B_p\xi_A)\right]^2 - \left(2J\left(J + \frac{\partial B_p}{\partial a}\right) + B_x\frac{\partial J}{\partial z}\right)\xi_A^2 + \mu\rho N^2\xi_z^2 + \\ & + \frac{\gamma\mu p}{B^2+\gamma\mu p}\left[B\left(B\frac{\partial \tilde{\xi}_\parallel}{\partial s} - \frac{g}{c_s^2}\xi_z\right) - 2\frac{B_p}{B}\left(J + \frac{\partial B_p}{\partial a} + \frac{B_p}{B}\frac{\partial S}{\partial a}\frac{\partial B_p}{\partial n}\right)\xi_A\right]^2 + \\ & + \left[B_p\frac{\partial}{\partial s}\left(\frac{\partial S}{\partial a}\xi_A\right) - 2\frac{B_y}{B}\left(J + \frac{\partial B_p}{\partial a}\right)\xi_A\right]^2\Bigg\}\cos^2 mS\; d\mathcal{V},\end{aligned} \tag{3.3.4}$$

where the subscript $_0$ has been suppressed for simplicity. This expression for δW_{ball} is equivalent to Equation (2.2.15) in the case of cylindrically symmetric arcades.

The Euler-Lagrange equations for the integral (3.3.4), generated by minimising with respect to the variables

$$\begin{aligned} y_1 &= B_p\xi_A, \\ y_2 &= \mathrm{e}^{-z/\gamma H}\tilde{\xi}_\parallel, \end{aligned}$$

are

$$\begin{aligned} & B\frac{\partial}{\partial s}\left[\left(1 + \left(\frac{B_p}{B}\frac{\partial S}{\partial a}\right)^2\right)\frac{B}{B_p^2}\frac{\partial y_1}{\partial s}\right] = -\Lambda\frac{f^2}{B_p^2}y_1 - \\ & -\frac{2}{B^2}\left(\left(J + \frac{\partial B_p}{\partial a}\right) + \frac{B_p}{B}\frac{\partial S}{\partial a}\frac{\partial B_p}{\partial n}\right)\left[\frac{\gamma\mu pB}{B^2+\gamma\mu p}\widetilde{SB}_\parallel + \mu\frac{\partial p}{\partial A}y_1\right] - \\ & \quad -\frac{1}{B_p^2}\left(-B_x + \frac{B_yB_z}{B^2}B_p\frac{\partial S}{\partial a}\right)\left[-\mu\rho N^2\xi_z + \frac{\gamma\mu pB}{B^2+\gamma\mu p}\frac{1}{\gamma H}\widetilde{SB}_\parallel + \frac{1}{H}\mu\frac{\partial p}{\partial A}y_1\right], \end{aligned} \tag{3.3.5a}$$

$$B\frac{\partial}{\partial s}\left[\frac{\gamma\mu pB}{B^2+\gamma\mu p}\,\mathrm{e}^{z/\gamma H}\widetilde{SB}_\parallel\right] = B_z\,\mathrm{e}^{z/\gamma H}\mu\rho N^2\xi_z, \tag{3.3.5b}$$

with

$$\begin{aligned}\widetilde{SB}_\parallel = \Bigg[B\Big(\mathrm{e}^{z/\gamma H}B\frac{\partial y_2}{\partial s} - \frac{1}{\gamma H}\frac{1}{B_p^2}\Big(-B_x + \frac{B_yB_z}{B^2}B_p\frac{\partial S}{\partial a}\Big)y_1\Big) - \\ - \frac{2}{B}\left(\left(J + \frac{\partial B_p}{\partial a}\right) + \frac{B_p}{B}\frac{\partial S}{\partial a}\frac{\partial B_p}{\partial n}\right)y_1\Bigg].\end{aligned}$$

The normalising condition, to exclude the trivial solution $\boldsymbol{\xi} \equiv \mathbf{0}$, is taken as

$$\int f^2 \xi_A^2 \, d\mathcal{V} = \text{constant}, \tag{3.3.6}$$

where f^2 is a strictly positive function. It introduces a Lagrange multiplier Λ which has the same sign as δW. In deriving Equations (3.3.5) the relation

$$B\frac{\partial}{\partial s}\left(\frac{1}{B_p}\frac{\partial S}{\partial a}\right) = -\frac{dB_y}{dA} + \frac{B_y}{B_p^2}\left(J + 2\frac{\partial B_p}{\partial a}\right) \tag{3.3.7}$$

was used (this equation is derived in Appendix G in the context of Chapter 5). At marginal stability, Equations (3.3.5) are equivalent to Equations (3.19)–(3.22) of Hood, Van der Linden, and Goossens (1989) in the case of ideal isothermal equilibria. They govern the stability of the configuration localised about any particular field line. If there is one field line (i.e., one value of A) for which δW can be made negative (i.e., $\Lambda < 0$), then the equilibrium is unstable.

The Euler-Lagrange equations (3.3.5) can be rewritten as a system of four coupled first order homogeneous ordinary differential equations plus an auxiliary equation, suitable for numerical computation :

$$\frac{\partial y_1}{\partial s} = \left(\frac{B}{B_p^2} + \frac{B_p^2}{B}y_5^2\right)^{-1} y_3, \tag{3.3.8a}$$

$$\frac{\partial y_2}{\partial s} = \mathrm{e}^{-z/\gamma H}\frac{1}{B}\left[\frac{B^2 + \gamma\mu p}{\gamma\mu p B^2}\tilde{y}_4 + \left(\frac{G}{\gamma H} - 2K_s\right)y_1\right], \tag{3.3.8b}$$

$$\frac{\partial y_3}{\partial s} = \frac{1}{B}\left[\left(2K_s - \frac{G}{H}\right)\mu\frac{\partial p}{\partial A}y_1 - \left(\frac{G}{\gamma H} - 2K_s\right)\tilde{y}_4 + G\tilde{\xi}_z - \Lambda\frac{f^2}{B_p^2}y_1\right], \tag{3.3.8c}$$

$$\frac{\partial y_4}{\partial s} = \frac{B_z}{B}\,\mathrm{e}^{z/\gamma H}\tilde{\xi}_z, \tag{3.3.8d}$$

$$\frac{\partial y_5}{\partial s} = \frac{1}{B}\left[-\frac{dB_y}{dA} + \frac{B_y}{B_p^2}\left(J + 2\frac{\partial B_p}{\partial a}\right)\right], \tag{3.3.8e}$$

where

$$y_5 = \frac{1}{B_p}\frac{\partial S}{\partial a},$$

$$G = -\frac{B_x}{B_p^2} + \frac{B_y B_z}{B^2}y_5,$$

$$K_s = -\frac{1}{B^2}\left(\left(J + \frac{\partial B_p}{\partial a}\right) + \frac{B_y}{2B}\frac{\partial B_p^2}{\partial s}y_5\right),$$

$$\tilde{y}_4 = \mathrm{e}^{-z/\gamma H}y_4,$$

$$\tilde{\xi}_z = \mu\rho N^2\xi_z = \mu\rho N^2\left(Gy_1 + B_z\,\mathrm{e}^{z/\gamma H}y_2\right).$$

Equation (3.3.8a) is the defining equation for y_3, while Equation (3.3.8b) defines y_4. Equation (3.3.8c) represents the Euler-Lagrange equation (3.3.5a) for y_1, while Equation (3.3.8d) is the analogous equation for y_2. Finally, the auxiliary equation

(3.3.8e) needed to compute $\partial S/\partial a$, comes from the relation (3.3.7). When the field is shearless, this equation is trivially satisfied by $y_5 = 0$.

3.3.2. Sufficient Conditions for Stability

A partial minimisation of δW can be performed by neglecting its non-negative $\mathcal{J}$-part. This time the variables used are

$$\begin{aligned} y_1 &= B_p \xi_A, \\ y_2 &= \mathrm{e}^{-z/\gamma H} \tilde{\xi}_\parallel, \\ y_5 &= \frac{B}{B_p} \xi_n. \end{aligned}$$

The $\mathcal{I}$-part of δW, (3.2.5), may then be expressed as

$$\begin{aligned} \delta W_{\mathcal{I}} = \frac{1}{2\mu} \int \Bigg\{ \frac{B^2}{B_p^2} \left[\frac{\partial y_1}{\partial s} \right]^2 - \left(2J \left(J + \frac{\partial B_p}{\partial a} \right) + B_x \frac{\partial J}{\partial z} \right) \frac{y_1^2}{B_p^2} + \mu \rho N^2 \xi_z^2 + \\ + \frac{\gamma \mu p}{B^2 + \gamma \mu p} \widetilde{SB}_\parallel{}^2 + \widetilde{SB}_n{}^2 \Bigg\} \, d\mathcal{V}, \end{aligned} \tag{3.3.9}$$

with

$$\begin{aligned} \xi_z &= -\frac{B_x}{B_p^2} y_1 + B_z \, \mathrm{e}^{z/\gamma H} y_2 + \frac{B_y B_z}{B^2} y_5, \\ \widetilde{SB}_\parallel &= B \Big(\mathrm{e}^{z/\gamma H} B \frac{\partial y_2}{\partial s} - \frac{1}{\gamma H} \Big(-\frac{B_x}{B_p^2} y_1 + \frac{B_y B_z}{B^2} y_5 \Big) \Big) - \\ &\quad - \frac{2}{B} \Big(\Big(J + \frac{\partial B_p}{\partial a} \Big) y_1 + \frac{B_y B_p}{B} \frac{\partial B_p}{\partial s} y_5 \Big), \\ \widetilde{SB}_n &= B_p \frac{\partial y_5}{\partial s} - 2 \frac{B_y}{B B_p} \Big(J + \frac{\partial B_p}{\partial a} \Big) y_1. \end{aligned}$$

Imposing the same normalising condition (3.3.6), the corresponding Euler-Lagrange equations become

$$\begin{aligned} B \frac{\partial}{\partial s} \left(\frac{B}{B_p^2} \frac{\partial y_1}{\partial s} \right) = \frac{\gamma \mu p}{B^2 + \gamma \mu p} \Big(\frac{1}{\gamma H} \frac{B B_x}{B_p^2} - \frac{2}{B} \Big(J + \frac{\partial B_p}{\partial a} \Big) \Big) \widetilde{SB}_\parallel - \\ - \frac{1}{B_p^2} \Big[2J \Big(J + \frac{\partial B_p}{\partial a} \Big) y_1 + B_x \Big(\mu \rho N^2 \xi_z + \frac{\partial J}{\partial z} y_1 \Big) + \\ + 2 \frac{B_y B_p}{B} \Big(J + \frac{\partial B_p}{\partial a} \Big) \widetilde{SB}_n \Big] - \Lambda \frac{f^2}{B_p^2} y_1, \end{aligned} \tag{3.3.10a}$$

$$B \frac{\partial}{\partial s} \left(\frac{\gamma \mu p B \, \mathrm{e}^{z/\gamma H}}{B^2 + \gamma \mu p} \widetilde{SB}_\parallel \right) = B_z \, \mathrm{e}^{z/\gamma H} \mu \rho N^2 \xi_z, \tag{3.3.10b}$$

$$\begin{aligned} B \frac{\partial}{\partial s} \left(\frac{B_p}{B} \widetilde{SB}_n \right) = -\frac{\gamma \mu p}{B^2 + \gamma \mu p} \left(\frac{1}{\gamma H} \frac{B_y B_z}{B} + 2 \frac{B_y B_p}{B^2} \frac{\partial B_p}{\partial s} \right) \widetilde{SB}_\parallel + \\ + \frac{B_y B_z}{B^2} \mu \rho N^2 \xi_z. \end{aligned} \tag{3.3.10c}$$

These equations prove definite stability of an equilibrium to all allowable (global and localised) perturbations when $\Lambda > 0$ for all field lines.

Written as a system of six coupled first order homogeneous ordinary differential equations suitable for numerical computation, the system (3.3.10) transforms to

$$\frac{\partial y_1}{\partial s} = \frac{B_p^2}{B} y_3, \tag{3.3.11a}$$

$$\frac{\partial y_2}{\partial s} = \mathrm{e}^{-z/\gamma H}\Big\{\frac{1}{B^3}\Big[\frac{B^2+\gamma\mu p}{\gamma\mu p}\,\mathrm{e}^{-z/\gamma H} y_4 + 2\Big(J + \frac{\partial B_p}{\partial a}\Big) y_1 + \\ + B_y\Big(\frac{1}{B}\frac{\partial B_p^2}{\partial s} + \frac{B_z}{\gamma H}\Big) y_5\Big] - \frac{1}{\gamma H}\frac{B_x}{B B_p^2} y_1\Big\}, \tag{3.3.11b}$$

$$\frac{\partial y_3}{\partial s} = -\frac{1}{B B_p^2}\Big[2J\Big(J + \frac{\partial B_p}{\partial a}\Big) y_1 + B_x\Big(\mu\rho N^2\xi_z + \frac{\partial J}{\partial z} y_1\Big) + 2B_y\Big(J + \frac{\partial B_p}{\partial a}\Big) y_6\Big] + \\ + \frac{1}{B^2}\,\mathrm{e}^{-z/\gamma H}\Big(\frac{1}{\gamma H}\frac{B B_x}{B_p^2} - \frac{2}{B}\Big(J + \frac{\partial B_p}{\partial a}\Big)\Big) y_4 - \Lambda\frac{f^2}{B B_p^2} y_1, \tag{3.3.11c}$$

$$\frac{\partial y_4}{\partial s} = \frac{B_z}{B}\,\mathrm{e}^{z/\gamma H}\mu\rho N^2\xi_z, \tag{3.3.11d}$$

$$\frac{\partial y_5}{\partial s} = \frac{1}{B_p^2}\Big[B y_6 + 2\frac{B_y}{B}\Big(J + \frac{\partial B_p}{\partial a}\Big) y_1\Big], \tag{3.3.11e}$$

$$\frac{\partial y_6}{\partial s} = \frac{1}{B^3}\Big[B_y B_z \mu\rho N^2\xi_z - B_y\,\mathrm{e}^{-z/\gamma H}\Big(\frac{1}{B}\frac{\partial B_p^2}{\partial s} + \frac{B_z}{\gamma H}\Big) y_4\Big]. \tag{3.3.11f}$$

Equations (3.3.11a), (3.3.11b) and (3.3.11e) are the defining equations for y_3, y_4, and y_6 respectively, while Equations (3.3.11c), (3.3.11d), and (3.3.11f) correspond to Equations (3.3.10a), (3.3.10b), and (3.3.10c), respectively. When the field is shearless (i.e., $B_y = 0$) it follows from the last two equations and the boundary conditions (1.4.2) that $y_5 = y_6 = 0$ and hence $\xi_n = 0$. The remaining four equations are then identical to the Equations (3.3.8a)–(3.3.8d) with $y_5 = 0$. This shows that when $B_y = 0$ the necessary conditions for stability blend into sufficient conditions and hence that the localised modes are the most unstable modes in shearless fields (see, for instance, Hood, 1986a). Equations (3.3.11) are also equivalent to the system (3.1) of Melville, Hood, and Priest (1986) when the magnetic field has no longitudinal component.

3.4. Application to Two Classes of Isothermal Arcades

3.4.1. Description of the Equilibria

The first class of equilibria that will be investigated is that of the linear force-free 2-D arcades, for which the magnetohydrostatic equation (1.2.8) reduces to

$$\nabla \times \mathbf{B} = \lambda \mathbf{B}, \qquad \lambda \text{ constant}.$$

This is equivalent to

$$\begin{aligned} \frac{dB_y}{dA} &= \lambda, \\ -\nabla^2 A &= B_y \frac{dB_y}{dA}\,. \end{aligned} \tag{3.4.1}$$

Requiring the total magnetic energy to be finite and the normal component of the magnetic field at the photosphere to be of the form

$$B_z(x,0) = -B_0 \sin\frac{\pi x}{L} \qquad \text{for} \qquad -\frac{L}{2} \le x \le \frac{L}{2}\,, \tag{3.4.2}$$

where L is the width of the arcade, the solution to (3.4.1) is

$$\begin{aligned} A &= A_0 \cos kx\ \mathrm{e}^{-\sqrt{k^2-\lambda^2}z}, \\ B_y(A) &= \lambda A, \end{aligned}$$

with $k = \pi/L$ and $A_0 = B_0/k$. After nondimensionalising by defining $\bar{A} = A/A_0$, $\bar{x} = kx$, $\bar{z} = kz$, $\bar{\lambda} = \lambda/k$, $\bar{B}_y = B_y/B_0$ and dropping the bars for simplicity, this becomes

$$\begin{aligned} A &= \cos x\ \mathrm{e}^{-\sqrt{1-\lambda^2}z}, \\ B_y(A) &= \lambda A, \end{aligned} \tag{3.4.3}$$

where $-\pi/2 \le x \le \pi/2$ to isolate one arcade. The value of λ is restricted to the interval $[0,1]$ for physically meaningful equilibria. A projection of the magnetic field lines on the x,z-plane corresponding to the solution (3.4.3) is plotted in Figure 3.1. Note that for force-free fields the expressions for $\mathcal{I}$ and $\mathcal{J}$ in (3.2.4) transform to

$$\begin{aligned} \mathcal{I} = \int\Bigg\{ &\frac{B^2}{B_p^2}\left[\frac{\partial}{\partial s}(B_p\xi_A)\right]^2 - 2J\Big(J + \frac{\partial B_p}{\partial a}\Big)\xi_A^2 + \\ &+ \left[B\frac{\partial \xi_n}{\partial s} - \frac{B_y}{B}\Big(2\Big(J + \frac{\partial B_p}{\partial a}\Big)\xi_A + \frac{\partial B_p}{\partial n}\xi_n\Big)\right]^2\Bigg\}\, d\mathcal{V} \end{aligned} \tag{3.4.4}$$

and

$$\begin{aligned} \mathcal{J} = \int\Bigg\{ B^2\Bigg[&B_p\frac{\partial \tilde{\xi}_A}{\partial a} + BB_p\frac{\partial \tilde{\xi}_n}{\partial n} - J\tilde{\xi}_A + \\ &+ 2\frac{B_p}{B^2}\Big(\Big(J + \frac{\partial B_p}{\partial a}\Big)\xi_A + \frac{\partial B_p}{\partial n}\xi_n\Big)\Bigg]^2\Bigg\}\, d\mathcal{V}, \end{aligned} \tag{3.4.5}$$

respectively. It follows trivially that the potential field, for which $J = 0$, is linearly stable. The system of coupled Euler-Lagrange equations (3.3.11) reduces to

$$\frac{\partial y_1}{\partial s} = \frac{B_p^2}{B} y_3, \tag{3.4.6a}$$

$$\frac{\partial y_3}{\partial s} = -\frac{2}{BB_p^2}\Big(J + \frac{\partial B_p}{\partial a}\Big)(Jy_1 + B_y y_6) - \Lambda\frac{f^2}{BB_p^2}y_1, \tag{3.4.6b}$$

$$\frac{\partial y_5}{\partial s} = \frac{1}{B_p^2}\Big(By_6 + 2\frac{B_y}{B}\Big(J + \frac{\partial B_p}{\partial a}\Big)y_1\Big), \tag{3.4.6c}$$

$$\frac{\partial y_6}{\partial s} = 0. \tag{3.4.6d}$$

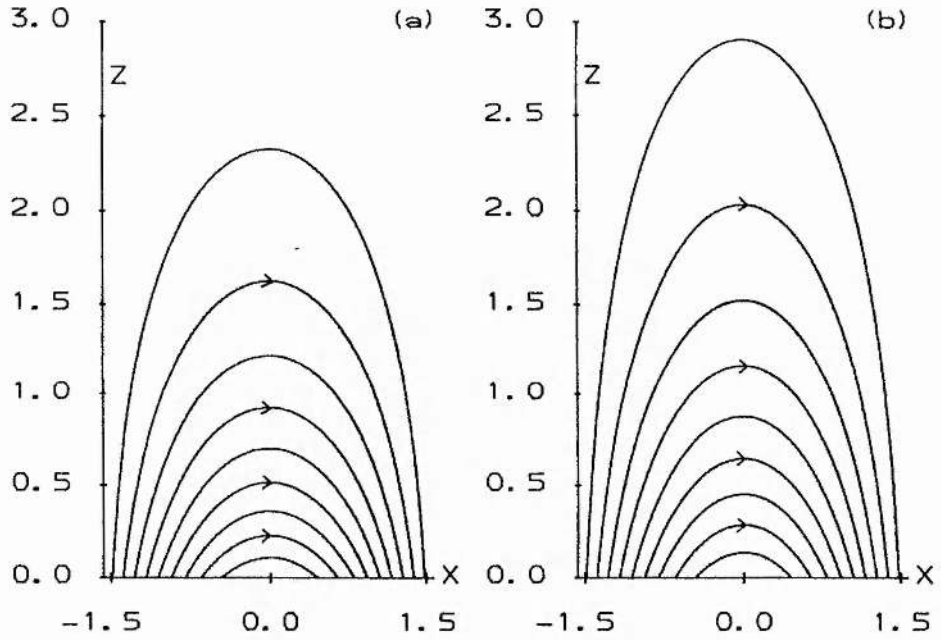

Fig. 3.1. Field lines projected on the x, z-plane corresponding to the equilibrium (3.4.3) for (a) $\lambda = 0$, the potential case, and (b) $\lambda = 0.6$, a sheared field. Arrows indicate the field direction.

The second class of equilibria is an extension of the equilibria presented by Zweibel and Hundhausen (1982) to sheared fields. The full stability study of the shearless fields was performed by Melville, Hood, and Priest (1986). The sheared version of the equilibrium presented here has been introduced in the context of flare build-up and flare trigger by Su Qing-rui (1984), who studied its equilibrium properties. Writing the plasma pressure as

$$p(x,z) = P(A)\ \mathrm{e}^{-z/H},$$

where H is the pressure scale height (see, for instance, Zweibel and Hundhausen, 1982), Equation (3.2.2c) transforms to

$$\nabla^2 A = -\frac{\partial}{\partial A}\left(\mu P(A)\ \mathrm{e}^{-z/H} + \frac{1}{2}B_y^2(A)\right). \tag{3.4.7}$$

Taking $P(A) = P_0 + \alpha^2 A^2$ and $B_y(A) = \lambda A$, where P_0 represents the background pressure and λ is a measure for the footpoint displacement, and requiring the boundary condition (3.4.2) to be satisfied, results in a finite energy solution to (3.4.7) of the form

$$A(x,z) = A_0 \cos kx\ J_{2\sqrt{k^2-\lambda^2}H}(2\sqrt{2\mu\alpha^2H^2}\mathrm{e}^{-z/2H}),$$

with

$$k = \frac{\pi}{L},$$

$$A_0 = \frac{B_0}{k}\left[J_{2\sqrt{k^2-\lambda^2}H}\left(2\sqrt{2\mu\alpha^2H^2}\right)\right]^{-1}.$$

J_n is the Bessel function of order n (see Abramowitz and Stegun, 1970, p. 355). After nondimensionalising by defining $\bar{A} = Ak/B_0$, $\bar{x} = x/H$, $\bar{z} = z/H$, $\bar{k} = kH$, $\bar{\lambda} = \lambda H$, $\beta = 2\mu\alpha^2H^2$, $\bar{B}_y = \bar{k}B_y/B_0$, and choosing $P_0 = qB_0^2/2\mu$, the expression for the flux function A, the longitudinal field component B_y and the plasma pressure p become

$$A = \cos\, kx \frac{J_{2\sqrt{k^2-\lambda^2}}(2\beta^{1/2}\mathrm{e}^{-z/2})}{J_{2\sqrt{k^2-\lambda^2}}(2\beta^{1/2})}, \tag{3.4.8a}$$

$$B_y = \lambda A, \tag{3.4.8b}$$

$$2\mu p = (qk^2 + \beta A^2)\ \mathrm{e}^{-z}, \tag{3.4.8c}$$

respectively, where, as before, the bars have been suppressed for simplicity. β is a measure for the importance of the plasma pressure in relation to the magnetic pressure. Magnetic field lines corresponding to the solution (3.4.8a) are plotted in Figure 3.2 as projected on the x, z-plane. When $2\beta^{1/2}$ is less than the first maximum of the Bessel function, $j'_{n,1}$ say, all field lines connect to the photosphere. When $2\beta^{1/2}$ is greater than $j'_{n,1}$ but smaller than the first zero of the Bessel function, $j_{n,1}$ say, an island with helical field lines (for which $A > 1$) forms, whose magnetic axis rises with increasing β. When $2\beta^{1/2}$ equals $j_{n,1}$, all field lines disconnect from the photosphere. The value of λ is restricted to the interval $[0, k]$ for physically meaningful equilibria. As $\lambda \to k$, the magnetic axis rises to infinity resulting in open field lines when $\lambda = k$. The advantage of this non-dimensionalisation over the one in Melville, Hood, and Priest (1986) is that

$$A = \cos\, kx \qquad \text{at the photosphere,}$$

independent of the value of β or λ. This implies that a field line with label A^*, say, $(A^* \leq 1)$ is always anchored to the photosphere at points $(\pm x^*, \pm y, 0)$, say, with the x-coordinate remaining fixed as β and λ evolve. This is clearly illustrated in Figure 3.3. In Figure 3.3.a the field line with label $A = 0.4$ is plotted for different values of β, while in Figure 3.3.b that same field line is plotted for different values of λ. It can be seen that the field is inflated by increasing either of these parameters.

The change in the distribution of the footpoints for varying β and λ is shown in Figure 3.4. The footpoint loci for different values of β (for fixed non-zero λ) are displayed in Figure 3.4.a, while Figure 3.4.b shows how the footpoints are displaced by varying λ. Increasing λ increases the footpoint displacement in most of the arcade. The shear is antisymmetric about the longitudinal axis of the structure. Note the

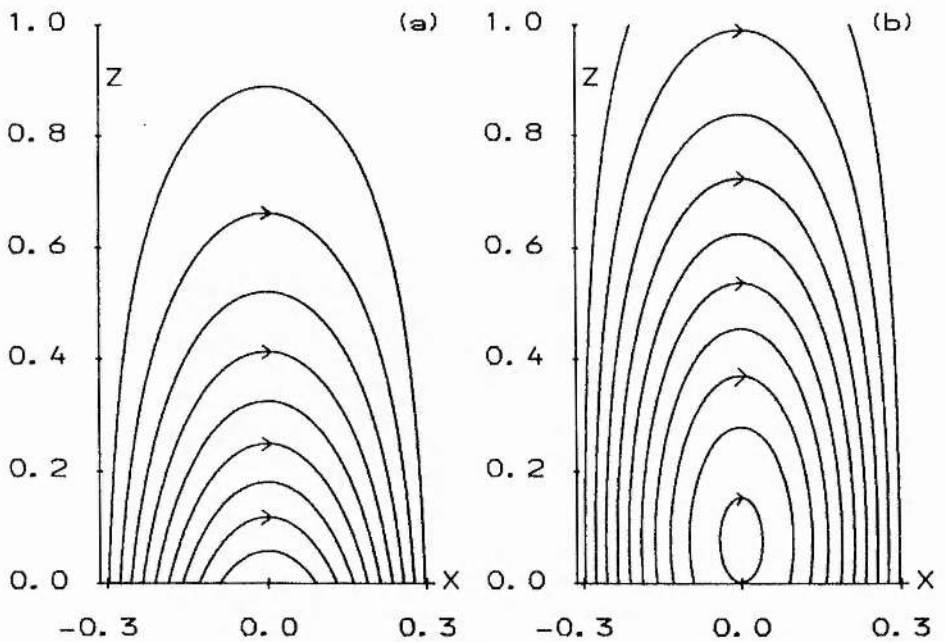

Fig. 3.2. Field lines projected on the x, z-plane corresponding to the equilibrium (3.4.8) when $k = 5, \lambda = 3$ for (a) $2\beta^{1/2} = 8$, where all field lines are connected to the photosphere, and (b) $2\beta^{1/2} = 10$, where a loop of helical field lines is embedded in the arcade. Arrows indicate the field direction.

discontinuity in the change of the footpoint distribution as $j'_{n,1}$ is passed, resulting from the emergence of the island.

3.4.2. Numerical Method

To integrate the systems (3.3.8), (3.3.11) or (3.4.6) we proceed as follows. Since the integration is along a field line, on which A is fixed, it is possible to replace the independent variable s by θ, for

$$B\frac{\partial}{\partial s} = \frac{B_\theta}{r}\frac{d}{d\theta},$$

where θ is the angular variable in a cylindrical coordinate system r, θ, y with y-axis on the photosphere. The integration along a field line is always performed from footpoint to footpoint, as opposed to Melville, Hood, and Priest (1986), who integrate from top to footpoint. The advantage of the former approach is that one does not need to integrate the system twice (once for even modes and once for odd modes). It is also applicable to equilibria that are asymmetric with respect to the y, z-plane. The rigid plate boundary conditions (1.4.2) require that at $\theta = \pm\pi/2$, $y_1 = y_2 = 0$ for system (3.3.8), $y_1 = y_2 = y_5 = 0$ for system (3.3.11), and $y_1 = y_5 = 0$ for system (3.4.6). The sign of δW is then determined by the sign of the Lagrange multiplier Λ.

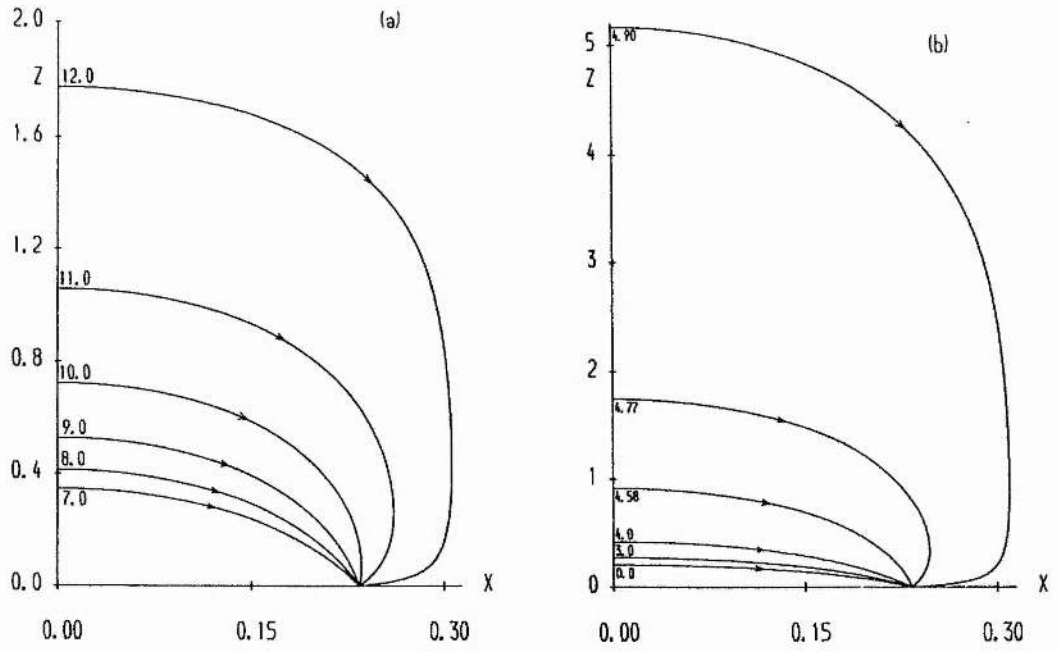

Fig. 3.3. Field line $A = 0.4$ projected on the x, z-plane corresponding to the equilibrium (3.4.8) when $k = 5$ for six values of (a) $2\beta^{1/2}$ ($\lambda = 3$), and (b) λ ($2\beta^{1/2} = 5$), demonstrating that increasing either parameter inflates the field. The projected field lines are symmetric about the y, z-plane. Arrows indicate the field direction.

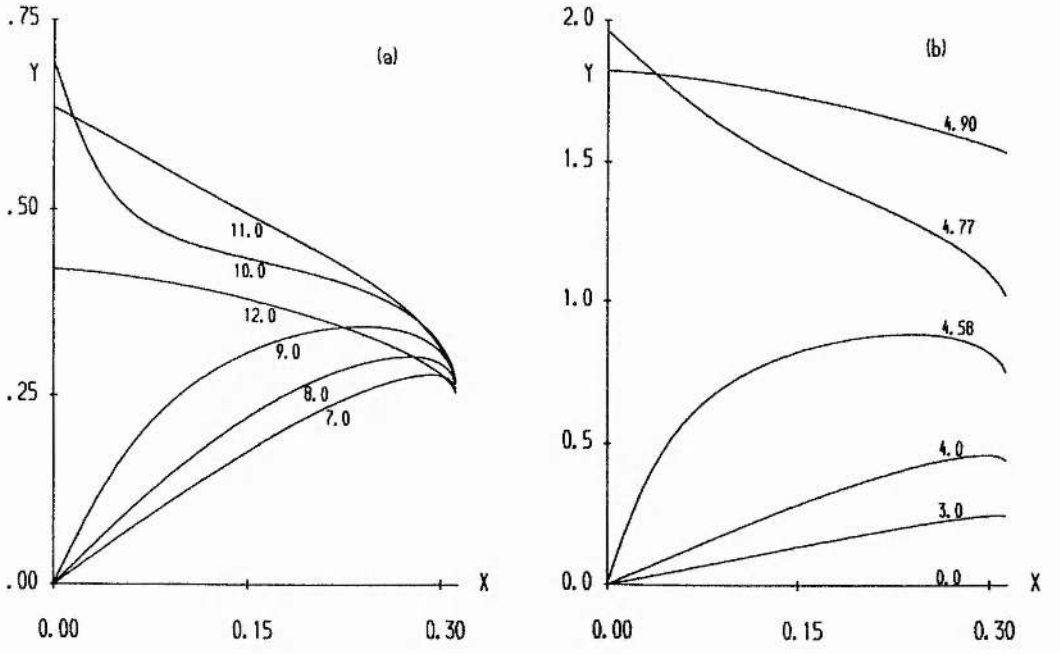

Fig. 3.4. Locus of the footpoints of equilibrium (3.4.8) for the same parameter values as in Figure 3.3. Since the shear is an odd function of x, it is clearly discontinuous at the y-axis when an island is embedded in the arcade. Figure 3.4.b shows that increasing λ increases the footpoint displacement over most of the width of the arcade.

The most efficient way of integrating system (3.3.8) for the second class of equilibria is as follows. Put $\Lambda = 0$, assume a value for k, γ, λ, q and select a value for A. To find the value of y_5 at the photosphere, Equation (3.3.8e) is first integrated from $\theta = 0$ (where $y_5 = 0$) to $\theta = -\pi/2$. To be able to satisfy the boundary condition at $\theta = \pi/2$ the system (3.3.8a)–(3.3.8d) is then integrated twice from $\theta = -\pi/2$ to $\theta = \pi/2$ for two different sets of left boundary values, both having $y_1 = y_2 = 0$, simultaneously with Equation (3.3.8e). This results in two linearly independent solutions $\boldsymbol{\xi}^I$ and $\boldsymbol{\xi}^{II}$. Putting $\Lambda = 0$ (which corresponds to marginal stability to ballooning modes) and demanding that a linear combination of $\boldsymbol{\xi}^I$ and $\boldsymbol{\xi}^{II}$ vanishes at $\theta = \pi/2$ determines a smallest value for β, say β_1^*. In this way an *instability curve* is computed which relates the β-values associated with the onset of ballooning instabilities to the A-values selected.

The integration of system (3.3.11) for that same class of equilibria progresses very similarly. There is no variable for which the starting value has to be determined before the actual integration can start. This time, however, the system is integrated three times simultaneously, for three different sets of left boundary values all having $y_1 = y_2 = y_5 = 0$, resulting in three linearly independent solutions $\boldsymbol{\xi}^I$, $\boldsymbol{\xi}^{II}$ and $\boldsymbol{\xi}^{III}$. The smallest value of β, say β_2^*, for which a linear combination of these vanishes at $\theta = \pi/2$ delimits the region of definite stability. In this way a *stability curve* can be plotted in the β, A-plane.

The same lines are followed for the integration of the force-free system (3.4.6). Once a value for λ and A are selected, it is integrated twice simultaneously, for two different sets of left boundary values satisfying $y_1 = y_5 = 0$. The normalising constraint is chosen to be

$$f^2 = B^2 B_p^2, \tag{3.4.9}$$

and the boundary condition at $\theta = \pi/2$ determines a smallest value for Λ, say Λ^*, and thus the sign of δW.

In all three cases a Bulirsch-Stoer shooting method is used to integrate the equations. This embodies Richardson polynomial function extrapolation (see, for instance, Press *et al.*, 1987, p. 563). The technique ensures high accuracy and is usually faster than a Runge-Kutta scheme. The iteration process to determine the critical value for β or Λ makes use of a Van Wijngaarden-Dekker-Brent root-finding method (see, for instance, Press *et al.*, 1987, p. 251), which converges much faster than linear interpolation. When β_1^*, β_2^*, or Λ^* is found, the system is reintegrated once more to calculate the eigenfunctions. Here a fourth order Runge-Kutta scheme offers the advantage that the number of meshpoints can be chosen a priori, allowing

high definition of the eigenfunction plots, whereas a Bulirsch-Stoer technique does not offer this freedom.

The numerical integration schemes were checked by applying them to the 1-D equilibria of Chapter 2, and the shearless Zweibel and Hundhausen (1982) arcades. In the former case the results agreed well with those found using the semi-analytical tests. In the latter case the instability thresholds of Melville, Hood, and Priest (1986) were recovered. A final note : the direction in which the relevant parameters are scanned is very important. To avoid finding 'higher harmonics' of the eigenfunctions, one must start at the stable side when scanning equilibrium parameters like β or λ, while for calculating the sign of δW or growth rates the starting point must lie in the unstable region. The reason for this is the Sturmian character of the unstable spectrum of the force operator $\mathbf{F}$ in the linearised momentum equation (1.3.12). See also Tayler (1957) and Goedbloed (1971a).

3.4.3. Stability Curves

The system (3.4.6) was integrated for the linear force-free arcade (3.4.3). It turns out that with the normalisation (3.4.9) the outer field lines (i.e., A very small) have the smallest corresponding Λ^*. These values of Λ^* are plotted against λ, a measure for the footpoint displacement, in Figure 3.5. It can be seen that for all values of λ between 0 and 1, Λ^* is positive. When $\lambda = 0$, $\Lambda^* = \pi^2/4$ and as $\lambda \rightarrow 1$, $\Lambda^* \rightarrow 0$. This implies that this finite energy line-tied 2-D linear force-free arcade is linearly stable to ideal disturbances. An analysis of the eigenfunctions shows that the least stable modes have an ξ_A that is even about $s = 0$ (the mid point).

An investigation of equilibrium (3.4.8) is much more complex. First the influence of a background pressure was assessed. A result is shown in Figure 3.6 for $k = 5, \lambda = 4$ and $\gamma = 1$. The full lines are the *instability curves* (from solving system (3.3.8)) to the right of which the equilibrium is unstable to ballooning modes. The broken lines are the *stability curves* (from solving system (3.3.11)) to the left of which the equilibrium is definitely stable. It can be seen that when there is no background pressure ($q = 0$) the outermost field lines ($A \rightarrow 0$) tend to be unstable to ballooning modes, however small β is. Hence no bounds on the (in-)stability exist in the absence of background pressure. As soon as $q \neq 0$ is allowed, definite bounds β_1 (the minimum of all β_1^* for A in the range $[0, 1]$) on stability and β_2 (the minimum of all β_2^* for A within $[0, 1]$) on instability can be found. Therefore q was fixed to 0.1 in the following investigation. A different q value will not invalidate the procedure used but merely change the bounds found, as will be indicated below. It is worth noting that when $k < 1$ no background

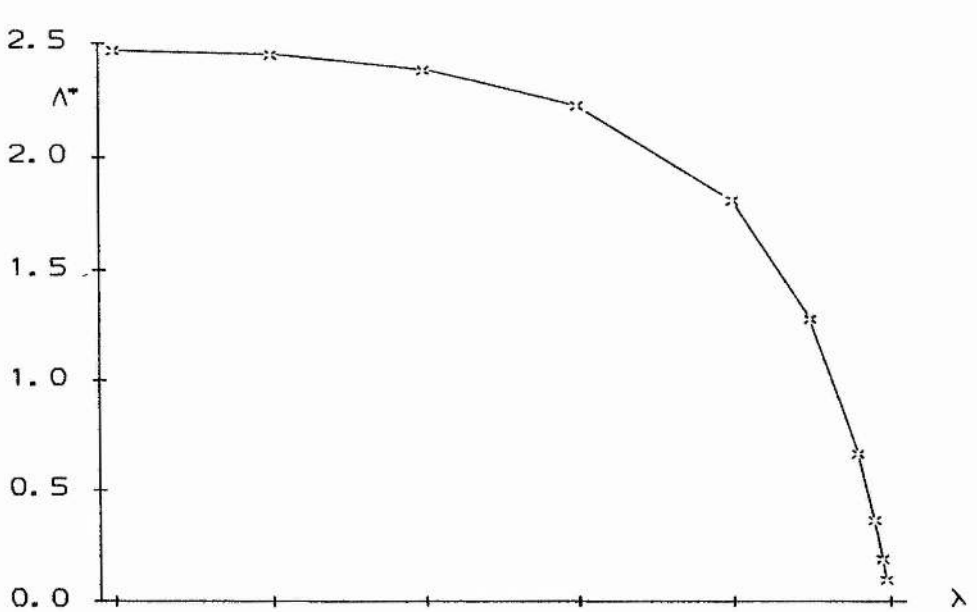

Fig. 3.5. Λ^*, a measure for δW, as a function of the shear parameter λ, showing that the linear force-free 2-D arcade (3.4.3) is linearly stable ($\Lambda^* > 0$) to ideal plasma displacements.

pressure seems needed to stabilise the outermost field lines, as was illustrated by Melville, Hood, and Priest (1986) for the case $k = 1/4, \lambda = 0$ and confirmed in our investigation.

Then the systems (3.3.8) and (3.3.11) were integrated for values of λ scanning the interval $[0, k]$ and for γ both 1 and 5/3. Figure 3.7 shows the change in the position of the *stability curve* as the footpoint displacement increases ($\gamma = 1$). All *stability curves* originate in their 'island point', i.e., the point $A = 1.0, 2\beta^{1/2} = j'_{n,1}$. There the magnetic axis coincides with the y-axis and helically shaped field lines are just about to form. This behaviour shows up for both $\gamma = 1$ and $\gamma = 5/3$, for all values of k. The *instability curves* however do not originate in the 'island point', except of course in the shearless case. This implies that this procedure does not allow one to prove that the equilibrium is definitely unstable as soon as field lines disconnect from the photosphere, as has been suggested by Melville, Hood, and Priest (1986). Marginally line-tied field lines $A = 1$ were investigated by letting the axis of the r, θ, z numerical coordinate system coincide with the magnetic axis of the arcade. Disconnected field lines ($A > 1$) were not studied, mainly because the boundary conditions (1.4.2) do not apply to them. It is obvious that their stability will crucially depend on the length of the loop structure (see, for instance, Hood and Priest, 1979, 1981).

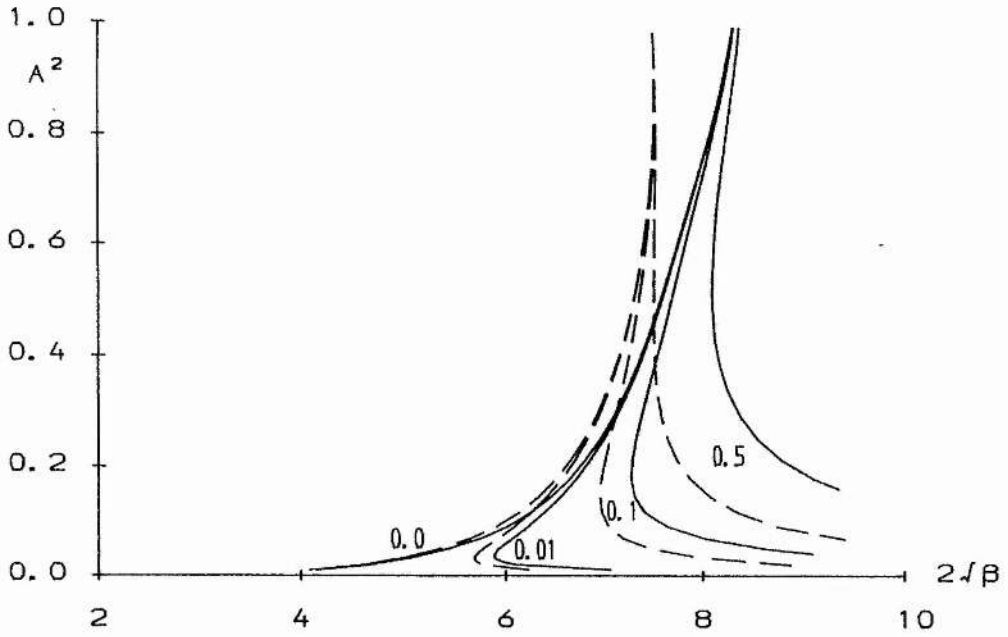

Fig. 3.6. Instability curves (full lines) and stability curves (broken lines) for four values of the background pressure parameter q for equilibrium (3.4.8) when $k = 5, \lambda = 4$, and $\gamma = 1$. When $q = 0$, i.e., without a background plasma pressure, no critical β (see text) can be found, since both curves tend towards the origin.

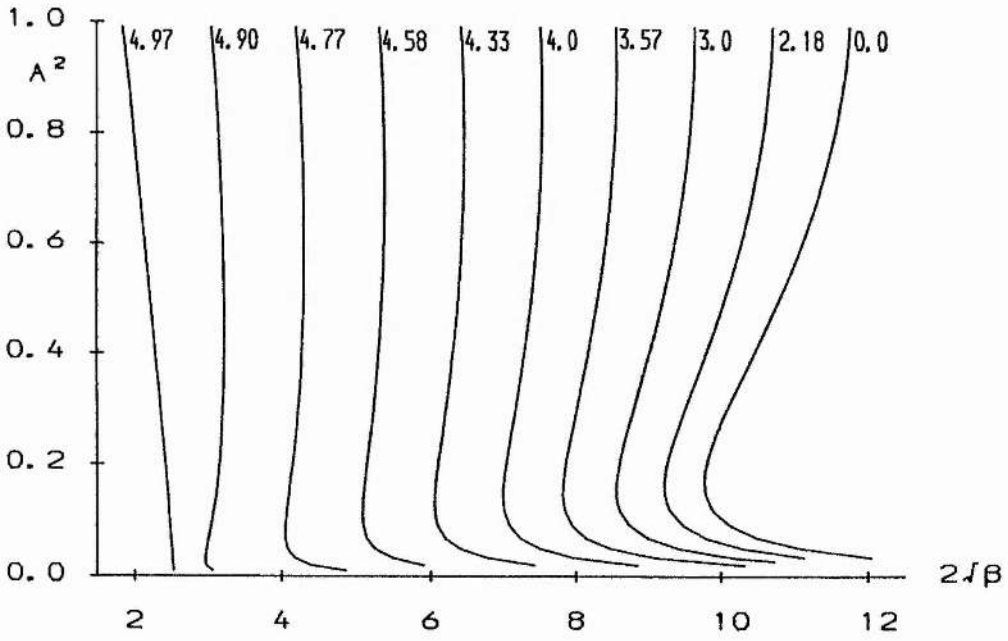

Fig. 3.7. Evolution of the stability curve for equilibrium (3.4.8) as the shear parameter λ is increased ($k = 5, q = 0.1, \gamma = 1$).

The results of the investigation for $k = 5$ are combined to produce Figure 3.8.a for $\gamma = 1$ and Figure 3.8.b for $\gamma = 5/3$. The line of dots is the locus in parameter space $(\lambda, 2\beta^{1/2})$ where the magnetic axis rises above the photosphere, $J_n(2\beta^{1/2}) = j'_{n,1}$, while the line of encircled dots indicates where all field lines disconnect from the photosphere, $J_n(2\beta^{1/2}) = j_{n,1}$. Below the line of triangles pointing upwards the equilibrium is definitely stable. Above the line of triangles pointing downwards the equilibrium is unstable to localised modes. When $\gamma = 1$ the field can be unstable before an island appears, while when $\gamma = 5/3$ it cannot. As can be expected the gap between the two triangle lines broadens as the shear is increased. Eventually it becomes impossible to predict instability before all field lines are disconnected from the photosphere.

Figure 3.9 shows the components of the plasma displacement on the field line $A = 0.9$ for $k = 5, \lambda = 3, q = 0.1$ and $\gamma = 5/3$. In Figure 3.9.a the eigenfunction of the system (3.3.8) is plotted, i.e., the ballooning perturbation that minimises the potential energy. The eigenfunction of the system (3.3.11) is depicted in Figure 3.9.b. The shapes of the components ξ_A and $\xi_\parallel$ of both displacements are fairly similar, but there is a big discrepancy between both ξ_n components. This is partly due to the fact that ξ_n is related to ξ_A via Equation (3.3.3) in the ballooning approximation while it is a genuine variable in the system (3.3.11), and partly because system (3.3.11) does not take into account the $\mathcal{J}$-contribution to δW. Both reasons constitute the difference between the necessary and the sufficient condition for stability.

3.5. Summary

The use of the energy principle (Bernstein *et al.*, 1958) to investigate the stability of line-tied 2-D magnetic fields normally requires solving a system of three coupled partial differential equations. This surely is a non-trivial and time-consuming task, whose inherent limitations might lead to unsatisfactory results, e.g., a possible overestimation of the stability of the equilibrium. We opted for a different approach. The expression for the perturbed potential energy integral is cast in the form (1.4.1), allowing the following manipulation. Firstly, localised modes are used as trial functions in an attempt to lower the potential energy, resulting in necessary conditions for stability. They are particularly useful since they minimise the stabilising effect of magnetic tension (Suydam, 1958) and are known to be the most unstable modes in shearless fields (Hood, 1986a). Secondly, the $\mathcal{J}$-contribution to δW is neglected and this partial minimisation yields a sufficient condition for stability. In both cases one only needs to solve two systems of coupled homogeneous linear ordinary differential

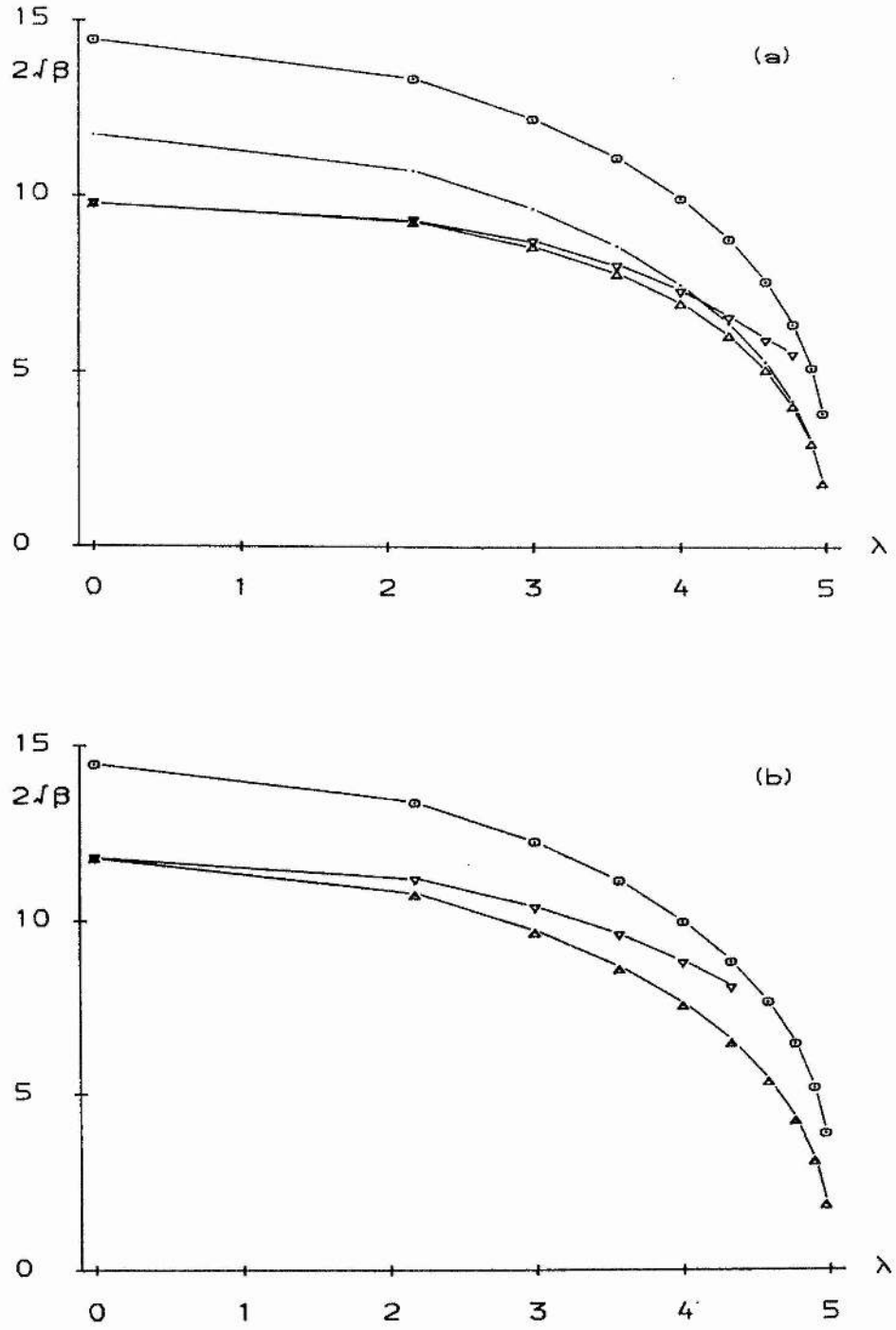

Fig. 3.8. A resumé of the results of the stability investigation for equilibrium (3.4.8) when $k = 5$, $q = 0.1$ for (a) $\gamma = 1$, and (b) $\gamma = 5/3$. See the text for an explanation of the symbols.

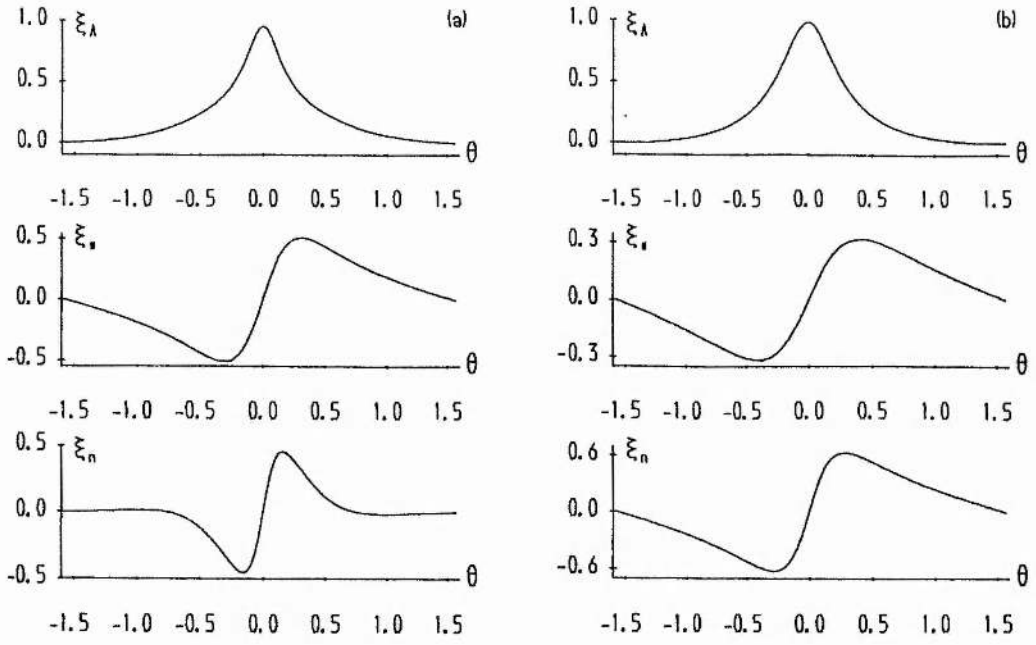

Fig. 3.9. Eigenfunction plots of (a) the system (3.3.8) determining the most unstable localised interchange mode, and (b) the system (3.3.11), for equilibrium (3.4.8) when $k = 5, \lambda = 3, q = 0.1$, and $\gamma = 5/3$.

equations along a field line, (3.3.8) and (3.3.11), subject to the boundary conditions (1.4.2). Combining both stability conditions yields three regions in parameter space : one in which the equilibrium is definitely stable, one in which it is unstable to localised modes and a third in which this procedure is unable to give a decisive answer. The success of this method can be measured by the size of that third region.

The method was applied to two classes of equilibria. The first one was a family of line-tied 2-D linear force-free arcades, with a flux function and longitudinal field component given by Equation (3.4.3). We proved this class is completely stable, in agreement with Berger (1985). It would be interesting to investigate the stability of some nonlinear force-free fields. Proving them to be stable as well would back up the conjecture that all line-tied force-free arcades are stable (Cargill, Hood, and Migliuolo, 1986; Hood and Anzer, 1987). The second class of investigated equilibria was that of Su Qing-rui (1984), an extension of the isothermal equilibria of Zweibel and Hundhausen (1982) to sheared magnetic fields. The stability bounds found are shown in Figure 3.8. The 'uncertainty region' between both marginal curves is pleasingly small, especially in view of the results of this method for cylindrically symmetric magnetic fields (Chapter 2). Decreasing the background pressure (i.e., the value of q) makes the gap even smaller, as Figure 3.6 indicates. Figure 3.8 shows that, for this

arcade at least, shearing is destabilising. This is contrary to the case of cylindrically symmetric fields, where the extended Suydam criterion (2.2.17) clearly assigns a stabilising role to footpoint displacements. One possible explanation for this apparent contradiction is that in cylindrically symmetric fields a field line is forced to stay on the same cylindrical flux surface, independent of the amount of shear, while this is not true for 2-D arcades. As can be seen in Figure 3.3, when the shear is increased the field line rises. This makes its length longer and hence the effect of line-tying, believed to be a major stabilising mechanism, is weakened. The destabilising role of shearing is well known from observations, showing evidence of shear in the magnetic fields of active regions (see, for instance, Foukal, 1971 and Hagyard *et al.*, 1986). However, in no case did we find that force-free fields were definitely unstable. It is also known that sheared equilibria can store an amount of 'free energy' in excess of the energy of the corresponding potential field (see, for instance, Klimchuk, Sturrock, and Yang, 1988). When they become unstable they can provide the energy for, e.g., solar flares. So it appears that the assumption of cylindrical symmetry is too strong a constraint on the realistic evolution of magnetic fields, and two-dimensional models match the observations much better.

The influence of gravity on the stability is briefly discussed in Appendix E. The method presented in this Chapter can easily be extended to loops that have a translational invariance, such as the disconnected helically shaped field lines forming an island in the equilibria of the second class, and to non-isothermal equilibria, as will be demonstrated in the next Chapter.

4

Prominence Stability

4.1. Introduction

Prominences are, quite literally, extra-ordinary objects. They might be defined as clouds of material visible in Hα (an emission line at 6563 Å) above a polarity inversion zone on the solar surface, which is about as accurate as defining the Eiffel Tower as a metal construction reaching 300 m in the Parisian air. Their beauty defies all description, let alone explanation.

Quiescent prominences, having temperatures of around 10 000 K or less, are situated in a corona which is heated up to 1 000 000 K or more. Their density can be over a hundred times higher than that of their environment, with plasma pressure and magnetic field strength not greatly exceeding coronal values. They are typically 200 Mm long, 50 Mm high, and 6 Mm wide. Seen against the solar disk they look like dark filaments, while projected onto the sky they appear as bright curtains. They can sit there quietly, growing slowly as the months pass, suddenly to erupt in a matter of hours. Observers wonder what holds them down (Zirin, 1988, p. 267), while theorists ponder on how they are supported against gravity (Priest, 1982, pp. 395–410). An up-to-date account of the subject can be found in, for example, Priest (1989) and the proceedings of the IAU Colloquium 117 on "Dynamics of Prominences" (1990).

A wide range of theoretical prominence models can be found in the astrophysical literature, ranging from the early 1-D model of Kippenhahn and Schlüter (1957), through 2-D structures such as those by Menzel (1951), Dungey (1953), and Kuperus and Raadu (1974), and 3-D static equilibria by, for example, Démoulin, Priest, and Anzer (1989) and Priest, Hood, and Anzer (1989), to fully dynamical 3-D descriptions by, e.g., Kuijpers (1989). Anzer (1989) presented a critical assessment of the existing models for magnetohydrostatic equilibrium of quiescent prominences and concluded that a lot still needs to be done.

The stability properties of only a fraction of these configurations are known. Kippenhahn and Schlüter (1957) studied the stability of their model against a subset

of perturbations, as did Brown (1958), whose family of equilibria also included that of Menzel (1951). Anzer (1969) derived stability criteria for the Kippenhahn–Schlüter model in the limit of vanishing prominence width. The equilibrium was re-examined by Zweibel (1982) and Migliuolo (1982) for special perturbations, and was found definitely stable by Galindo Trejo and Schindler (1984). Low, Hundhausen, and Zweibel (1983) proved their nonlinear shearless isothermal filament model to be unstable to localised perturbations. Wu (1987) showed that the curved current sheet models of Wu and Low (1987) are also unstable. Vršnak *et al.* (1990) compared the observed oscillatory motions in an active prominence with those of a curved current-carrying loop, while Vršnak (1990) examined the eruptive instability of a magnetic arcade containing a filament. Numerical investigations were performed by, for example, Sakurai (1976), who studied the nonlinear stability of a filament modelled as a 1-D flux tube, Galindo Trejo (1987), who investigated the stability properties of four models of quiescent prominences (Menzel, 1951; Dungey, 1953; Kippenhahn and Schlüter, 1957; Lerche and Low, 1980) and found them stable in the observed parameter range, and Van Ballegooijen and Martens (1989), who modelled formation and eruption of solar prominences.

Among the few models that are non-isothermal, have a magnetic field component along the prominence axis, and describe both the internal magnetic field and its coupling to the bipolar coronal field (all prerequisites for a realistic model) are those of Low (1981a) and Hood and Anzer (1990). In Section 4.2 we will concentrate on the former one, while the latter one will be dealt with in Section 4.3. The stability of the Low (1981a) model has been examined by Galindo Trejo (1989a,b) but not in a completely satisfactory way, as will be discussed in due course. The Hood and Anzer (1990) equilibrium, being relatively new, has to our knowledge not been subjected to a stability investigation before. The Chapter is rounded off with a summary in Section 4.4.

4.2. The Low (1981a) Prominence Model

4.2.1. Equilibrium and Stability Equations

Low (1981a) constructed an analytical 2-D model for a finite size static filament embedded in an arcade straddling a bipolar photospheric region. The filament may be cooler than the surrounding corona, representing a prominence, or it may be hotter, a configuration displaying an X-ray coronal loop. Here, the reader's attention is drawn to the former case.

Using the coronal pressure scale height $H_0 = \mathcal{R}T_0/\tilde{\mu}g$ and a characteristic magnetic field strength B_0 as a normalisation, such that

$$\begin{aligned} \mathbf{r} &= H_0\bar{\mathbf{r}}, \quad & A &= B_0H_0\bar{A}, \quad & \mathbf{B} &= B_0\bar{\mathbf{B}}, \quad & \mathbf{j} &= \frac{B_0}{\mu H_0}\bar{\mathbf{j}}, \\ p &= \frac{B_0^2}{\mu}\bar{p}, \quad & \rho &= \frac{B_0^2}{\mu H_0 g}\bar{\rho}, \quad & T &= T_0\bar{T}, \quad & \phi &= H_0 g\bar{z}, \end{aligned} \tag{4.2.1}$$

the components of the magnetohydrostatic equation (1.2.8) and the ideal gas law (1.2.7) read

$$B_y = B_y(A), \tag{4.2.2a}$$

$$\frac{\partial p}{\partial z} = -\rho, \tag{4.2.2b}$$

$$\nabla^2 A = -\frac{\partial}{\partial A}\left(p + \frac{1}{2}B_y^2\right), \tag{4.2.2c}$$

$$p = \rho T. \tag{4.2.2d}$$

Bars have been dropped for simplicity, and the geometry and notation of Chapter 3 is used, so that all quantities are functions of the flux function A and height z. Prescribing the bipolar normal field as

$$B_z(x,0) = \frac{-2x}{x^2+\delta^2}\,, \tag{4.2.3}$$

where δ is a constant fixing the length scale of the bipolar region, determines a potential field with flux function

$$A_0 = -\ln\,[x^2 + (z+\delta)^2], \qquad B_{y0} = \text{constant}. \tag{4.2.4}$$

This background potential field may be thought of as being produced by an infinitely long line-current located at $x = 0, z = -\delta$, running in the positive y-direction. The coronal background plasma distribution is then in strictly hydrostatic equilibrium with the uniform gravity field. A plasma concentration will introduce electric currents such that a net Lorentz force $\mathbf{j} \times \mathbf{B}$ acts upwards and supports the plasma weight. Let the currents be such that they generate a magnetic field with flux function

$$A_c = \ln\,[x^2 + (z-z_1)^2 + a^2]. \tag{4.2.5}$$

This field is due to a current density symmetrically distributed about $x = 0, z = z_1$, and declining in strength over a characteristic radius a from the axis. The current produces an image current below the corona, responsible for a field with flux function

$$A_i = -\ln\,[x^2 + (z+\delta)^2]. \tag{4.2.6}$$

Hence, since Maxwell's equations are linear, the total flux function is

$$A = A_0 + A_c + A_i = \ln\frac{x^2 + (z-z_1)^2 + a^2}{[x^2 + (z+\delta)^2]^2}\,. \tag{4.2.7}$$

The normal field distribution (4.2.3) then implies that $a^2 = \delta^2 - z_1^2$. So, if one fixes

the length scale of the bipolar region, δ, a one-parameter family of magnetic fields is obtained as the height of the coronal current distribution, z_1, varies between $-\delta$ and δ.

To construct a plasma distribution consistent with magnetohydrostatic equilibrium, the variable

$$U = x^2 + (z - z_1)^2 + a^2 \tag{4.2.8}$$

is introduced, so that

$$A(U, z) = \ln \frac{U}{[2(z_1 + \delta)z + U]^2} \,. \tag{4.2.9}$$

From the Grad-Shafranov equation (4.2.2c) it then follows that

$$p(U, z) = \frac{2a^2}{(z_1 + \delta)^2 z^2}\left[\frac{(z_1 + \delta)^2 z^2}{U^2} - \frac{2(z_1 + \delta)z}{U} + \ln\left(1 + \frac{2(z_1 + \delta)z}{U}\right)\right] + \\ + \frac{\beta}{2}\exp\,(z_1 - z) - \frac{1}{2}B_y^2(A), \tag{4.2.10}$$

where β is a characteristic ratio of background plasma to magnetic pressure. The mass density ρ is obtained from the equation of hydrostatic equilibrium along a field line (4.2.2b), yielding

$$\rho(U, z) = \frac{4a^2}{(z_1 + \delta)^2 z^3}\left[\frac{2(z_1 + \delta)^2 z^2}{U^2} - \frac{2(z_1 + \delta)z}{U} + \ln\left(1 + \frac{2(z_1 + \delta)z}{U}\right)\right] + \\ + \frac{\beta}{2}\exp\,(z_1 - z). \tag{4.2.11}$$

Finally, the temperature distribution is determined by the ideal gas law (4.2.2d).

Notice from Equation (4.2.10) that the longitudinal field $\mathbf{B}_y$ is introduced solely through the plasma pressure. The requirement that p must be positive severely restricts the ranges of δ, z_1, β, and B_y. For example, Equation (4.2.10) evaluated at the origin gives

$$p(x = 0, z = 0) = -\frac{2(\delta^2 - z_1^2)}{\delta^4} + \frac{\beta}{2}\mathrm{e}^{z_1} \tag{4.2.12}$$

for a shearless configuration (i.e., $B_y = 0$). Now since, from the ideal gas law (4.2.2d),

$$\lim_{z_1 \to \delta} T(x = 0, z = \delta) = \frac{\delta}{4} \,, \tag{4.2.13}$$

one wants δ as small as possible in order to obtain a cool filament. Unfortunately,

$$\lim_{z \to +\infty} T = -\infty, \tag{4.2.14}$$

so the equilibrium becomes meaningless at large height. Therefore the stability investigation is restricted to the parameter values $\delta = 1, \beta = 1$, $0.7 < z_1 \leq 1$, and $0 \leq B_y \leq 0.2$. This is hardly a justifiable choice in the light of what is to be modelled; it will do, however, to demonstrate the viability of the stability procedure employed. A projection of the magnetic field lines on the x, z-plane is plotted in Figure 4.1 for two values of z_1. From the flux function (4.2.7) it follows that the

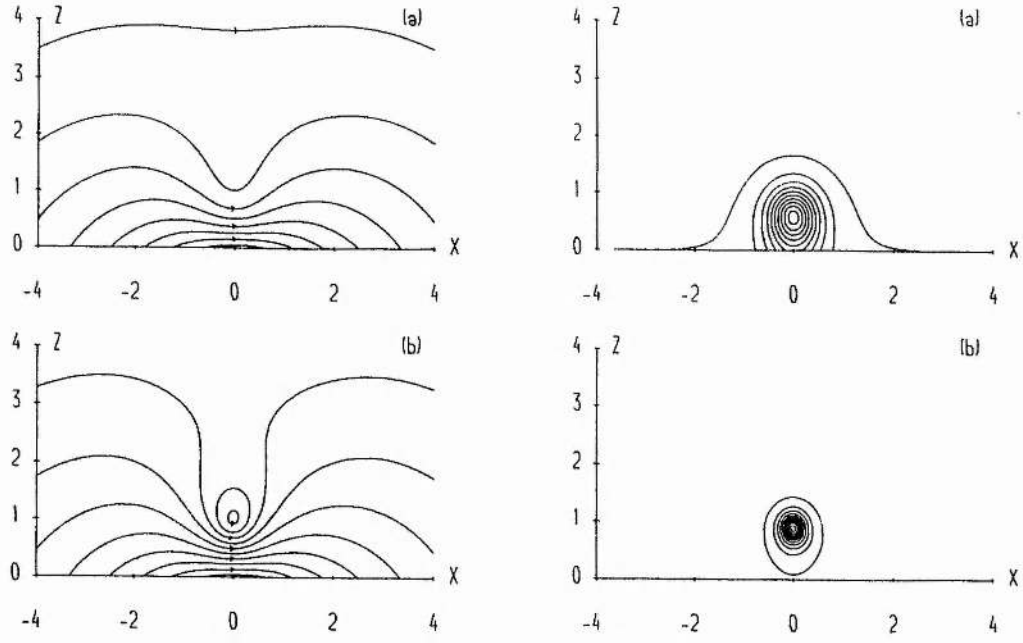

Fig. 4.1 (left) and Fig. 4.2 (right). A projection of the magnetic field lines (left) and density contours (right) of the equilibrium (4.2.9)–(4.2.11) on the x, z-plane when $\delta = 1, \beta = 1$ for (a) $z_1 = 0.75$, and (b) $z_1 = 0.95$.

magnetic field can have two neutral points, situated at

$$x = 0, \qquad z_{\pm} = \frac{1}{2}\Big[(3z_1 + \delta) \pm \sqrt{(z_1 + \delta)(9z_1 - 7\delta)}\Big]. \tag{4.2.15}$$

When $z_1 \leq 7\delta/9$ all field lines connect to the photosphere, while for $7\delta/9 < z_1 \leq \delta$ a magnetic island is embedded in the field. At $z_1 = \delta$ with $B_y(A) = 0$, the field is potential and the plasma pressure is purely hydrostatic, except at the singular axis $x = 0, z = \delta$. Figure 4.2 depicts density contours for the same two values of z_1. Comparing Figures 4.1 and 4.2, it can be seen that the density enhancement is concentrated below the O-type neutral point.

To derive necessary conditions and sufficient conditions for stability, the approach used in Chapter 3 is adapted to fit non-isothermal equilibria. To minimise the ballooning integral (3.3.4) the variables

$$y_1 = B_p \xi_A,$$
$$\tilde{y}_2 = \tilde{\xi}_{\|},$$

are selected. Using the non-dimensionalisation (4.2.1), the Euler-Lagrange equations (3.3.8), determining a necessary condition for stability, transform into

$$\frac{\partial y_1}{\partial s} = \left(\frac{B}{B_p^2} + \frac{B_p^2}{B} y_5^2\right)^{-1} y_3, \tag{4.2.16a}$$

$$\frac{\partial \tilde{y}_2}{\partial s} = \frac{1}{B}\left[\frac{B^2+\gamma p}{\gamma p B^2}\tilde{y}_4 + \left(L_1 + \frac{L_2}{\gamma T}\right)\tilde{y}_1\right] + \frac{1}{\gamma T}\frac{B_z}{B}\tilde{y}_2, \tag{4.2.16b}$$

$$\frac{\partial y_3}{\partial s} = \frac{-1}{BB_p}\left[\left(\Lambda f^2 + L_1\frac{\partial p}{\partial A}B_p + L_2\frac{\partial \rho}{\partial A}B_p\right)\tilde{y}_1 + L_2\tilde{y}_\phi + \left(L_1 + \frac{L_2}{\gamma T}\right)\tilde{y}_4\right], \tag{4.2.16c}$$

$$\frac{\partial \tilde{y}_4}{\partial s} = -\frac{B_z}{B}\tilde{y}_\phi - \frac{1}{\gamma T}\frac{B_z}{B}\tilde{y}_4, \tag{4.2.16d}$$

$$\frac{\partial y_5}{\partial s} = \frac{1}{B}\left[-\frac{dB_y}{dA} + \frac{B_y}{B_p^2}\left(J + 2\frac{\partial B_p}{\partial a}\right)\right], \tag{4.2.16e}$$

where

$$\tilde{y}_1 = \frac{y_1}{B_p}, \qquad y_5 = \frac{1}{B_p}\frac{\partial S}{\partial a},$$
$$\tilde{y}_\phi = \rho\tilde{A}(L_2\tilde{y}_1 + B_z\tilde{y}_2),$$
$$\tilde{A} = \frac{1}{\gamma T} + \frac{1}{\rho}\frac{\partial \rho}{\partial z},$$
$$L_1 = \frac{B_p}{B^2}\left(2\left(J + \frac{\partial B_p}{\partial a}\right) + \frac{B_y}{B}\frac{\partial B_p^2}{\partial s}y_5\right),$$
$$L_2 = -\frac{B_x}{B_p} + \frac{B_y B_z B_p}{B^2}y_5.$$

Similarly, choosing the variables

$$y_1 = B_p\xi_A,$$
$$y_2 = \tilde{\xi}_\parallel,$$
$$y_5 = \frac{B}{B_p}\xi_n,$$

the Euler-Lagrange equations (3.3.11), determining a sufficient condition for stability, turn into

$$\frac{\partial y_1}{\partial s} = \frac{B_p^2}{B}y_3, \tag{4.2.17a}$$

$$\frac{\partial \tilde{y}_2}{\partial s} = \frac{1}{B}\left[\frac{B^2+\gamma p}{\gamma p B^2}\tilde{y}_4 + G_1\tilde{y}_1 + G_2\frac{B_y}{B}y_5\right] + \frac{1}{\gamma T}\frac{B_z}{B}\tilde{y}_2, \tag{4.2.17b}$$

$$\frac{\partial y_3}{\partial s} = \frac{-1}{BB_p}\left[(\Lambda f^2 + \tilde{V})\tilde{y}_1 - \frac{B_x}{B_p}\tilde{y}_\phi + G_1\tilde{y}_4 + G_3B_y\tilde{y}_6\right], \tag{4.2.17c}$$

$$\frac{\partial \tilde{y}_4}{\partial s} = -\frac{B_z}{B}\tilde{y}_\phi - \frac{1}{\gamma T}\frac{B_z}{B}\tilde{y}_4, \tag{4.2.17d}$$

$$\frac{\partial y_5}{\partial s} = B\tilde{y}_6 + G_3\frac{B_y}{BB_p^2}\tilde{y}_1, \tag{4.2.17e}$$

$$\frac{\partial y_6}{\partial s} = -\frac{B_y}{B^2}\left[\frac{B_z}{B}\tilde{y}_\phi + G_2\tilde{y}_4\right], \tag{4.2.17f}$$

where

$$\tilde{y}_1 = \frac{y_1}{B_p}\,, \qquad \tilde{y}_6 = \frac{y_6}{B_p^2}\,,$$

$$\tilde{y}_\phi = \rho\tilde{A}\left(-\frac{B_x}{B_p}\tilde{y}_1 + B_z\tilde{y}_2 + \frac{B_yB_z}{B^2}y_5\right),$$

$$\tilde{A} = \frac{1}{\gamma T} + \frac{1}{\rho}\frac{\partial\rho}{\partial z}\,,$$

$$\tilde{V} = 2J\Big(J + \frac{\partial B_p}{\partial a}\Big) - B_x\frac{\partial\rho}{\partial A}\,,$$

$$G_1 = \frac{2B_p}{B^2}\Big(J + \frac{\partial B_p}{\partial a}\Big) - \frac{1}{\gamma T}\frac{B_x}{B_p}\,,$$

$$G_2 = \frac{1}{B^2}\frac{\partial B_p^2}{\partial s} + \frac{1}{\gamma T}\frac{B_z}{B}\,,$$

$$G_3 = 2B_p\Big(J + \frac{\partial B_p}{\partial a}\Big).$$

As before, the systems (4.2.16) and (4.2.17) are identical when the prominence model does not have a longitudinal field component (i.e., $B_y = 0$).

4.2.2. Results of the Linear Stability Analysis

The MHD stability of the Low (1981a) filament model has been investigated before, namely by Galindo Trejo (1989a,b). He too used the Bernstein *et al.* (1958) energy method (p. 71; in this and the following paragraph page numbers will refer to Galindo Trejo, 1989a), but minimised δW by the variational method of finite elements (p. 76). He found the equilibrium stable for the parameter range observed in quiescent prominences and associated the computed stable horizontal oscillations with the observed short-period variations in the velocity field (p. 87). For other parameter ranges he demonstrated instability driven by compressional effects and assigned this to macroscopic drift instabilities (p. 88).

However, his conclusions have to be viewed with some caution, mainly for the following reasons : the boundary conditions on the plasma disturbance are very restrictive (pp. 71–72), possibly leading to an overestimation of the stability; a maximum of 32 elements is taken in each mesh direction (p. 76), eliminating localised modes from the analysis; T is normalised with respect to the prominence temperature (p. 77), yielding a corona with a pressure scale height characteristic of a prominence; Equation (4.2.13) is derived incorrectly (p. 77), leading to the wrong equilibrium parameter choice; many of the equilibria investigated are purely hydrostatic backgrounds embedded in a potential field with a singular prominence axis invisible in the numerical mesh (pp. 78–81), which explains the stable oscillations; others have negative pressure and temperature regions, see Equations (4.2.12) and (4.2.14) (pp. 78–89), responsible for

instabilities driven by compressional effects. Similar criticisms apply to Galindo Trejo (1989b). It was therefore thought that a second stability investigation was not wholly out of place.

The way to integrate the systems (4.2.16) and (4.2.17) governing stability is very similar to that used in Chapter 3. For line-tied field lines the numerical polar coordinate system r, θ, y has its axis on the photosphere, while for closed field lines it is placed at the prominence axis $x = 0, z = z_-$. Rigid plate boundary conditions (1.4.2) are imposed on the photosphere and periodicity is assumed for the perturbations of the closed field lines. Here too, the Bulirsch-Stoer and Van Wijngaarden-Dekker-Brent (Press *et al.*, 1987) numerical routines are employed to determine marginal stability parameters, while a Runga-Kutta scheme provides the eigenfunctions. The ratio of specific heats γ is taken to be 5/3 throughout.

Figure 4.3 depicts the stability diagram for the shearless field (i.e., $B_y = 0$), where the field lines have been labelled by z_0, the height at which they pass through the y, z-plane. The absciss is the height z_1 of the symmetric current distribution above the photosphere. The full curve is the marginal stability curve for even modes (i.e., ξ_A is even in x), while the dashed curve represents that for odd modes (ξ_A odd in x). A field line is stable to the right and unstable to the left of these curves. The region underneath the lower dotted line has a negative pressure at $x = 0$, while field lines above the upper dotted line are disconnected from the photosphere. It is clear that only a slight departure from the potential state $z_1 = 1$ is needed for the configuration to become unstable. Note that the marginal stability curves match across the upper dotted line, indicating that line-tying plays an insignificant role in stabilising this equilibrium. The instability is due to an unstable stratification, which triggers a Rayleigh-Taylor instability. Since there is no shear here, the field lines are free to interchange. All field lines above the magnetic island are linearly stable in the region where the pressure is positive.

The introduction of a shear component B_y does not suppress the instability. This is counter-intuitive, as one would expect a sheared field to oppose the interchanging of field lines (characteristic of a Rayleigh-Taylor instability) much more efficiently than its shearless counterpart, see Section 2.3. The explanation for this somewhat surprising result lies in the fact that a longitudinal field component decreases the plasma pressure, see Equation (4.2.10), without altering the density profile and hence reduces the stabilising effect of compression, tipping the balance in favour of an instability. The marginal stability curves hardly change when a longitudinal field component is introduced. This can be seen by comparing Figure 4.3, where $B_y = 0$, with Figure 4.4,

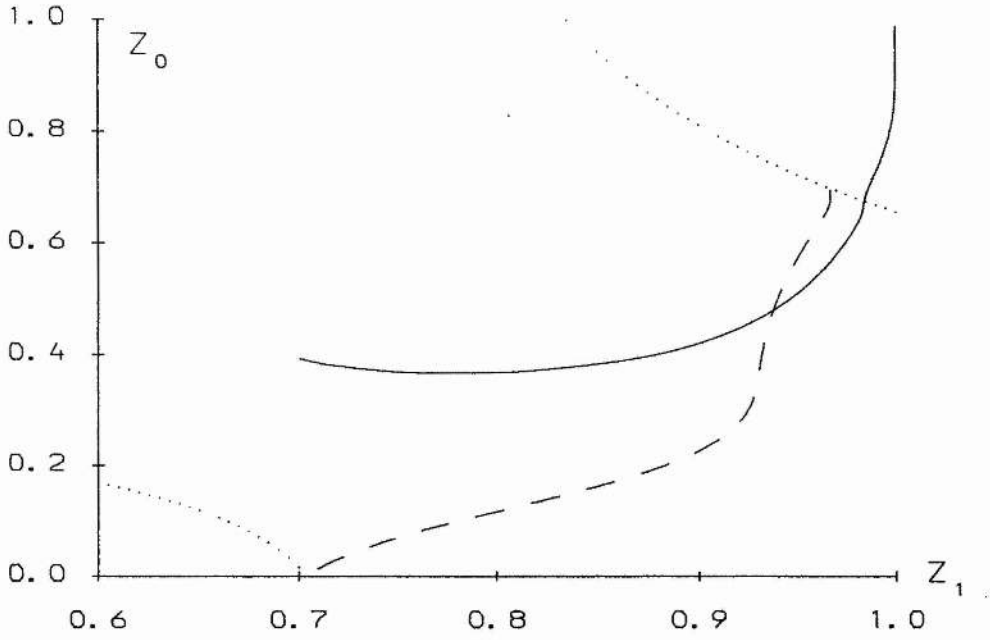

Fig. 4.3. Stability diagram for the shearless equilibrium (4.2.9)–(4.2.11) when $\delta = 1, \beta = 1$, and $\gamma = 5/3$, showing the marginal stability thresholds for even modes (full curve) and odd modes (broken curve). A field line, labelled by z_0 (see text) is stable to the right and unstable to the left of these curves. Below the lower dotted curve the pressure at $x = 0$ is negative, while the field lines above the upper dotted curve are disconnected from the photosphere.

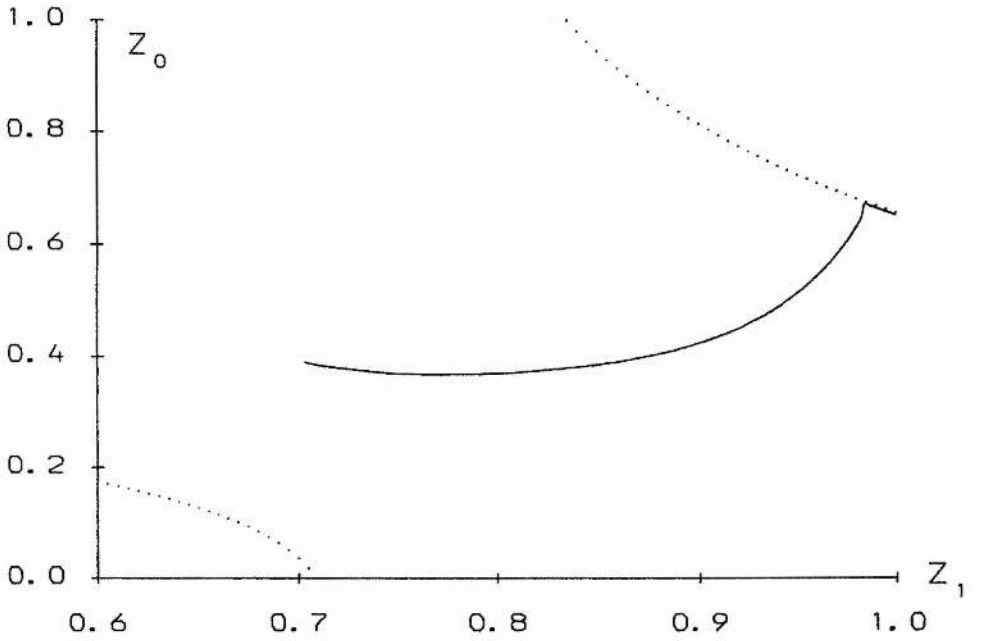

Fig. 4.4. Counterpart of Figure 4.3 for even modes when $B_y = 0.2$.

displaying the (in-)stability curves for even modes when $B_y = 0.2$. The stability and instability curve are indistinguishable on this scale. Only line-tied field lines have been investigated, since the stability of the helical field lines is dependent on the length of the prominence. Figure 4.5 depicts marginal eigenfunctions for $B_y = 0.2$ and (a) odd modes at $z_0 = 0.3$, (b) even modes at $z_0 = 0.5$. As in Figure 3.9, the shape of the components ξ_A and $\xi_\parallel$ of the systems (4.2.16) and (4.2.17) is strikingly similar, with the main difference lying in the component ξ_n.

4.3. The Hood and Anzer (1990) Prominence Model

4.3.1. Equilibrium and Stability Equations

Hood and Anzer (1990) developed a 2-D extension of the original Kippenhahn-Schlüter (1957) prominence model. They matched the cool filament configuration onto a hot external force-free coronal field, and took account of a longitudinal field component that affects the internal structure of the prominence.

Assume the following functional form for the magnetic field $\mathbf{B}$, the plasma pressure p, the temperature T, and the mean molecular weight $\tilde{\mu}$:

$$\begin{aligned} \mathbf{B} &= (X(x), Y(x), Z(x))\ \mathrm{e}^{-kz}, \\ p &= P(x)\ \mathrm{e}^{-2kz}, \\ T &= T(x), \\ \tilde{\mu} &= \tilde{\mu}(x). \end{aligned} \tag{4.3.1}$$

The flux function A is then of the form

$$A(x,z) = \frac{1}{k} X(x)\ \mathrm{e}^{-kz}, \tag{4.3.2}$$

up to an additive constant, while it follows from the ideal gas law (1.2.7) that

$$\rho(x) = \frac{P(x)}{gH(x)}\ \mathrm{e}^{-2kz}, \qquad \text{with } H(x) = \frac{\mathcal{R}T(x)}{\tilde{\mu}(x)g}\ . \tag{4.3.3}$$

The magnetohydrostatic equation (1.2.8) and Gauss's law (1.2.6) then yield

$$2\mu P + X^2 + Y^2 + Z^2 = \text{constant} = 2\mu P_T, \tag{4.3.4a}$$

$$Y = \lambda X, \tag{4.3.4b}$$

$$\frac{1}{k} X' = Z, \tag{4.3.4c}$$

$$\frac{1}{k} X Z' = \left(1 - \frac{1}{2kH}\right) Z^2 - \frac{1+\lambda^2}{2kH} X^2 - \left(1 - \frac{1}{2kH}\right) 2\mu P_T, \tag{4.3.4d}$$

where primes denote derivatives with respect to x. Equation (4.3.4a) entails constant total pressure in the horizontal direction, while Equation (4.3.4b) implies that the equilibrium is laminated, i.e., the magnetic field lines lie in parallel vertical planes.

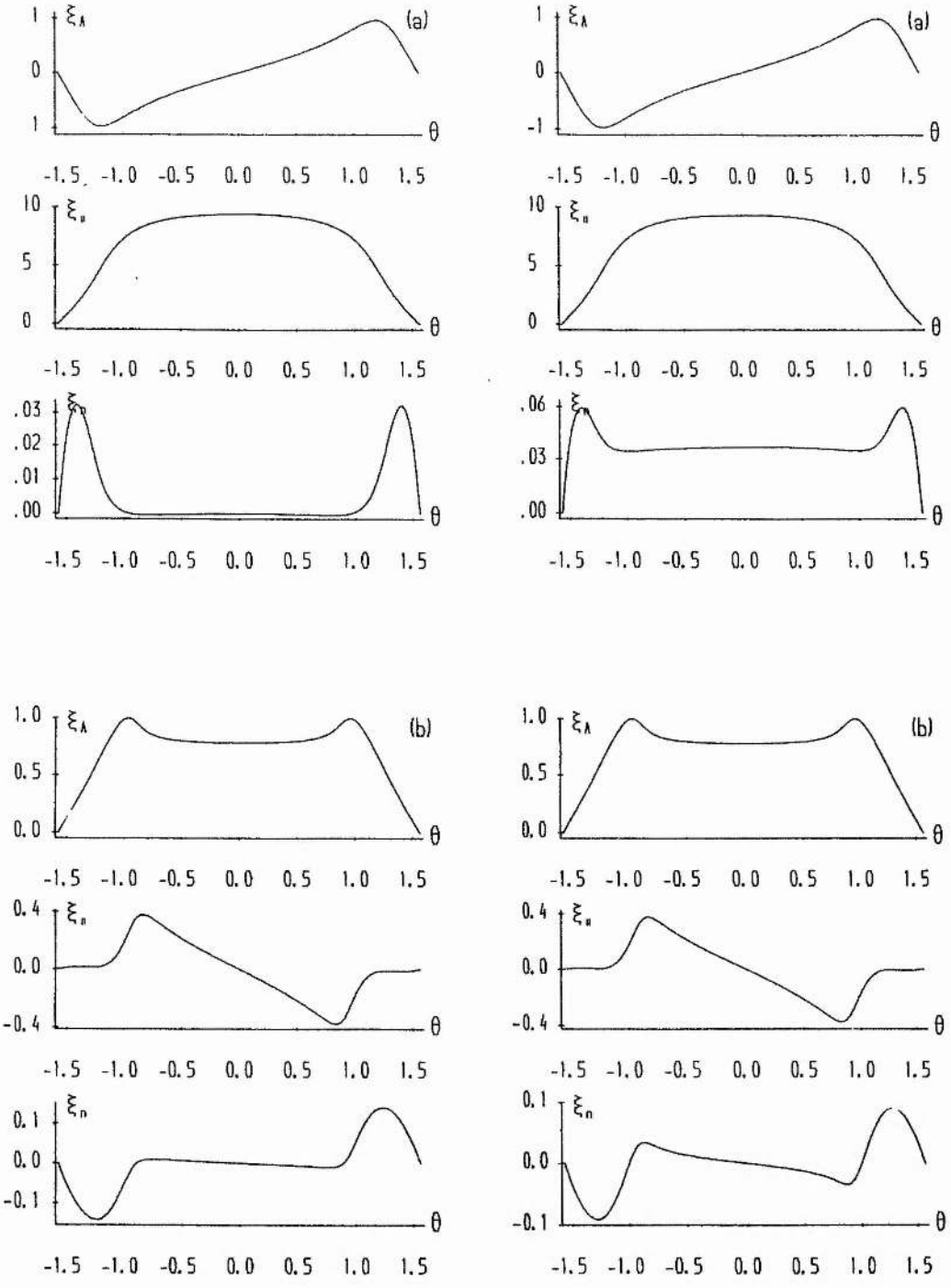

Fig. 4.5. Eigenfunctions of the system (4.2.16) determining a necessary condition for stability (left) and the system (4.2.17) determining a sufficient condition for stability (right) for the equilibrium (4.2.9)–(4.2.11) along the field lines (a) $z_0 = 0.3$, and (b) $z_0 = 0.5$, when $\delta = 1, \beta = 1, B_y = 0.2$, and $\gamma = 5/3$.

Equations (4.3.4c–d) then form a nonlinear system of two first order ordinary differential equations governing the magnetic field configuration. Since there is no energy equation, a temperature distribution can be chosen at will. Because the prominence-corona transition region is very narrow, the T- and $\tilde{\mu}$-profiles are selected to consist of two uniform regions, such that

$$H(x) = \begin{cases} H_{\rm cool} & |x| < x_{\rm prom}, \\ H_{\rm hot} & |x| > x_{\rm prom}, \end{cases} \tag{4.3.5}$$

where $x_{\rm prom}$ is the prominence half width and $H_{\rm cool} \ll H_{\rm hot}$. Note that the special case $k = 0, T(x) = T_0, \tilde{\mu}(x) = \tilde{\mu}_0$ retrieves the Kippenhahn-Schlüter (1957) model. For the corona to be force-free, the choice $kH_{\rm hot} = 1/2$ is made.

To non-dimensionalise, the inverse wave number $1/k$, the field strength $X_0{=}X(0)$ and the coronal mean molecular weight $\tilde{\mu}_{\rm hot}$ are used as a normalisation, such that

$$\begin{aligned} &\mathbf{r} = \bar{\mathbf{r}}/k, \qquad A = X_0\bar{A}/k, \qquad \mathbf{B} = X_0\bar{\mathbf{B}}, \qquad \mathbf{j} = \frac{X_0 k}{\mu}\bar{\mathbf{j}}, \\ &p = \frac{X_0^2}{\mu}\bar{p}, \qquad \rho = \frac{X_0^2 k}{\mu g}\bar{\rho}, \qquad T = \frac{\tilde{\mu}_{\rm hot} g}{\mathcal{R}k}\bar{T}, \qquad \phi = g\bar{z}/k. \end{aligned} \tag{4.3.6}$$

Four parameters then govern the equilibrium, $P_0 = P(0), \lambda, H_{\rm cool}$, and $x_{\rm prom}$. Bars have been dropped for simplicity.

To obtain a prominence configuration, Equations (4.3.4c–d) with $H = H_{\rm cool}$ are numerically integrated from $x = 0$ (since the model is symmetric in x), with initial conditions $X(0) = 1, Z(0) = 0$, out to $x = x_{\rm prom}$. At the prominence-corona interface, continuity of $\mathbf{B}$ and p is imposed (Roberts, 1967, p. 103). The system is then integrated with $H = H_{\rm hot} = 1/2$ out to $x = x_{\rm edge}$ where $X = 0$. Due to the choice of H, discontinuities in ρ and Z' at $x = x_{\rm prom}$ will occur. A projection of the magnetic field lines on the x, z-plane is plotted in Figure 4.6 for a given set of parameter values. It can be seen that, although a central dip in the field lines is present, it is very shallow. From Equation (4.3.4d) for Z it follows that the condition for a dip, which can contain the enhanced plasma density, is approximately

$$P_0 \geq (1 + \lambda^2)H_{\rm cool} \tag{4.3.7}$$

when $H_{\rm hot} \gg H_{\rm cool}$. It indicates that, as the longitudinal field component Y increases, the dip disappears, a somewhat unfortunate result. Two prominence pressure profiles are displayed in Figure 4.7.

To derive necessary conditions and sufficient conditions for stability, it is convenient to eliminate the z-dependence from the equations. This is possible only because of the special choice (4.3.1) for the equilibrium profiles. To minimise the ballooning

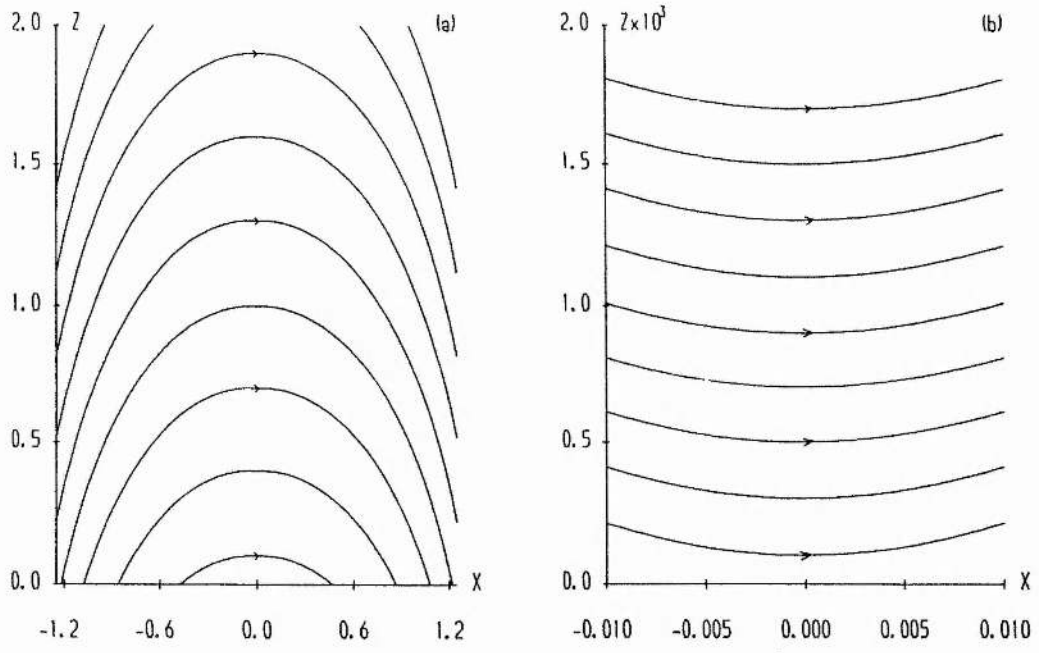

Fig. 4.6. A projection of the magnetic field lines of the equilibrium (4.3.4) on the x, z-plane for $P_0 = 0.0025$, $\lambda = 0.1$, $x_{\text{prom}} = 0.01$, and $H_{\text{cool}} = 0.00075$, showing (a) the overall arcade structure, and (b) the prominence slab itself. Arrows indicate the field direction.

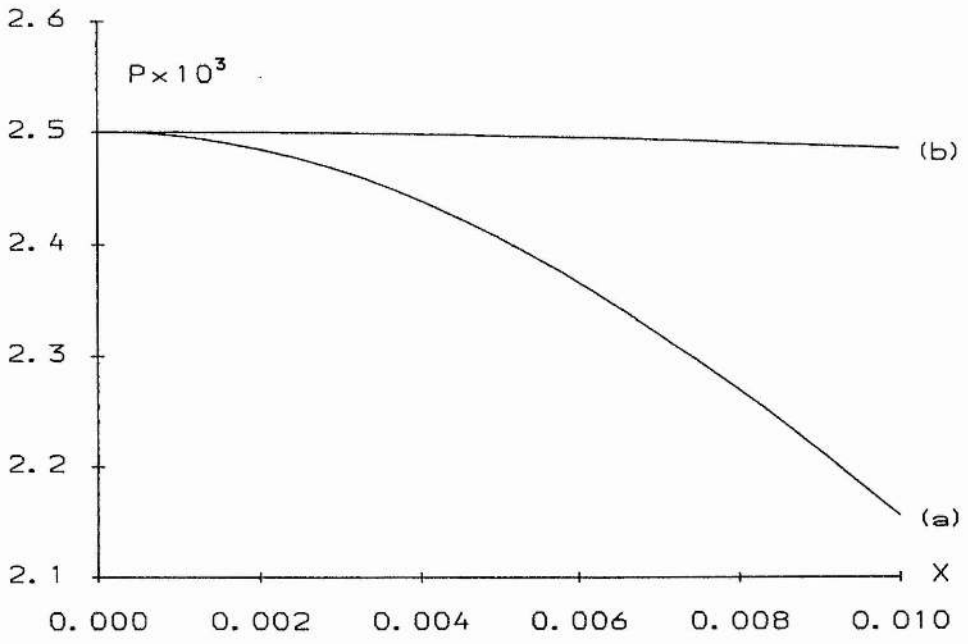

Fig. 4.7. The prominence pressure profile of the equilibrium (4.3.4) when $P_0 = 0.0025$, $\lambda = 0.1$, $x_{\text{prom}} = 0.01$ for (a) $H_{\text{cool}} = 0.00075$, and (b) $H_{\text{cool}} = 0.002$.

integral (3.3.4) the variables

$$y_1 = \xi_A,$$

$$y_2 = \xi_\parallel,$$

are selected. Using the non-dimensionalisation (4.3.6), the Euler-Lagrange equations (3.3.8), determining a necessary condition for stability, transform into

$$\frac{\partial y_1}{\partial s} = \left(\frac{B}{B_p} + \frac{B_p}{B}y_5^2\right)^{-1} y_3 - \frac{1}{2B_p^2}\frac{\partial B_p^2}{\partial s}y_1, \tag{4.3.8a}$$

$$\frac{\partial y_2}{\partial s} = \frac{B^2+\gamma p}{\gamma p}y_4 + \left(L_1 + \frac{L_2}{\gamma H}\right)y_1 + \left(\frac{1}{\gamma H}\frac{B_z}{B} + \frac{1}{2B^2}\frac{\partial B_p^2}{\partial s}\right)y_2, \tag{4.3.8b}$$

$$\frac{\partial y_3}{\partial s} = \frac{-1}{BB_p}\left[\left(\Lambda f^2 + L_1\frac{\partial p}{\partial A}B_p + L_2\frac{\partial \rho}{\partial A}B_p\right)y_1 + L_2\tilde{y}_\phi + \left(L_1 + \frac{L_2}{\gamma H}\right)B^2 y_4\right], \tag{4.3.8c}$$

$$\frac{\partial y_4}{\partial s} = -\left[\frac{B_z}{B^3}\tilde{y}_\phi + \left(\frac{1}{\gamma H}\frac{B_z}{B} + \frac{1}{B^2}\frac{\partial B_p^2}{\partial s}\right)y_4\right], \tag{4.3.8d}$$

$$\frac{\partial y_5}{\partial s} = \frac{B_p}{B}\left[-\frac{dB_y}{dA} + \frac{B_y}{B_p^2}\left(J + 2\frac{\partial B_p}{\partial a}\right)\right] + \frac{1}{2B_p^2}\frac{\partial B_p^2}{\partial s}y_5, \tag{4.3.8e}$$

where

$$y_5 = \frac{\partial S}{\partial a}, \qquad \tilde{y}_\phi = \rho\tilde{A}\left(L_2 y_1 + \frac{B_z}{B}y_2\right),$$

$$\tilde{A} = \frac{1}{\gamma H} + \frac{1}{\rho}\frac{\partial \rho}{\partial z},$$

$$L_1 = \frac{1}{B^2}\left(2B_p\left(J + \frac{\partial B_p}{\partial a}\right) + \frac{B_y}{B}\frac{\partial B_p^2}{\partial s}y_5\right),$$

$$L_2 = -\frac{B_x}{B_p} + \frac{B_y B_z}{B^2}y_5.$$

Note that, since the exponential z-factors cancel out, all coefficients in the equations are x-dependent only. Similarly, choosing the variables

$$y_1 = \xi_A,$$

$$y_2 = \xi_\parallel,$$

$$y_5 = \xi_n,$$

the Euler-Lagrange equations (3.3.11), determining a sufficient condition for stability, turn into

$$\frac{\partial y_1}{\partial s} = \frac{B_p}{B}y_3 - \frac{1}{2B_p^2}\frac{\partial B_p^2}{\partial s}y_1, \tag{4.3.9a}$$

$$\frac{\partial y_2}{\partial s} = \frac{B^2+\gamma p}{\gamma p}y_4 + G_1 y_1 + G_2\frac{B_y}{B_p}y_5 + \left(\frac{1}{\gamma H}\frac{B_z}{B} + \frac{1}{2B^2}\frac{\partial B_p^2}{\partial s}\right)y_2, \tag{4.3.9b}$$

$$\frac{\partial y_3}{\partial s} = \frac{-1}{BB_p}\left[(\Lambda f^2 + \tilde{V})y_1 - \frac{B_x}{B_p}\tilde{y}_\phi + G_1 B^2 y_4 + G_3\frac{B_y}{B_p}y_6\right], \tag{4.3.9c}$$

$$\frac{\partial y_4}{\partial s} = -\left[\frac{B_z}{B^3}\tilde{y}_\phi + G_2 y_4\right], \tag{4.3.9d}$$

$$\frac{\partial y_5}{\partial s} = y_6 + G_3\frac{B_y}{B^2B_p}y_1 + \frac{B_y^2}{2B^2B_p^2}\frac{\partial B_p^2}{\partial s}y_5, \tag{4.3.9e}$$

$$\frac{\partial y_6}{\partial s} = -\frac{B_y}{B_p}\left[\frac{B_z}{B^3}\tilde{y}_\phi + G_2 y_4\right] - \frac{1}{2B_p^2}\frac{\partial B_p^2}{\partial s}y_6, \tag{4.3.9f}$$

where

$$\tilde{y}_\phi = \rho\tilde{A}\left(-\frac{B_x}{B_p}y_1 + \frac{B_z}{B}y_2 + \frac{B_yB_z}{BB_p}y_5\right),$$

$$\tilde{A} = \frac{1}{\gamma H} + \frac{1}{\rho}\frac{\partial \rho}{\partial z},$$

$$\tilde{V} = 2J\left(J + \frac{\partial B_p}{\partial a}\right) - B_x\frac{\partial \rho}{\partial A},$$

$$G_1 = \frac{2B_p}{B^2}\left(J + \frac{\partial B_p}{\partial a}\right) - \frac{1}{\gamma H}\frac{B_x}{B_p},$$

$$G_2 = \frac{1}{B^2}\frac{\partial B_p^2}{\partial s} + \frac{1}{\gamma H}\frac{B_z}{B},$$

$$G_3 = 2B_p\left(J + \frac{\partial B_p}{\partial a}\right).$$

Again, all coefficients are functions of x only. As before, the systems (4.3.8) and (4.3.9) are identical when the prominence model does not have a longitudinal field component (i.e., $\lambda = 0$).

The correct boundary conditions at the prominence-corona interface are the continuity of the Lagrangian displacement and magnetic field and pressure perturbations (Roberts, 1967, p. 228). They can be derived by integrating the stability equations (4.3.8) and (4.3.9) across the interface. One then arrives at

$$\text{continuity of } \begin{cases} y_1, \\ y_2, \\ y_3 + \frac{L_2}{B_xB_z}\left(u_1 + \frac{B_x}{B_p}y_\phi\right)\rho, \\ y_4 + \frac{1}{B^2}y_\phi\rho, \\ y_5, \end{cases} \tag{4.3.10}$$

for the solutions of system (4.3.8), and

$$\text{continuity of } \begin{cases} y_1, \\ y_2, \\ y_3 - \frac{1}{B_xB_p}\left(u_1 + \frac{B_x}{B_p}y_\phi\right)\rho, \\ y_4 + \frac{1}{B^2}y_\phi\rho, \\ y_5, \\ y_6 + \frac{B_y}{B^2B_p}y_\phi\rho, \end{cases} \tag{4.3.11}$$

for the solutions of system (4.3.9), with $y_\phi = \xi_z$.

Finally, the non-dimensionalised x-dependent equilibrium equations read

$$X' = Z, \tag{4.3.12a}$$

$$Z' = \frac{1}{X}\left[\left(1 - \frac{1}{2H}\right)Z^2 - \frac{1+\lambda^2}{2H}X^2 - \left(1 - \frac{1}{2H}\right)2P_T\right], \tag{4.3.12b}$$

with

$$P = P_T - \frac{1}{2}(X^2 + Y^2 + Z^2), \tag{4.3.13a}$$

$$Y = \lambda X. \tag{4.3.13b}$$

4.3.2. Results of the Linear Stability Analysis

The systems (4.3.8)–(4.3.13) are x-dependent only. Hence the geometry of the field lines is independent of z and the photosphere is merely a reference level. The equilibrium is symmetric in x, so it suffices to consider the region $x \geq 0$. The integrations are performed in x via

$$B\frac{\partial}{\partial s} = B_x \frac{d}{dx} .$$

The integration is started off at $x = 0$, where all functions are known, with $X = 1$, $Z = 0$, and ξ chosen to be either even or odd. The stability equations (4.3.8) or (4.3.9) are integrated together with the equilibrium equations (4.3.12). At the prominence-corona interface $x = x_{\text{prom}}$ the boundary conditions (4.3.10) or (4.3.11) are applied. The integration is then continued until the rigid boundary conditions (1.4.2) are satisfied at $x = x_0$, say. At that point, the photospheric level is fixed, so that from Equation (4.3.2) for the flux function,

$$A_{\text{crit}} = X(x_0) \tag{4.3.14}$$

labels the critical field line. All field lines below $A = A_{\text{crit}}$ are stable due to line-tying, while field lines above $A = A_{\text{crit}}$ are unstable. So, the maximum height of the stable prominence is

$$z_0 = -\ln\,(X(x_0)). \tag{4.3.15}$$

If $z_0 < 0$, the model is completely unstable. If, on the other hand, the boundary conditions (1.4.2) cannot be satisfied before $x = x_{\text{edge}}$ is reached, the whole prominence is stable. Note that, since the equilibrium is laminated (see Equation (4.3.4b)), necessary conditions and sufficient conditions for stability will coincide, and hence integrating one of Equations (4.3.8) or (4.3.9) will yield the stability curves.

The choice of the parameters $P_0, \lambda, H_{\text{cool}}$, and x_{prom} is determined by observational data (see, for instance, Leroy, Bommier, and Sahal-Bréchot, 1983; Hirayama, 1985; Leroy, 1989; Hirayama, 1989). Typical values are : coronal temperatures $T_c = 1.2\times10^6 - 2\times10^6$ K, coronal mean molecular weight $\tilde{\mu}_{\text{hot}} = 0.6$, coronal number density $N_c = 2\times10^{14}$ m^{-3}, prominence temperatures $T_p = 5\times10^3 - 8\times10^3$ K, prominence mean molecular weight $\tilde{\mu}_{\text{cool}} = 1$, prominence number density $N_p = 2\times10^{17}$ m^{-3}, prominence width $2\,x_{\text{prom}} = 4\times10^6 - 6\times10^6$ m, prominence magnetic field $B = 5$ G – 20 G, horizontal angle between prominence magnetic field vector and

normal to prominence plane Arctan(λ) = 0° - 80°. This led to the following choice for the parameter ranges : $P_0 \in [0.0005, 0.1]$, $\lambda \in [0, 4]$, $H_{\text{cool}} \in [0.00075, 0.002]$, $x_{\text{prom}} \in [0.01, 0.025]$.

The prevailing trends in the stability results are now summarised. Increasing the prominence pressure P_0 is destabilising, as a heavier prominence is more likely to trigger a Rayleigh-Taylor instability. Increasing the magnetic field via λ somewhat counteracts this, but, more importantly, it flattens the central dip in the field (see Equation (4.3.7)), which is again destabilising. Increasing the prominence pressure scale height H_{cool} is stabilising, as the ideal gas law (1.2.7) implies a lower density for a given pressure when the temperature is raised. Increasing the prominence width $2x_{\text{prom}}$ is destabilising, because the field lines then tend to attain their maximum height inside the prominence, allowing the cool plasma to slide down under gravity.

Figure 4.8 depicts contours of prominence height z_0 in the λ, P_0-parameter space, for $x_{\text{prom}} = 0.01$ and (a) $H_{\text{cool}} = 0.00075$, (b) $H_{\text{cool}} = 0.002$. Above the dashed line, the equilibrium has a central dip, below it the field has an arcade structure as in Figure 3.1. Above the highest curve ($z_0 = 0$) the model is completely unstable. No stable prominence with a height exceeding 7 000 km was found, which does not match observations. Figure 4.9 shows the two marginal eigenfunctions for the parameters of Figure 4.7. Note that $\xi_{\|}$ has the largest amplitude. This is not surprising, since a force-free corona is largely unaffected by displacements parallel to its field lines.

4.4. Summary

Prominences are beautiful and highly interesting objects, but they do not easily lend themselves to a theoretical analysis. Many models exist, but most of them have some serious drawbacks (see, for instance, Anzer, 1989, for a review). Among the static equilibria that are nearest to reality, we selected the Low (1981a) and the Hood and Anzer (1990) prominences for a stability analysis.

Low's (1981a) magnetohydrostatic atmosphere seems not wholly appropriate for modelling a cool filament. The requirement of a positive plasma pressure severely restricts the available parameter ranges. Moreover, it turns out that, apart from the singular case of a line-current embedded in a potential field, the model is unstable to localised disturbances. The magnetic field below the O-type neutral point is not capable of suppressing a Rayleigh-Taylor instability. Increasing the shear does not counteract this, as it forces the pressure to decrease, which in turn diminishes the stabilising effect of compression.

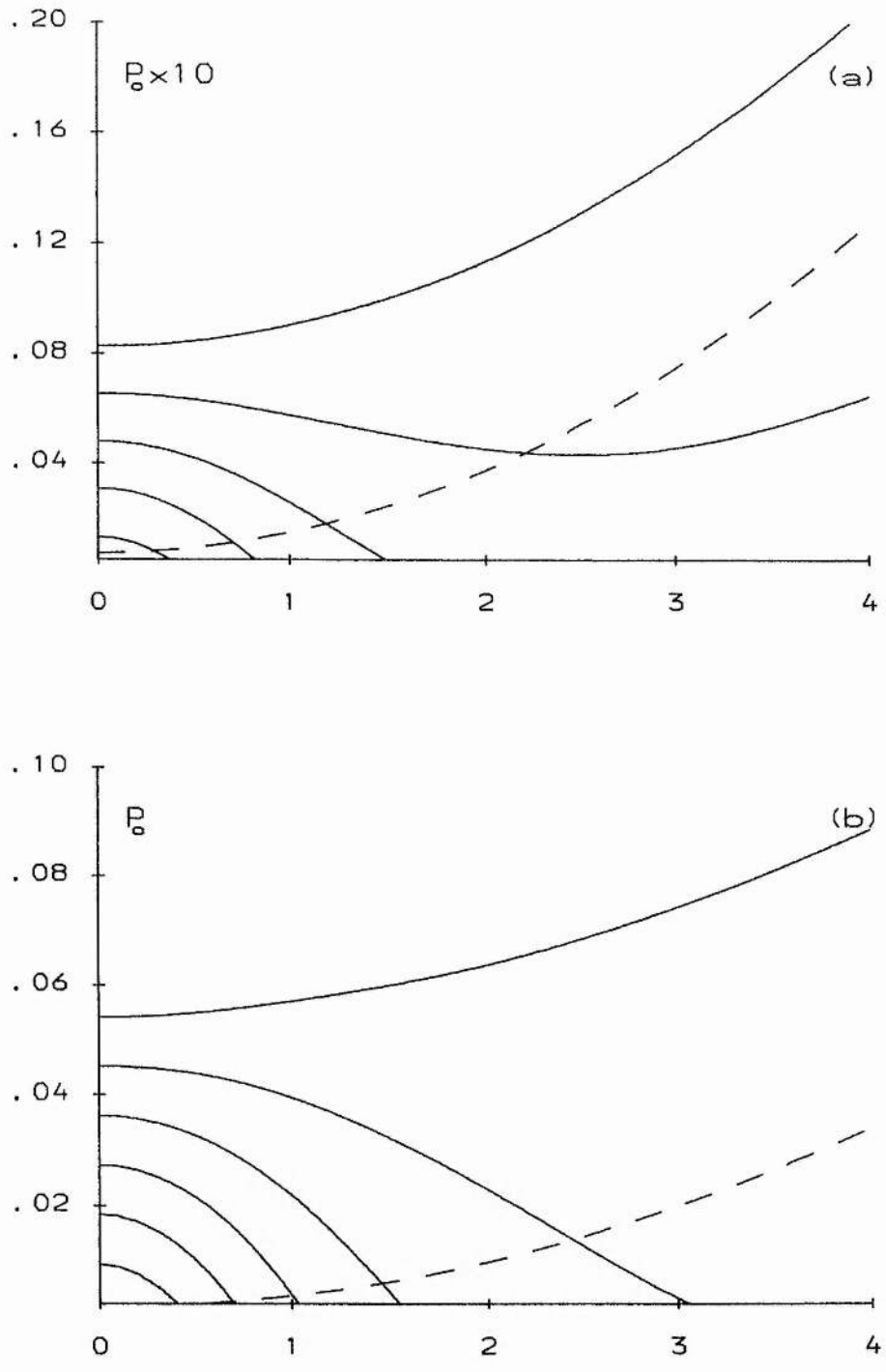

Fig. 4.8. Stability diagram for the equilibrium (4.3.4)–(4.3.5) when $x_{\text{prom}} = 0.01$ and $\gamma = 5/3$ for (a) $H_{\text{cool}} = 0.00075$, and (b) $H_{\text{cool}} = 0.002$. Shown are contours of z_0 (see text), starting off at $z_0 = 0$ (upper curve) with consecutive increments of (a) 0.002, and (b) 0.01. The magnetic field has a central dip for equilibria above the dashed curve.

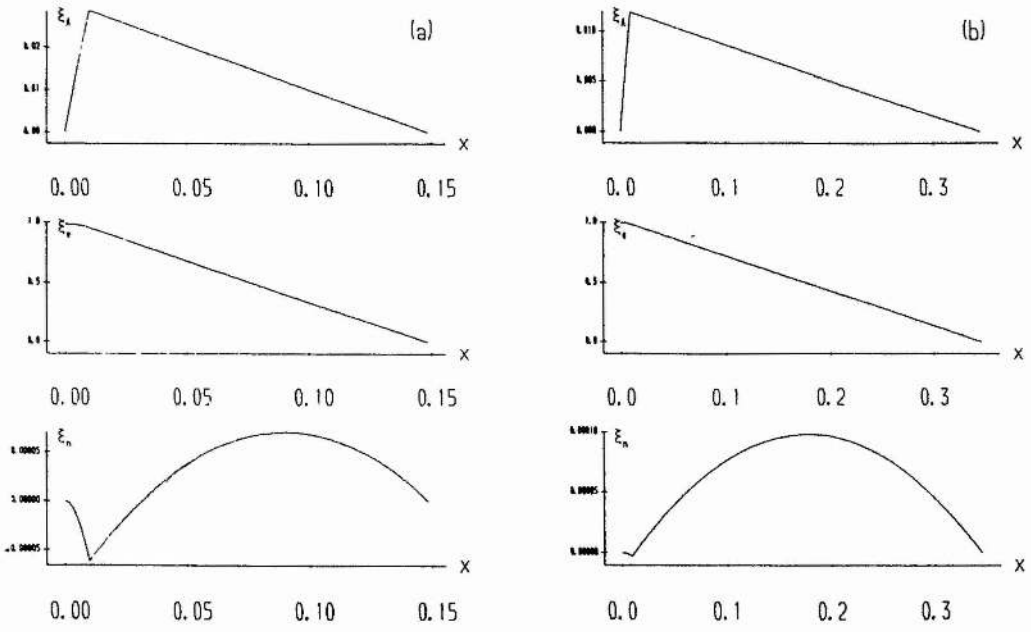

Fig. 4.9. Marginal displacements of the equilibrium (4.3.4) when $P_0 = 0.0025$, $\lambda = 0.1$, $x_{\text{prom}} = 0.01$, and $\gamma = 5/3$ for (a) $H_{\text{cool}} = 0.00075$, and (b) $H_{\text{cool}} = 0.002$.

The Hood and Anzer (1990) model is a natural extension of the Kippenhahn-Schlüter prominence configuration in that it takes account of the non-isothermal nature of a prominence-corona configuration. However, the fact that the equilibrium is laminated renders it prone to interchange instabilities. The only stabilising mechanism that discriminates beween the different field lines is the effect of line-tying, which is most efficient when the field lines are short. This restricts the height of the prominence to values that are well below those observed.

Many observers are convinced that a prominence cannot be modelled as a static structure in equilibrium (Hirayama, Leroy, Sara Martin, private communications). Videos made from filament observations show non-steady flows, continual changes in fibril structure, a four-dimensional "beast". Maybe theorists will have to resort to dynamical models, such as that by Kuijpers (1989), before they can begin to understand what remains one of the great enigmas of solar physics.

5

An Ideal MHD Stability Procedure for General Line-Tied Symmetric Equilibria

5.1. Introduction

Magnetic fields play an important role in many astrophysical objects and phenomena (for a discussion see, for instance, Chapter 1 of Parker, 1979). Magnetohydrodynamics provides a tool for modelling such diverse systems as large-scale coronal structures on the Sun, the global magnetic field of Ap stars, and the interstellar medium. It also enables one to study their stability.

To simplify the mathematical treatment the structure of interest is often assumed to be in static equilibrium and free from dissipation, thus satisfying a magnetohydrostatic equation and conservation of energy. Also, the equilibrium is frequently taken to be symmetric, i.e., all quantities depend on only two spatial coordinates q^1 and q^2, being independent of the third coordinate q^3 (Solov'ev, 1967). Therefore, the structures considered possess a helical symmetry, with translational and rotational invariance as limiting cases. This immediately follows from the existence of only six independent Killing vectors in a three-dimensional Euclidean space (Edenstrasser, 1980b; see also Woolley, 1990, who treats a more general equilibrium theory).

In order to construct equilibrium models one then has to find solutions of a generalised Grad-Shafranov equation, as derived by, for example, Edenstrasser (1980a). He presented a unified treatment of symmetric magnetostatic equilibria in a non-orthogonal coordinate system. In an earlier paper (Edenstrasser, 1978) he derived stability criteria for modes that possess the same symmetry as the equilibria considered. His formulation was confined to situations where gravitational forces are negligible, as in nuclear fusion theory. Hu (1987) included gravity, but restricted his analysis to orthogonal bases. He constructed an energy integral for general symmetric equilibria. For magnetic fields without a component in the ignorable direction, he rearranged δW in a form that reduces the problem of minimisation to one along individual field lines, similar to the approach in Chapter 3. This allowed him to prove that localised modes are the most dangerous perturbations, in that they have

the lowest thresholds for instability, a generalisation of previous results. In a subsequent paper (Hu, 1988) the method was tailored to fit a particular class of analytical solutions, for which specific stability criteria were derived. These were then applied to a family of large-scale axisymmetric magnetohydrostatic atmospheres.

In this Chapter the stability analysis technique of Chapter 3 is extended to non-isothermal non-constant gravity equilibria with an ignorable space variable in a general orthogonal coordinate system. A single formulation is developed which unifies previous work on structures with translational, rotational or helical symmetry. In Section 5.2, the equilibrium is presented and its energy integral is rearranged in the by now familiar form (1.4.1),

$$\delta W = \frac{1}{2\mu}(\mathcal{I} + \mathcal{J}),$$

where $\mathcal{I}$ does not contain derivatives of the plasma displacement across the magnetic field, and $\mathcal{J} > 0$. A necessary condition for stability to localised modes and a sufficient condition for stability to all modes satifying the rigid plate boundary conditions (1.4.2) are derived in Section 5.3. The only demand they make is the integration of a set of ordinary differential equations along the magnetic field lines. Section 5.4 presents a discussion.

5.2. Equilibrium and Energy integral

Consider ideal magnetohydrostatic equilibria governed by the force balance equation (1.2.8) and the ideal gas law (1.2.7). Introduce an orthogonal coordinate system q^1, q^2, q^3 with right-handed natural contravariant basis $\mathbf{g}^1, \mathbf{g}^2, \mathbf{g}^3$ where $\mathbf{g}^i = \nabla q^i$. The corresponding covariant basis $\mathbf{g}_1, \mathbf{g}_2, \mathbf{g}_3$ is found using the identity $\mathbf{g}_i = g_{ii}\mathbf{g}^i$ where $g_{ii} = 1/g^{ii}$ are the metric coefficients. Assume all equilibrium quantities and the metric coefficients are independent of q^3. This is equivalent to the requirement of helical symmetry in the problem (Solov'ev, 1967). Write the equilibrium magnetic field $\mathbf{B}(q^1, q^2)$ in the form

$$\begin{aligned} \mathbf{B} &= \mathbf{B}_p + \mathbf{B}_3, \\ \mathbf{B}_p &= \nabla A \times \mathbf{g}^3, \\ \mathbf{B}_3 &= B_3\mathbf{g}^3 = B^3\mathbf{g}_3, \end{aligned} \tag{5.2.1}$$

where A is the flux function and $B_3 = g_{33}B^3$ is the covariant field component in the ignorable direction. Provided the Jacobian

$$\frac{\partial(A, \phi)}{\partial(q^1, q^2)}$$

only vanishes at isolated points along a field line, A, ϕ may be used as independent variables instead of q^1, q^2. The magnetohydrostatic equation (1.2.8) can then be

decomposed into its components (Low, 1975a; Hu, 1987)

$$B_3 = B_3(A), \tag{5.2.2a}$$

$$\frac{\partial p}{\partial \phi} + \rho = 0, \tag{5.2.2b}$$

$$\nabla \cdot \left(\frac{\nabla A}{g_{33}} \right) + J(A, \phi) = 0, \tag{5.2.2c}$$

with

$$J(A, \phi) = \mu \frac{\partial p}{\partial A} + B^3 B_3' = \mu j^3, \tag{5.2.3a}$$

$$B_3' = \frac{dB_3}{dA} . \tag{5.2.3b}$$

Compare this with Equations (3.2.2) and (3.2.3) for an equilibrium with translational invariance. Note that $\partial/\partial A$ stands for the derivative with respect to A while ϕ is kept constant, and likewise $\partial/\partial\phi$ stands for the derivative with respect to ϕ while A is kept constant. Substituting the ideal gas law (1.2.7) into the equation (5.2.2b) for hydrostatic equilibrium along a field line yields the following expression for the pressure (Low, 1975a):

$$p = P(A)\, \mathrm{e}^{-D}, \qquad D = \int_{\phi_o}^{\phi} \frac{\tilde{\mu} \mathrm{d}\phi'}{\mathcal{R} T(A, \phi')} , \tag{5.2.4}$$

where $P(A)$ is determined by the photospheric pressure distribution. Finding solutions of the nonlinear elliptic differential equation (5.2.2c) that satisfy certain imposed boundary conditions is a highly complicated task. For a discussion see, for example, Low (1975a, 1980) and Edenstrasser (1980a).

To rewrite the perturbed potential energy integral δW in a form suitable for manipulation, the notation of Appendix A.4 is used. For displacements $\boldsymbol{\xi}$ satisfying the rigid plate boundary conditions (1.4.2), δW then reads (see Appendix F)

$$\delta W = \frac{1}{2\mu}(\mathcal{I} + \mathcal{J}), \tag{5.2.5}$$

where

$$\mathcal{I} = \int \Bigg\{ \frac{g^{33} B^2}{B_p^2} \left[\frac{\partial}{\partial s}(B_p^2 \tilde{\xi}_A) \right]^2 - \left(2J\Big(J + \frac{\partial B_p}{\partial a}\Big) + \mu \frac{\partial \rho}{\partial A} B_p \frac{\partial \phi}{\partial a} - B_3 B_3' B_p \frac{\partial g^{33}}{\partial a} \right) \xi_A^2 -$$

$$- \mu \rho \tilde{A} \tilde{\xi}_\phi^2 + \frac{\gamma \mu p}{B^2 + \gamma \mu p} \left[B\Big(B \frac{\partial \tilde{\xi}_\parallel}{\partial s} - \frac{\tilde{\xi}_\phi}{c_s^2} \Big) - \frac{1}{B} \Big(\Big(2\mu \frac{\partial p}{\partial A} B_p + \frac{\partial B^2}{\partial a} \Big) \xi_A + \frac{\partial B^2}{\partial n} \xi_n \Big) \right]^2 +$$

$$+ g_{33} \left[B_p \frac{\partial}{\partial s}(B^2 \tilde{\xi}_n) - \frac{B^3}{B B_p} \Big(2\mu \frac{\partial p}{\partial A} B_p + g^{33} \frac{\partial}{\partial a}\Big(g_{33} B^2 \Big) \Big) \xi_A \right]^2 \Bigg\} \, d\mathcal{V} \tag{5.2.6}$$

and

$$\mathcal{J} = \int \Bigg\{ (B^2 + \gamma \mu p) \left[B_p \frac{\partial \tilde{\xi}_A}{\partial a} + B B_p \frac{\partial \tilde{\xi}_n}{\partial n} - J \tilde{\xi}_A + \frac{\gamma \mu p}{B^2 + \gamma \mu p} \Big(B \frac{\partial \tilde{\xi}_\parallel}{\partial s} - \frac{\tilde{\xi}_\phi}{c_s^2} \Big) + \right.$$

$$\left. + \frac{1}{B^2 + \gamma \mu p} \Big(\Big(2\mu \frac{\partial p}{\partial A} B_p + \frac{\partial B^2}{\partial a} \Big) \xi_A + \frac{\partial B^2}{\partial n} \xi_n \Big) \right]^2 \Bigg\} \, d\mathcal{V}. \tag{5.2.7}$$

Note that, as opposed to an upper index 3, an upper index 2 stands for an exponent (except in q^2 and $\mathbf{g}^2$). For the sake of completeness the following definitions from Chapter 3 are repeated :

$$\tilde{A} = \left(\frac{\rho}{\gamma p} + \frac{1}{\rho}\frac{\partial \rho}{\partial \phi}\right),$$
$$\tilde{\xi}_\phi = \nabla\phi \cdot \boldsymbol{\xi}.$$

Setting $g_{33} = 1$ reduces this formulation of δW to Equations (3.2.4)–(3.2.6) for equilibria with a translational invariance described in Cartesian geometry. Axisymmetry is often expressed in cylindrical or spherical polar coordinates, for which $g_{33} = r^2$ and $r^2 \sin^2\theta$, respectively.

5.3. Stability Equations

5.3.1. Necessary Conditions for Stability

As in Chapter 3, consider perturbations with wavenumbers $k_\perp \gg k_\parallel$ (Conner, Hastie, and Taylor, 1979; Hood, 1986a), i.e., take plasma displacements

$$\boldsymbol{\xi}(q^1, q^2, q^3) = \boldsymbol{\xi}(q^1, q^2) \cos mS, \tag{5.3.1}$$

with $m \gg 1$, $\mathbf{B} \cdot \nabla S = 0$, and $\cos mS$ is periodic in q^3. A simple solution for S is

$$S = q^3 - \int^s \left(\frac{B^3}{B}\right)_{\text{A=const.}} ds. \tag{5.3.2}$$

The lower boundary of the integral has to be chosen such that it minimises the perturbed potential energy integral (Conner, Hastie, and Taylor, 1979). Expanding the amplitude factor $\boldsymbol{\xi}(q^1, q^2)$ in inverse powers of m and defining the variables

$$y_1 = B_p^2 \tilde{\xi}_A,$$
$$y_2 = \mathrm{e}^{-D/\gamma}\tilde{\xi}_\parallel,$$

with D from Equation (5.2.4), one gets for the leading order contribution to δW in the ballooning ordering

$$\begin{aligned}
\delta W_{\text{ball}} = \frac{1}{2\mu}\int d\mathcal{V}\, \cos^2 mS \Bigg\{ & \frac{g^{33}B^2}{B_p^2}\left[\frac{\partial y_1}{\partial s}\right]^2 - \mu\rho\tilde{A}\tilde{\xi}_\phi^2 - \\
& - \left(2J\left(J + \frac{\partial B_p}{\partial a}\right) + \mu\frac{\partial \rho}{\partial A}B_p\frac{\partial \phi}{\partial a} - B_3 B_3' B_p \frac{\partial g^{33}}{\partial a}\right)\frac{y_1^2}{B_p^2} + \\
& + \frac{\gamma\mu p}{B^2 + \gamma\mu p}\left[B\left(\mathrm{e}^{D/\gamma}B\frac{\partial y_2}{\partial s} - \frac{1}{c_s^2}\left(\frac{\partial \phi}{\partial a} + \frac{\nabla A \cdot \nabla S}{g_{33}B}\frac{\partial \phi}{\partial n}\right)\frac{y_1}{B_p}\right) - \right. \\
& \left. - \frac{1}{B}\left(2\mu\frac{\partial p}{\partial A}B_p + \frac{\partial B^2}{\partial a} + \frac{\nabla A \cdot \nabla S}{g_{33}B}\frac{\partial B^2}{\partial n}\right)\frac{y_1}{B_p}\right]^2 + \\
& + g_{33}\left[B_p\frac{\partial}{\partial s}\left(\frac{\nabla A \cdot \nabla S}{g_{33}B_p^2}y_1\right) - \frac{B^3}{BB_p^2}\left(2\mu\frac{\partial p}{\partial A}B_p + g^{33}\frac{\partial}{\partial a}\left(g_{33}B^2\right)\right)y_1\right]^2\Bigg\}.
\end{aligned} \tag{5.3.3}$$

This expression for δW_{ball} reduces to Equation (3.3.4) when $g_{33} = 1$. The minimisation of this integral, subject to the normalising condition

$$\frac{1}{2\mu}\int g^{33} f^2 \xi_A^2 \, d\mathcal{V} = \text{constant}, \tag{5.3.4}$$

where f^2 is a strictly positive function, produces a set of two second order Euler-Lagrange equations containing a Lagrange multiplier Λ that has the same sign as δW. As in Chapter 3, this set can be transformed to a system of four coupled first order homogeneous ordinary differential equations plus an auxiliary equation, suitable for numerical computation :

$$\begin{aligned}
\frac{\partial y_1}{\partial s} &= \left(\frac{B}{g_{33}B_p^2} + \frac{g_{33}B_p^2}{B}y_5^2\right)^{-1} y_3, \\
\frac{\partial \tilde{y}_2}{\partial s} &= \frac{1}{B}\left[\frac{B^2+\gamma\mu p}{\gamma\mu p B^2}\tilde{y}_4 + \left(L_1 + \frac{L_2}{c_s^2}\right)\tilde{y}_1\right] + \frac{1}{c_s^2}\frac{\partial \phi}{\partial s}\tilde{y}_2, \\
\frac{\partial y_3}{\partial s} &= \frac{-1}{BB_p}\left[\left(\Lambda g^{33} f^2 + \mu\frac{\partial p}{\partial A}B_p L_1 + \mu\frac{\partial \rho}{\partial A}B_p L_2\right)\tilde{y}_1 + L_2\tilde{y}_\phi + \left(L_1 + \frac{L_2}{c_s^2}\right)\tilde{y}_4\right], \\
\frac{\partial \tilde{y}_4}{\partial s} &= -\frac{\partial \phi}{\partial s}\tilde{y}_\phi - \frac{1}{c_s^2}\frac{\partial \phi}{\partial s}\tilde{y}_4, \\
\frac{\partial y_5}{\partial s} &= \frac{1}{B}\left[-g^{33}\frac{dB_3}{dA} + \frac{B^3}{B_p^2}\left(J + 2\frac{\partial B_p}{\partial a} - g_{33}B_p\frac{\partial g^{33}}{\partial a}\right)\right],
\end{aligned} \tag{5.3.5}$$

where

$$\begin{aligned}
\tilde{y}_1 &= \frac{y_1}{B_p}, \qquad \tilde{y}_2 = \tilde{\xi}_\parallel, \qquad y_5 = \frac{\nabla A \cdot \nabla S}{g_{33}B_p^2}, \\
\tilde{y}_\phi &= \mu\rho\tilde{A}\tilde{\xi}_\phi = \mu\rho\tilde{A}\left(L_2\tilde{y}_1 + B\frac{\partial \phi}{\partial s}\tilde{y}_2\right), \\
L_1 &= \frac{1}{B^2}\left(2\mu\frac{\partial p}{\partial A}B_p + \frac{\partial B^2}{\partial a} + \frac{B_3 B_p}{B}\frac{\partial B^2}{\partial s}y_5\right), \\
L_2 &= \frac{\partial \phi}{\partial a} + \frac{B_3 B_p}{B}\frac{\partial \phi}{\partial s}y_5.
\end{aligned}$$

A derivation of the auxiliary equation for y_5 is given in Appendix G. Equations (5.3.5) reduce to Equations (3.3.8) and (4.2.16) in Cartesian geometry. Putting $\Lambda = 0$, this system yields the condition for marginal stability to localised modes satisfying the rigid plate boundary conditions (1.4.2).

5.3.2. Sufficient Conditions for Stability

Once more, the non-negative $\mathcal{J}$-part of δW is neglected and $\delta W_{\mathcal{I}}$ is minimised with respect to the variables

$$\begin{aligned}
y_1 &= B_p^2\tilde{\xi}_A, \\
\tilde{y}_2 &= \tilde{\xi}_\parallel, \\
y_5 &= B^2\tilde{\xi}_n,
\end{aligned}$$

subject to the same constraint (5.3.4). This results in three second order Euler-Lagrange equations that can be rearranged into a system of six coupled first order homogeneous ordinary differential equations, suitable for numerical computation :

$$\begin{aligned}
\frac{\partial y_1}{\partial s} &= \frac{g_{33}B_p^2}{B}y_3,\\
\frac{\partial \tilde{y}_2}{\partial s} &= \frac{1}{B}\left[\frac{B^2+\gamma\mu p}{\gamma\mu p B^2}\tilde{y}_4 + G_1\tilde{y}_1 + \frac{B_3}{B}G_2 y_5\right] + \frac{1}{c_s^2}\frac{\partial\phi}{\partial s}\tilde{y}_2,\\
\frac{\partial y_3}{\partial s} &= \frac{-1}{BB_p}\left[\left(\Lambda g^{33}f^2 + \tilde{V}\right)\tilde{y}_1 + \frac{\partial\phi}{\partial a}\tilde{y}_\phi + G_1\tilde{y}_4 + B^3G_3\tilde{y}_6\right],\\
\frac{\partial \tilde{y}_4}{\partial s} &= -\frac{\partial\phi}{\partial s}\tilde{y}_\phi - \frac{1}{c_s^2}\frac{\partial\phi}{\partial s}\tilde{y}_4,\\
\frac{\partial y_5}{\partial s} &= g^{33}B\tilde{y}_6 + \frac{B^3}{BB_p^2}G_3\tilde{y}_1,\\
\frac{\partial y_6}{\partial s} &= -\frac{B_3}{B^2}\left[\frac{\partial\phi}{\partial s}\tilde{y}_\phi + G_2\tilde{y}_4\right],
\end{aligned} \tag{5.3.6}$$

where

$$\begin{aligned}
&\tilde{y}_1 = \frac{y_1}{B_p}\,, \qquad \tilde{y}_6 = \frac{y_6}{B_p^2}\,,\\
&\tilde{y}_\phi = \mu\rho\tilde{A}\tilde{\xi}_\phi = \mu\rho\tilde{A}\left(\frac{\partial\phi}{\partial a}\tilde{y}_1 + B\frac{\partial\phi}{\partial s}\tilde{y}_2 + \frac{\partial\phi}{\partial s}\frac{B_3}{B}y_5\right),\\
&\tilde{V} = -B_p^2V = 2J\Big(J + \frac{\partial B_p}{\partial a}\Big) + \mu\frac{\partial\rho}{\partial A}B_p\frac{\partial\phi}{\partial a} - B_3B_3'B_p\frac{\partial g^{33}}{\partial a}\,,\\
&G_1 = \frac{1}{B^2}\left(2\mu\frac{\partial p}{\partial A}B_p + \frac{\partial B^2}{\partial a}\right) + \frac{1}{c_s^2}\frac{\partial\phi}{\partial a}\,,\\
&G_2 = \frac{1}{B^2}\frac{\partial B^2}{\partial s} + \frac{1}{c_s^2}\frac{\partial\phi}{\partial s}\,,\\
&G_3 = 2\mu\frac{\partial p}{\partial A}B_p + g^{33}\frac{\partial}{\partial a}\big(g_{33}B^2\big).
\end{aligned}$$

Equations (5.3.6) reduce to Equations (3.3.11) and (4.2.17) in Cartesian geometry. The system proves definite stability to all allowable perturbations satisfying the boundary conditions (1.4.2) when $\Lambda > 0$ on every field line. For a field that has no component in the ignorable direction, i.e., $B_3 = 0$, the systems (5.3.5) and (5.3.6) are equivalent and hence one obtains the necessary and sufficient conditions for stability by solving either of them (cf. Hu, 1987).

5.4. Discussion

We have extended the procedure for investigating the stability of line-tied MHD equilibria with a translational invariance, as presented in Chapter 3, to equilibria with a general symmetry. Taking a formulation of the energy integral by Hu (1987)

as a starting point, a new expression for δW is given in Equations (5.2.5)–(5.2.7). From this it is readily seen that an equilibrium is obviously stable if

$$\tilde{V} \equiv 2J\Big(J + \frac{\partial B_p}{\partial a}\Big) + \mu \frac{\partial \rho}{\partial A} B_p \frac{\partial \phi}{\partial a} - B_3 B_3' B_p \frac{\partial g^{33}}{\partial a} \leq 0 \qquad (5.4.1a)$$

and

$$\tilde{A} \equiv \frac{\rho}{\gamma p} + \frac{1}{\rho} \frac{\partial \rho}{\partial \phi} \leq 0 \qquad (5.4.1b)$$

everywhere. The former condition inhibits current and pressure driven instabilities. The latter is the Schwarzschild criterion for stability against convection (Schwarzschild, 1906; see also Schwarzschild, 1958, Chapter 2), which is always satisfied for isothermal equilibria. If both inequalities do not hold everywhere, and this happens more often than not, one must proceed further. The form (5.2.5) of δW allows for two simple lines of approach.

Firstly, inserting a trial function (5.3.1) results in the ballooning integral (5.3.3) that governs the plasma stability to localised modes. One can then integrate the associated system (5.3.5) of ordinary differential equations that minimises this integral. Alternatively one can select an appropriate form for the amplitude factor $\boldsymbol{\xi}(q^1, q^2)$, that has to vanish at the photosphere, and derive a generalised Mercier criterion (Mercier, 1960), including gravity and line-tying (cf. the extended Suydam criteria in Chapter 2).

Secondly, neglecting the non-negative $\mathcal{J}$-part of δW produces the system (5.3.6) of ordinary differential equations that can prove definite stability to all allowable perturbations. This could, for instance, be a useful means for substantiating or falsifying the conjecture by Cargill, Hood, and Migliuolo (1986) and Hood and Anzer (1987) that line-tied force-free arcades with a magnetic axis on or below the photosphere are stable.

Note that the developed procedure is also applicable to force-free equilibria (cf. Chapter 3), and in the absence of gravity. In the latter case the pressure p becomes a function of A alone (hence, $D \equiv 0$ in Equation (5.2.4)), and all terms involving the external gravitational potential ϕ disappear from the equations.

The combined power of the two stability conditions thus obtained has proved successful in the investigations carried out in Chapters 2–4. The systems (5.3.5) and (5.3.6) can easily be implemented in a numerical code for computing 2-D equilibria, such as that developed by Fiedler and Cally (1990), and provide a straightforward test for stability. The results of such tests could help in finding answers to important questions such as (i) can shear (i.e., the generation of a component of the magnetic field in the ignorable direction due to footpoint motions) destabilise an arcade, as observations seem to predict (Hagyard *et al.*, 1986); (ii) what is the effect of gravity

on the stability of an equilibrium (Low, 1985b; Melville, Hood, and Priest, 1987); (iii) can coronal mass ejections (CME's) be explained as coronal structures that become unstable and erupt (Low, 1981b, 1984b; Wolfson, 1982); (iv) how much energy can be stored in coronal loops (Chiueh and Zweibel, 1989) and arcades (Klimchuk, Sturrock, and Yang, 1988); and (v) does a field go unstable before a point of non-equilibrium can be reached (Birn, Goldstein, and Schindler, 1978; Birn and Schindler, 1981).

The stability procedure developed in this Chapter can be applied to a wide variety of situations : (i) more realistic prominence models, including gravity, a predominant longitudinal field and a varying temperature profile (Low, 1975b); (ii) sheared arcades (Melville, Hood, and Priest, 1984); (iii) twisted axisymmetric loops (Lothian and Hood, 1989; Browning and Hood, 1989); (iv) sunspot models (Barnes and Sturrock, 1972; Bogdan, 1985); (v) large-scale coronal structures (Hundhausen, Hundhausen, and Zweibel, 1981; Low, 1984b); and (vi) helically twisted hydromagnetic fields (Tsinganos, 1982). Replacing the rigid plate boundary conditions (1.4.2) appropriate for the Sun by periodic boundary conditions, one can extend the investigations of stellar magnetic fields (Tayler, 1973; Van Assche, Tayler, and Goossens, 1982) and the interstellar medium (Asseo *et al.*, 1978, 1980) to include a third component of the magnetic field. It would also allow one to test the stability of tokamak (no line-tied field lines) and spheromak (part of the field lines are line-tied to the plasma gun) equilibria in nuclear fusion research (see, for instance, Taylor, 1986).

In summary, a tractable method for investigating the linear ideal MHD stability of a wide range of equilibria has been presented. The energy integral and stability equations were derived, and their applications were discussed.

6

Stability of Line-Tied 1-D Coronal Loops : Significance of the Extended Suydam Criterion

6.1. Introduction

Flux tubes, suitably called coronal loops in the corona, have aroused a lot of interest from solar physicists, mainly because they form, together with current sheets, the building blocks of the Sun's magnetic field. Since their observed lifetime is much longer than the typical dynamical time scale, they are often regarded as being in or near static mechanical and thermodynamical equilibrium. An appropriate mathematical model is then constructed by solving the corresponding magnetohydrostatic force and energy balance equations. Usually they are modelled as straight plasma cylinders because the observed aspect ratio L/a, where L is the loop length and a is a characteristic transverse length scale, is large enough for toroidal coupling to be neglected. Constructing equilibria is often a complicated problem in itself (for an introduction to the subject, see, for instance, Chapters 3 and 6 of Priest, 1982). It is, however, only half the story, for if small disturbances, which inevitably occur on a seething Sun, lead to a gradual departure of the equilibrium from its initial state then the model is unstable. Hence it is important to study the effect of small perturbations on an equilibrium.

Infinitely long 1-D cylinders are prone to instabilities (see, for instance, Kruskal and Schwarzschild, 1954; Hain and Lüst, 1958; Voslamber and Callebaut, 1962; Anzer, 1968; Shafranov, 1970). This tendency can be neutralised, or at least weakened, by a variety of mechanisms : axial field reversals (Robinson, 1971), surrounding force-free fields (Goedbloed, 1971b; Goedbloed and Schuurman, 1972) or potential fields (Chiuderi *et al.*, 1980; Chiuderi and Einaudi, 1981), special pressure profiles (Giachetti, Van Hoven, and Chiuderi, 1977), neighbouring loops (Goedbloed, 1990), or line-tying (Raadu, 1972; Hood and Priest, 1979). The latter mechanism, caused by the inertial anchoring of coronal field lines in the dense photosphere, probably offers the best scope for explaining the observed longevity of coronal loops.

A careful study of the different terms in the perturbed potential energy integral

provides some insight into the effects that tend to drive instabilities and those that tend to be stabilising. The change in potential energy due to a coronal disturbance, $\boldsymbol{\xi}$, can be written in the following physically illuminating way (Bateman, 1978, p. 97) :

$$\delta W = \frac{1}{2}\int_{\text{plasma}} d\mathcal{V}\left\{\frac{1}{\mu}|\mathbf{B}_\perp^1|^2 + \mu\left|\frac{1}{\mu}\mathbf{B}_\parallel^1 - \frac{\boldsymbol{\xi}\cdot\nabla p}{B^2}\mathbf{B}\right|^2 + \gamma p|\nabla\cdot\boldsymbol{\xi}|^2 + \right. \\ \left. + \frac{\mathbf{j}\cdot\mathbf{B}}{B^2}\mathbf{B}\times\boldsymbol{\xi}\cdot\mathbf{B}^1 - 2\boldsymbol{\xi}\cdot\nabla p\,\boldsymbol{\xi}\cdot\boldsymbol{\kappa}\right\}, \tag{6.1.1}$$

where the subscripts $_\perp$ and $_\parallel$ refer to vectors perpendicular and parallel to the equilibrium magnetic field, respectively. The first three terms are positive and thus stabilising. They represent the effect of bending and compressing the field, causing Alfvén and magneto-acoustic waves to propagate. The last two terms are potentially destabilising. A decrease in the parallel current, $(\mathbf{j}\cdot\mathbf{B})\mathbf{B}/B^2$, may lead to a *kink mode*, while an unfavourable interplay of the pressure gradient, ∇p, and the field line curvature $\boldsymbol{\kappa} = [(\mathbf{B}\cdot\nabla)\mathbf{B}]/B^2$, can drive *interchange modes* (for a classification of instabilities, see, for instance, Freidberg, 1982). Gravity is assumed to be unimportant here.

It is well known from fusion research that the two most dangerous ideal MHD instabilities are precisely the helical kink modes and the interchange (or, in fusion terminology, *ballooning*) modes. The kink mode is a current driven global instability distorting the axis of the coronal loop into what resembles a helix. It might well be nonlinearly unstable and will then destroy the equilibrium. An instructive geometrical explanation of these modes can be found in Bateman (1978, p. 107). Its impact on coronal loop stability has been widely investigated (Hood and Priest, 1981; Einaudi and Van Hoven, 1983; Craig, McClymont, and Sneyd, 1988; Foote and Craig, 1990; Velli, Einaudi, and Hood, 1990b; Mikić, Schnack, and Van Hoven, 1990, and references therein). Interchange modes, on the other hand, are very localised about a flux surface, producing ripples that follow the field lines. They are likely to be sensitive to hitherto neglected physical effects such as finite Larmor radius, resistivity and viscosity. Also, they might well saturate at an early stage, leaving the equilibrium relatively untouched. They have been studied in a solar context by Hood (1986a), among others.

In a 1-D cylinder, each perturbation $\boldsymbol{\xi}$ can be decomposed into its Fourier components as

$$\boldsymbol{\xi}(\mathbf{r},t) = \sum_m\sum_n \boldsymbol{\xi}(r)\exp\left[i(m\theta + \frac{2n\pi}{L}z - \omega t)\right], \tag{6.1.2}$$

where m, n, ω are the poloidal and axial mode number and the angular frequency (imaginary in the case of an instability, where $-i\omega$ is referred to as the growth rate) respectively. Different instabilities are then characterised by their poloidal mode

number : the $m = 0$ sausage mode, $m = 1$ kink mode, $m \geq 2$ flute modes, and $m \gg 1$ localised interchange modes. When end effects due to line-tying are neglected, the stability analysis is one-dimensional and purely analytical stability criteria, involving equilibrium profiles only, can be derived. For a plasma column of length L to be stable to low-m modes, one needs

$$nq > m, \tag{6.1.3}$$

where $q(r) = 2\pi r B_z / L B_\theta$ has to be evaluated at the outer radius (see, for instance, Lowder and Thomassen, 1973, who also present a clear geometrical and physical picture of these modes). When $m = n = 1$, this is known as the *Kruskal-Shafranov criterion*. The condition for stability of a loop to localised interchange modes is

$$\frac{B_z^2}{4}\left(\frac{q'}{q}\right)^2 + \frac{2\mu p'}{r} > 0. \tag{6.1.4}$$

This is referred to as *Suydam's criterion* (Suydam, 1958).

Since much is known about these two types of modes, it is surprising that their relationship has hardly been touched upon in the astrophysical literature. It has been established that there is a smooth transition from kink modes to localised interchange modes as the Suydam criterion becomes satisfied by varying the wave vector (Freidberg, 1970), and that the most dangerous modes go from kinks to interchanges as $|\nabla p|$ increases (Goedbloed and Hagebeuk, 1972). In toroidal equilibria, stability thresholds for low-m global modes were shown to blend into those of ballooning modes as m increases (Dewar *et al.*, 1981). These are however results from fusion research, where configurations, boundary conditions, and parameter regimes are different from the ones applicable to the corona. The first aim of our present investigation is to discover how, for coronal loops, the stability properties of kink modes transform into these of localised modes as the poloidal mode number m is increased.

From the relative weakness of interchange modes one could be drawn to the conclusion that an equilibrium need not be tested for stability to this kind of perturbation. The contrary was proved by Goedbloed and Sakanaka (1974) for an infinite 1-D cylinder. They showed that violation of Suydam's criterion implies instability of the global kink mode. It is the second aim of this investigation to demonstrate that this powerful result applies equally well, *mutatis mutandis*, to (near force-free) coronal loops. For these finite-length plasma cylinders, the anchoring of the field lines in the dense photosphere is simulated by line-tying boundary conditions in the axial direction. In linear ideal MHD, neglecting dissipative effects and assuming adiabatic disturbances, the rigid plate conditions should be used (Rosner, Low, and Holzer, 1986; Cargill, Hood, and Migliuolo, 1986; Hood, 1986b; Hood, Van der Lin-

den, and Goosens, 1989). They impose the constraint that the coronal displacement $\boldsymbol{\xi}$ vanishes at the photosphere, and thereby render the stability analysis intrinsically two-dimensional.

In Section 6.2 a general method for investigating low-m modes, developed by Velli, Einaudi, and Hood (1990a) and based on a normal mode analysis, is presented. The plasma perturbation in the linearised equation of motion is expanded in a truncated Fourier series in the poloidal and axial directions. The resulting system of ordinary differential equations for the radial displacement can then be solved as an eigenvalue problem for the critical loop length or the growth rate. In Section 6.3 the method is applied to two classes of equilibria and the results are compared with those of Chapter 2 for the localised interchange modes. This juxtaposition will reveal the significance of the extended Suydam criterion. The Chapter is concluded with a summary in Section 6.4.

6.2. Normal Mode Analysis

A coronal loop is modelled as a cylindrically symmetric current-carrying plasma column of constant density $\rho = \rho_0$, rooted in the much denser photosphere at $z = -L/2$ and $z = L/2$. In cylindrical coordinates r, θ, z the equilibrium magnetic field and plasma pressure

$$\begin{aligned} \mathbf{B} &= (0, B_\theta(r), B_z(r)), \\ p &= p(r), \end{aligned} \tag{6.2.1}$$

satisfy the magnetohydrostatic equation

$$\frac{d}{dr}\left(p + \frac{B^2}{2\mu}\right) = -\frac{B_\theta^2}{\mu r}, \tag{6.2.2}$$

where gravity has been assumed negligible. Line-tying is simulated by imposing the rigid plate boundary conditions (1.4.2) on the coronal displacement $\boldsymbol{\xi}$ at $z = \pm L/2$. Making use of the notation of Appendix A.1, the perturbed and linearised equation of motion (1.3.9) with $\nabla\phi = \mathbf{0}$ can be decomposed into its components

$$\begin{aligned} -\mu\rho\omega^2\xi_r = {} & B^2\frac{\partial^2\xi_r}{\partial s^2} + \frac{\partial}{\partial r}\left(\frac{B^2}{r}\frac{\partial}{\partial r}(r\xi_r)\right) - \frac{\partial}{\partial r}\left(\frac{B_\theta^2}{r^2}\right) r\xi_r + \\ & + \frac{\partial}{\partial r}\left(B\frac{\partial\zeta}{\partial n}\right) + 2\frac{B_\theta}{r}\frac{\partial\zeta}{\partial z} + \frac{\partial}{\partial r}(\gamma\mu p\nabla\cdot\boldsymbol{\xi}), \end{aligned} \tag{6.2.3a}$$

$$-\mu\rho\omega^2\xi_\parallel = B\frac{\partial}{\partial s}(\gamma\mu p\nabla\cdot\boldsymbol{\xi}), \tag{6.2.3b}$$

$$\begin{aligned} -\mu\rho\omega^2\zeta = {} & B^2\frac{\partial^2\zeta}{\partial s^2} + B^2\frac{\partial^2\zeta}{\partial n^2} + \frac{B^3}{r}\frac{\partial}{\partial n}\left(\frac{\partial}{\partial r}(r\xi_r)\right) - \\ & - 2\frac{B^2 B_\theta}{r}\frac{\partial\xi_r}{\partial z} + B\frac{\partial}{\partial n}(\gamma\mu p\nabla\cdot\boldsymbol{\xi}), \end{aligned} \tag{6.2.3c}$$

where a normal mode time dependence, $e^{-i\omega t}$, has been assumed.

To cast Equations (6.2.3) with axial boundary conditions (1.4.2) in the form of an eigenvalue problem, the displacement $\boldsymbol{\xi}$ is expanded in a Fourier series in the poloidal and axial directions (see, for instance, Einaudi and Van Hoven, 1981, 1983, and Velli, Einaudi, and Hood, 1990a, for an extensive discussion). So,

$$\begin{aligned}
\xi_r(\mathbf{r}) &= \mathrm{Re} \sum_{m=-\infty}^{+\infty} \sum_{n=-\infty}^{+\infty} \xi_{nm}(r) \exp[i(m\theta + n\pi(\frac{2z}{L}+1))], \\
\xi_\parallel(\mathbf{r}) &= \mathrm{Re} \sum_{m=-\infty}^{+\infty} \sum_{n=-\infty}^{+\infty} \eta_{nm}(r) \exp[i(m\theta + n\pi(\frac{2z}{L}+1)+\frac{\pi}{2})], \\
\zeta(\mathbf{r}) &= \mathrm{Re} \sum_{m=-\infty}^{+\infty} \sum_{n=-\infty}^{+\infty} \zeta_{nm}(r) \exp[i(m\theta + n\pi(\frac{2z}{L}+1)+\frac{\pi}{2})].
\end{aligned} \tag{6.2.4}$$

Phases have been chosen in such a way that the r-dependent amplitudes are real. The rigid plate conditions (1.4.2) then imply

$$\forall r, m : \sum_{n=-\infty}^{+\infty} \xi_{nm}(r) = 0, \tag{6.2.5a}$$

$$\forall r, m : \sum_{n=-\infty}^{+\infty} \eta_{nm}(r) = 0, \tag{6.2.5b}$$

$$\forall r, m : \sum_{n=-\infty}^{+\infty} \zeta_{nm}(r) = 0. \tag{6.2.5c}$$

These boundary conditions do not couple the harmonics in the poloidal coordinate, hence each value of m can be treated separately. However, Equations (6.2.5) cause coupling of the axial harmonics and this renders the stability analysis intrinsically two-dimensional, as opposed to the one-dimensional investigation of Newcomb (1960).

On multiplying the equations (6.2.3) by the appropriate phase factors and integrating in θ and z, unknown surface terms arise that allow the constraints (6.2.5) to be applied. An infinite set of coupled second order ordinary differential equations in the radial direction for the components ξ_{nm} (with m fixed) is then obtained. Truncation to N Fourier harmonics, ξ_i, results in a system of $(N-1)$ differential equations that can be written in the form

$$(\mathcal{U}\mathbf{y}')' + \mathcal{V}\mathbf{y}' + \mathcal{W}\mathbf{y} = \mathbf{0}, \tag{6.2.6}$$

where $\mathbf{y}(r) = r(\xi_1, \ldots, \xi_{N-1})^{\mathrm{T}}$, $\mathcal{U}, \mathcal{V}, \mathcal{W}$ are $(N-1)\times(N-1)$ matrices, and a prime denotes differentiation with respect to r. The corresponding boundary conditions are

$$y_i = 0 \qquad \text{at} \quad r = 0 \quad \text{and} \quad r = \infty, \qquad i = 1, \ldots, N-1. \tag{6.2.7}$$

For full details, see Velli, Einaudi, and Hood (1990a), and Appendix H. Convergence of the solutions of the eigenvalue problem (6.2.6)–(6.2.7) as the order of truncation, N, is increased, has been studied in detail by Van der Linden, Goossens, and Kerner (1990). They showed that a convergence rate of at least $O(N^{-1})$ may be expected.

Convergence is ensured by physical arguments, as it is well known that high-n global modes are stable even without the effect of line-tying (see, for instance, Sneyd and Craig, 1989, and Craig *et al.*, 1990). At marginal stability (i.e., $\omega^2 = 0$), the system (6.2.6) is the counterpart of that obtained by Einaudi and Van Hoven (1983) through minimisation of the perturbed potential energy integral δW subject to a different set of axial boundary conditions.

6.3. Application to Two Classes of Loop Equilibria

6.3.1. Choice of the Equilibria

The equilibria selected for a stability analysis were the constant-twist Gold-Hoyle field (Gold and Hoyle, 1960),

$$B_\theta = B_0 \frac{\bar{r}}{1+\bar{r}^2}\,, \qquad B_z = B_0 \frac{\bar{\lambda}}{1+\bar{r}^2}\,, \qquad \mu p = B_0^2 \frac{1-\bar{\lambda}^2}{2\left(1+\bar{r}^2\right)^2}\,, \tag{E1}$$

and a variable-twist field (Anzer, 1968),

$$\begin{aligned} B_\theta = B_0 \bar{r} \mathrm{e}^{-\bar{r}/2}, \qquad B_z = B_0 \bar{\lambda} [\sigma + (2 + 2\bar{r} - \bar{r}^2)\mathrm{e}^{-\bar{r}}]^{1/2}, \\ \mu p = B_0^2 \frac{1-\bar{\lambda}^2}{2} [\sigma + (2 + 2\bar{r} - \bar{r}^2)\mathrm{e}^{-\bar{r}}], \end{aligned} \tag{E3}$$

where $\bar{r} = r/a$ and $\bar{\lambda} = \lambda/a$. B_0 and a are the characteristic equilibrium magnetic field strength and length scale, respectively. Both equilibria were described in Subsection 2.2.3. Recall that $\bar{\lambda}$ governs the departure from a force-free state, with $\bar{\lambda} = 1$ implying a purely force-free loop, while σ accounts for a constant component in the axial field.

The first field, E1, was selected because it had previously been investigated by a number of authors using different techniques, and hence provided an excellent test for our numerical code. The force-free case was studied by Hood and Priest (1981) using a finite difference scheme, by Einaudi and Van Hoven (1983) who Fourier decomposed the perturbation in the energy integral, and by Foote and Craig (1990) by integrating a 'fictitious' force equation in time. They all found a critical loop length $L/a \approx 2.5\pi$ for the $m = 1$ kink mode. The non-force-free case was investigated in Subsection 2.2.3, where a sufficient condition for stability and the instability region for localised modes ($m = \infty$) were calculated. However, the field is somewhat pathological, as pointed out by, for example, Goedbloed (1971c). Moreover, coronal loops are not expected to have a constant twist profile, since this would require increasingly large footpoint motions as one moves away from the axis. Hence, it might be dangerous to extrapolate stability results for this particular equilibrium, and therefore a second field, E3, was selected for analysis. It has a much more realistic twist profile,

and was also investigated in Subsection 2.2.3. Throughout this Section, the value of σ is fixed to 0.15. Results for these two fields should give a fairly good indication of the general stability properties of coronal loops.

6.3.2. Numerical Method

To solve the system (6.2.6) with boundary conditions (6.2.7) we proceeded as follows. A value for the poloidal mode number m and the equilibrium parameters $\bar{\lambda}$ and σ was chosen, while $\gamma = 5/3$ throughout. One could look for marginal stability, or the growth rates. In the first case, ω^2 was set equal to zero, and the eigenvalue of the system (6.2.6) was the critical loop length $\bar{L}_{\rm crit}$, i.e., the shortest length for which the loop becomes unstable. In the second case, the loop length was fixed, and the eigenvalue, Γ, was a measure for the growth rate, namely

$$\Gamma = \frac{1}{2}\log_{10}\left(L^2\frac{\mu\rho_0}{B_0^2}(-\omega^2)\right). \tag{6.3.1}$$

Note that the growth rate was normalised to the Alfvén travel time *along* the loop, as this is the time needed for the field to communicate the existence of the photospheric boundaries (see also Velli, Einaudi, and Hood, 1990b, and Mikić, Schnack, and Van Hoven, 1990).

Because the axis $r = 0$ is a regular singular point of the system (6.2.6), the left boundary of the integration interval was taken to be $\bar{r} = \epsilon$, and the first boundary condition was replaced by (see, for instance, Hood and Priest, 1981)

$$\bar{r} \to 0 : \xi_r \propto \begin{cases} \bar{r}^{|m|} & m \neq 0, \\ \bar{r} & m = 0. \end{cases} \tag{6.3.2}$$

Since integration to infinity is impractical, the second boundary condition was replaced by the requirement that the eigenfunctions vanish at a finite radius $\bar{r}_f$. This radius was chosen so far out that the eigenvalue did not strongly depend on its actual position. To speed up convergence, a central axial wavenumber $\bar{k}_0 = \frac{2n_0\pi}{L}$ was selected and sidebands at $\bar{k}_0 \pm \frac{2\pi}{L}, \bar{k}_0 \pm \frac{4\pi}{L}, \ldots$ were added. Note that n_0 need not be an integer, as it simply introduces a factor $\exp[in_0\pi(\frac{2z}{L}+1)]$ in the expression (6.2.4) for $\boldsymbol{\xi}$. A good initial guess for $\bar{k}_0$ turned out to be the most unstable axial wavenumber for the infinite loop. This allowed for a large contribution of modes that are unstable in the infinite length case without having to add too many stable modes. With this judicious choice of harmonics a convergence rate of order $N^{-1.4}$ was obtained and five harmonics normally yielded a satisfactory result. Note that the pairs $(m, \bar{k}_0)$ and $(-m, -\bar{k}_0)$ are equivalent, so that only positive m need to be investigated.

Two different numerical codes were employed to solve the two point boundary value problem (6.3.6)–(6.3.7). Originally, it was integrated using the standard Lentini-Pereyra method (Lentini and Pereyra, 1977), an implementation of which is

readily available (NAG library routine D02RAF). Comments on the code and illustrative examples can be found in, for example, Kirby (1985). It makes use of finite differences on a variably spaced mesh, which allows the resolution of steep gradients. Because the solution is sought globally, a global error estimate is obtained. This enables one to place considerable confidence in the final solution. Its accuracy is increased using a deferred correction technique, in which a Newton iteration on the truncation error of the finite difference approximation is performed. Yet, the numerous internal tests for convergence render this reliable routine rather slow compared to, for instance, a shoot-and-match method. Moreover, in the non-force-free case, it often finds difficulty in converging unless accurate initial guesses for the eigenfunctions are supplied. Nevertheless, when used interactively, it is a very rewarding routine that simultaneously produces eigenvalues and eigenfunctions (the eigenvalue is nothing but a constant eigenfunction). The code was run on a VAX 11/785, which limited the number of Fourier components to five or seven. To study higher N-values, it needs to be transferred to a more powerful mainframe, such as a CRAY X-MP.

To scan a wide range of parameters, a code was needed that could be run in batch mode. For this purpose, the robust Bulirsch-Stoer and Van Wijngaarden-Dekker-Brent numerical routines were used (Press *et al.*, 1987; see also Subsection 3.4.2). The shoot-and-match method was employed in a configuration that is well known from stellar oscillation research (see, for instance, Gautschy and Glatzel, 1990). $(N-1)$ independent solutions of Equations (6.2.6) were advanced from the 'axis' $\bar{r}=\epsilon$ outward, and another $(N-1)$ were integrated from $\bar{r}=\bar{r}_f$ inward. They were matched at some point $\bar{r}=\bar{r}_{\rm match}$ by demanding continuity of the solutions and their derivatives. This required the vanishing of the determinant of a $2(N-1)\times 2(N-1)$ matrix, which yielded the dispersion relation of the problem. To construct the eigenfunctions, a singular value decomposition (Press *et al.*, 1987, p. 52) of that matrix produced the correct coefficients for the linear combination of the $(N-1)$ independent solutions that satisfies both radial boundary conditions. The main advantage of this configuration is that the presence of decaying exponentials in the solution is not lost in the process of shooting. If one shoots too far out, growing exponentials completely dominate the solution and, since all accuracy is lost, the integration routine effectively becomes an expensive random number generator. The code was run on a SUN SPARCstation 1, which, when optimised, proved almost an order of magnitude faster than on the VAX 11/785.

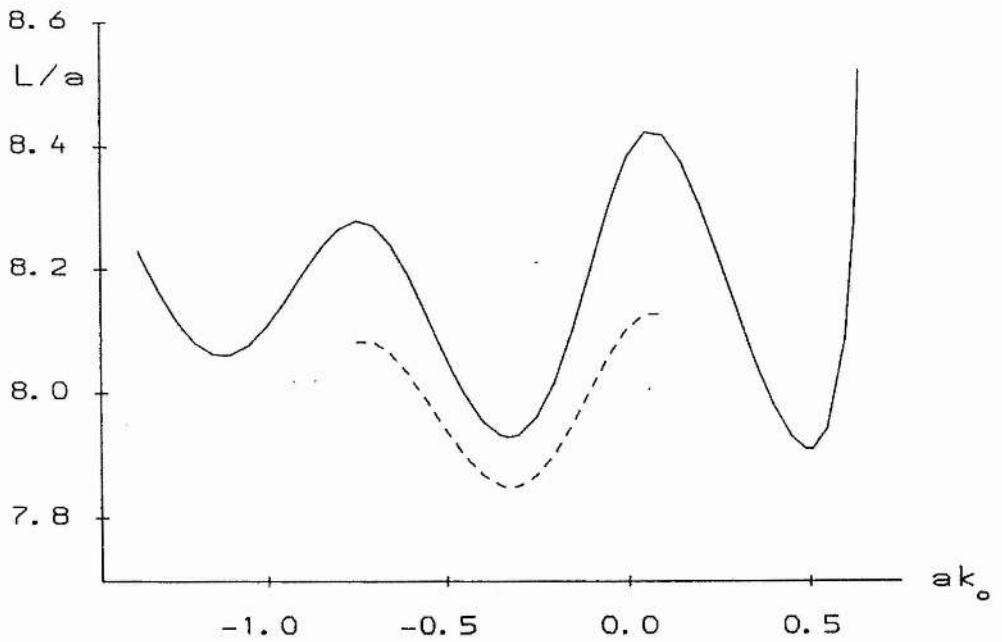

Fig. 6.1. The critical loop length $\bar{L}_{\rm crit}$ of the equilibrium E1 as a function of the central wavenumber $\bar{k}_0$ for five (full curve) and seven (dashed curve) Fourier harmonics, when $m = 1, \bar{\lambda} = 1, \bar{r}_f = 20$. Note the extended vertical scale.

6.3.3. Stability Results

Figure 6.1 shows the dependence of the critical loop length of equilibrium E1 on the choice of the central wavenumber $\bar{k}_0$ for five (full curve) and seven (dashed curve) harmonics, when $m = 1, \bar{\lambda} = 1, \bar{r}_f = 20$. The different minima roughly correspond to $\bar{k}_0 = -0.32 + \frac{2n\pi}{L}$ with $n = -1, 0, 1$. They agree well with the 2.5π cited above. As the number of harmonics is increased the amplitude of the oscillations decreases. This is not surprising, since in the limit of $N \to \infty$ the critical loop length is independent of the 'central' wavenumber. We selected $\bar{k}_0$ such that the central harmonic had the largest amplitude. The amplitudes of the other Fourier harmonics then tend to fall off as $1/n^2$. From here on, the number of Fourier harmonics, N, is fixed to 5, as it is clear that increasing N to its upper limit for feasibility on the SUN, say 11, will not yield qualitatively different results (again, see Van der Linden, Goossens, and Kerner, 1990).

Figures 6.2 and 6.3 depict the stability diagrams for (a) E1, and (b) E3. For a force-free field ($\bar{\lambda} = 1$) the critical loop length increases with increasing m, as was suggested by Einaudi and Van Hoven (1981). As $\bar{\lambda}$ decreases, the order reverses. This extrapolates the result of Section 5.3 that localised interchange modes ($m \to \infty$) are

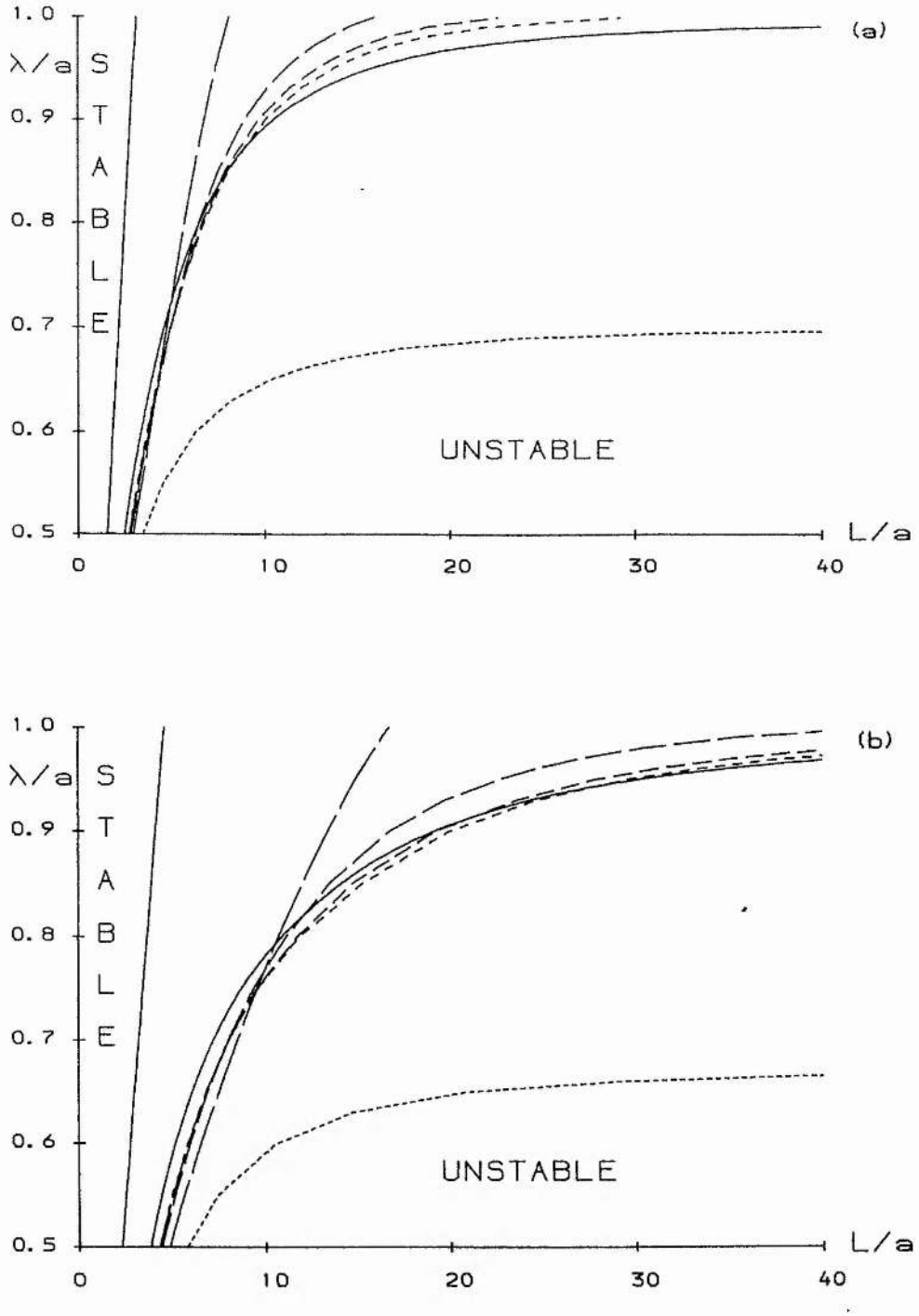

Fig. 6.2. Stability diagram for (a) E1, and (b) E3. The equilibria are absolutely stable for parameter values to the left of the straight line. They are unstable for parameter values to the right of the curved lines; these are the marginal instability curves for the localised interchange modes (full curve) and the $m = 1,2,3,4,0$ modes (in order of decreasing dash length).

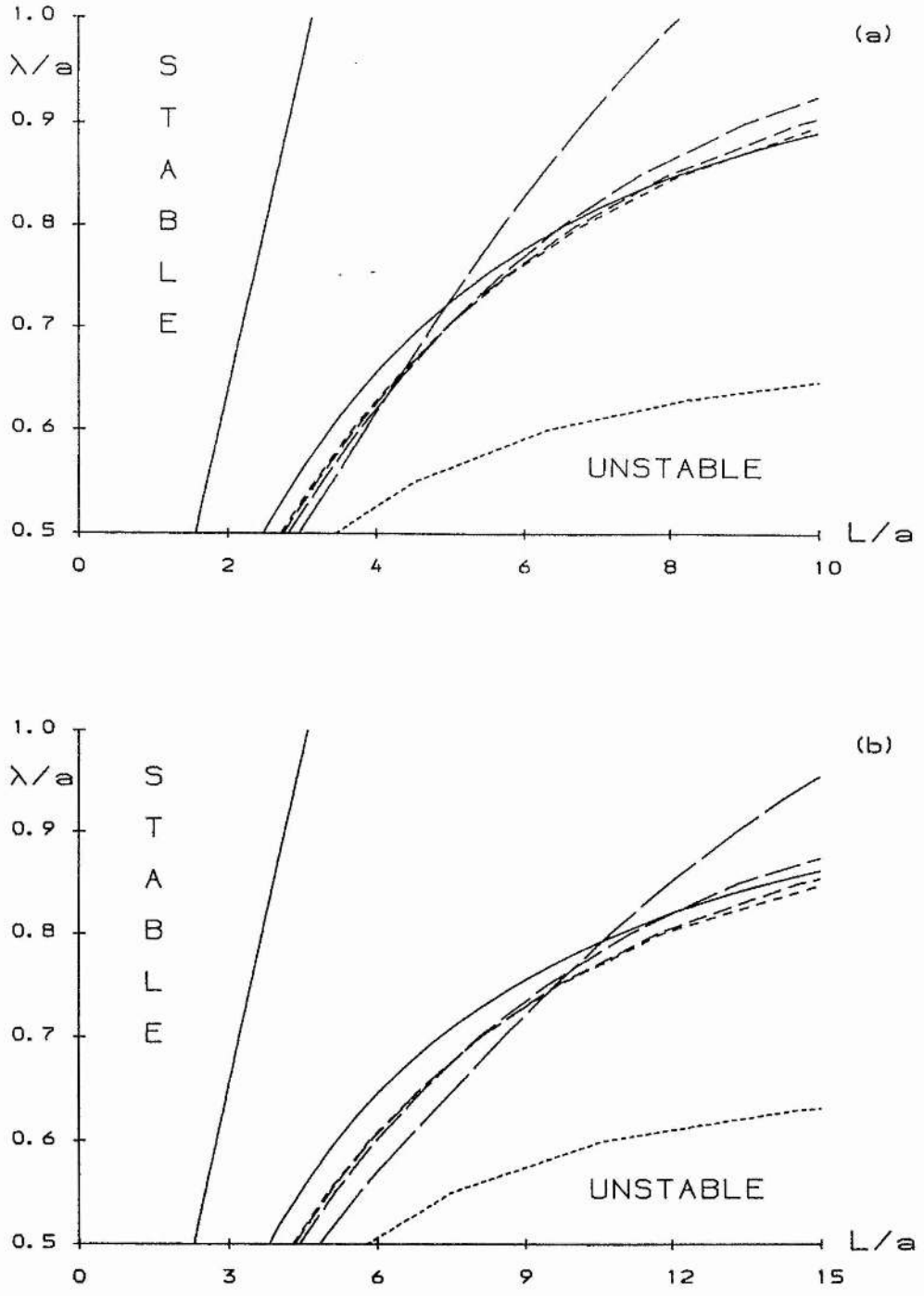

Fig. 6.3. Blow-up of the shorter loop length region of Figure 6.2 for (a) E1, and(b) E3, to highlight the crossing-over of the marginal instability curves.

the most unstable perturbations in laminated equilibria ($\bar{\lambda} = 0$ for these loops) to low-shear configurations. The instability curve for localised interchange modes (full curved line, computed in Subsection 2.2.3) intersects the instability curve for the $m = 1$ kink mode (broken line with longest dashes) at $\bar{\lambda} \approx 0.72$ and 0.8, respectively. Given that the corona is assumed to be near force-free, it follows that for coronal values of $\bar{\lambda}$ a localised interchange instability implies a global $m = 1$ kink instability. Note that both equilibria are also unstable to the $m = 0$ sausage mode, albeit that other instabilities clearly dominate. Sausage modes are stable in an infinitely long 1-D force-free loop (Newcomb, 1960), and this obviously holds for line-tied loops as well. Another of Newcomb's (1960) results that applies equally well to finite loops is the fact that the most unstable sausage mode can be found by concentrating on the case $\bar{k}_0 \rightarrow 0$.

Figure 6.4 shows the marginal radial eigenfunctions $\xi_r(\bar{r})$ at the midplane $z = 0$ of the force-free loops (a) E1 and(b) E3. As the poloidal mode number m increases, the perturbations become more peaked about the radius predicted by the local analysis of Section 2.2, shown here by means of a vertical line (remember that applying the extended Suydam criterion (2.2.17) not only provides a necessary condition for stability, it also determines the flux surface around which localised modes are concentrated). This effect is even more pronounced when pressure gradients are present, as demonstrated in Figure 6.5 where $\bar{\lambda} = 0.6$. Unstable modes peak in the region where they are driven. The present analysis therefore seems to indicate that the standard classification of kink modes as being current-driven, and of localised modes as being pressure-driven, might have to be relaxed.

Figure 6.6 depicts the marginal eigenfunctions $\xi_r(z/L)$ along a magnetic field line, at the radius where $\xi_r(\bar{r}, z = 0)$ peaks, for the force-free loops (a) E1, and (b) E3. It is clear that all perturbations have a similar shape, dictated by the heuristic principle of minimal bending. The logic behind this principle is straightforward : since bending the magnetic field lines requires a lot of energy while interchanging them does not, it seems reasonable to expect that those displacements which bend the field lines the least are the most dangerous (see, for instance, Suydam, 1958). The trial function (2.2.19),

$$\xi_r = \cos xz/L - \cos x/2,$$

used to determine a necessary condition for stability to localised interchange modes in Chapter 2, is drawn here as a full curve. It yields a good approximation of the field line distortion by low-m modes, Increasing pressure gradients only enhances this similarity, as can be seen in Figure 6.7, where $\lambda = 0.6$.

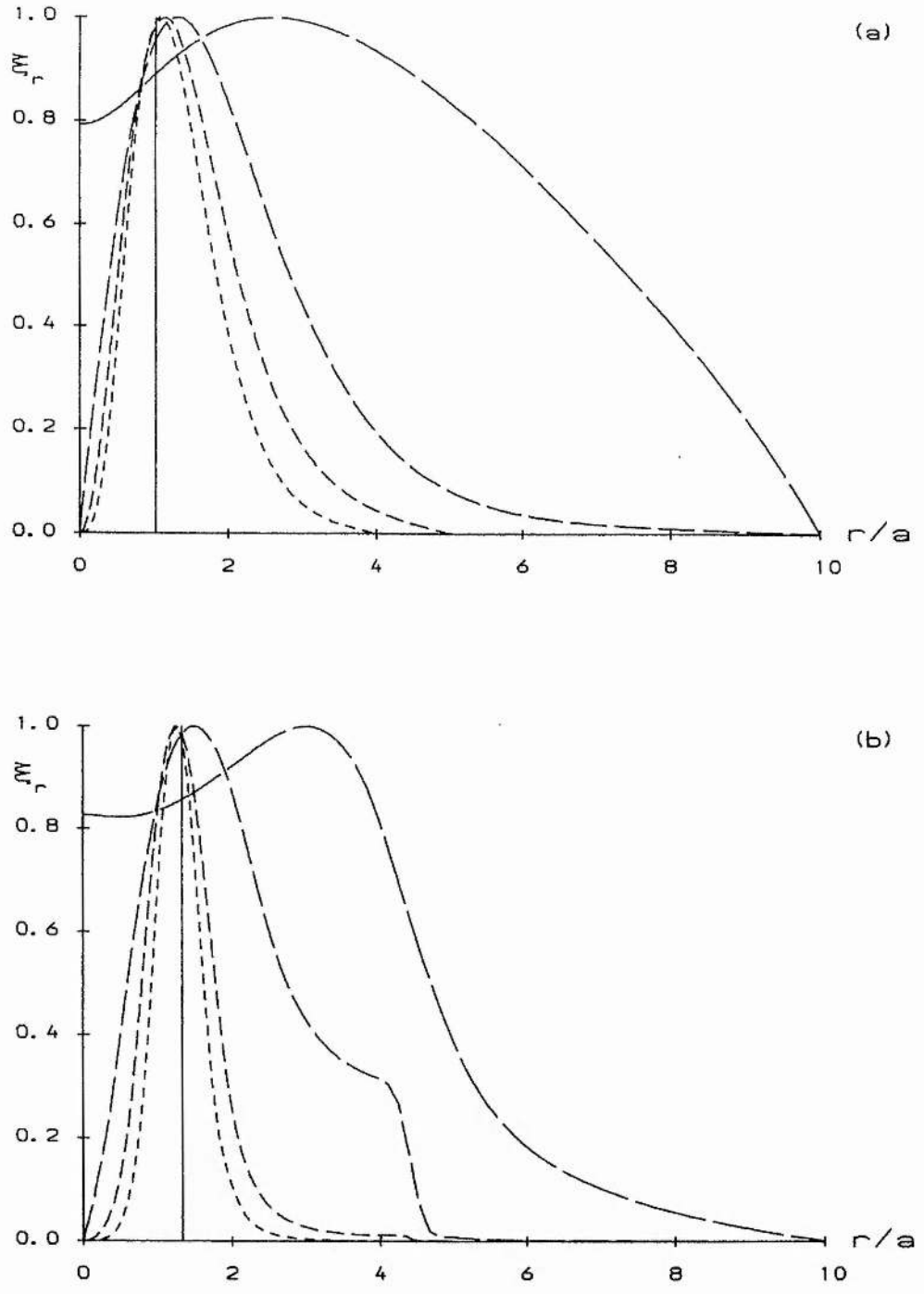

Fig. 6.4. Marginal radial eigenfunctions ξ_r versus $\bar{r}$ at the midplane $z = 0$ of the force-free loops (a) E1, and (b) E3. The broken lines are the eigenfunctions for the m =1,2,3,4 modes (in order of decreasing dash length). The solid line indicates the radius where the localised interchange modes are driven in the case of a slight departure ($\bar{\lambda} = 0.99$) from the force-free state.

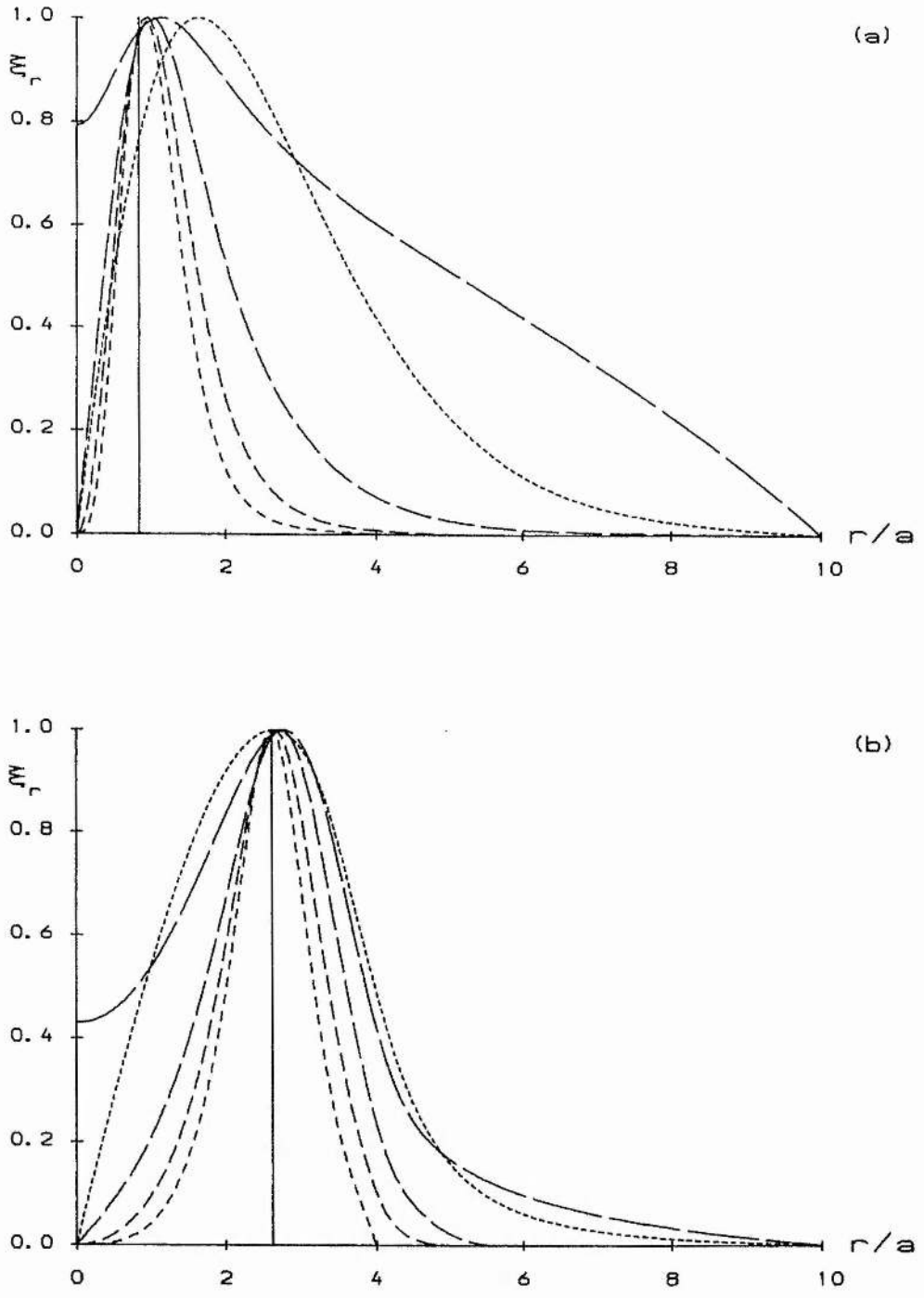

Fig. 6.5. Counterpart of Figure 6.4 when $\bar{\lambda} = 0.6$ for (a) E1, and (b) E3. In both of these diagrams, the broken line with the shortest dashes is the eigenfunction for the $m = 0$ sausage mode.

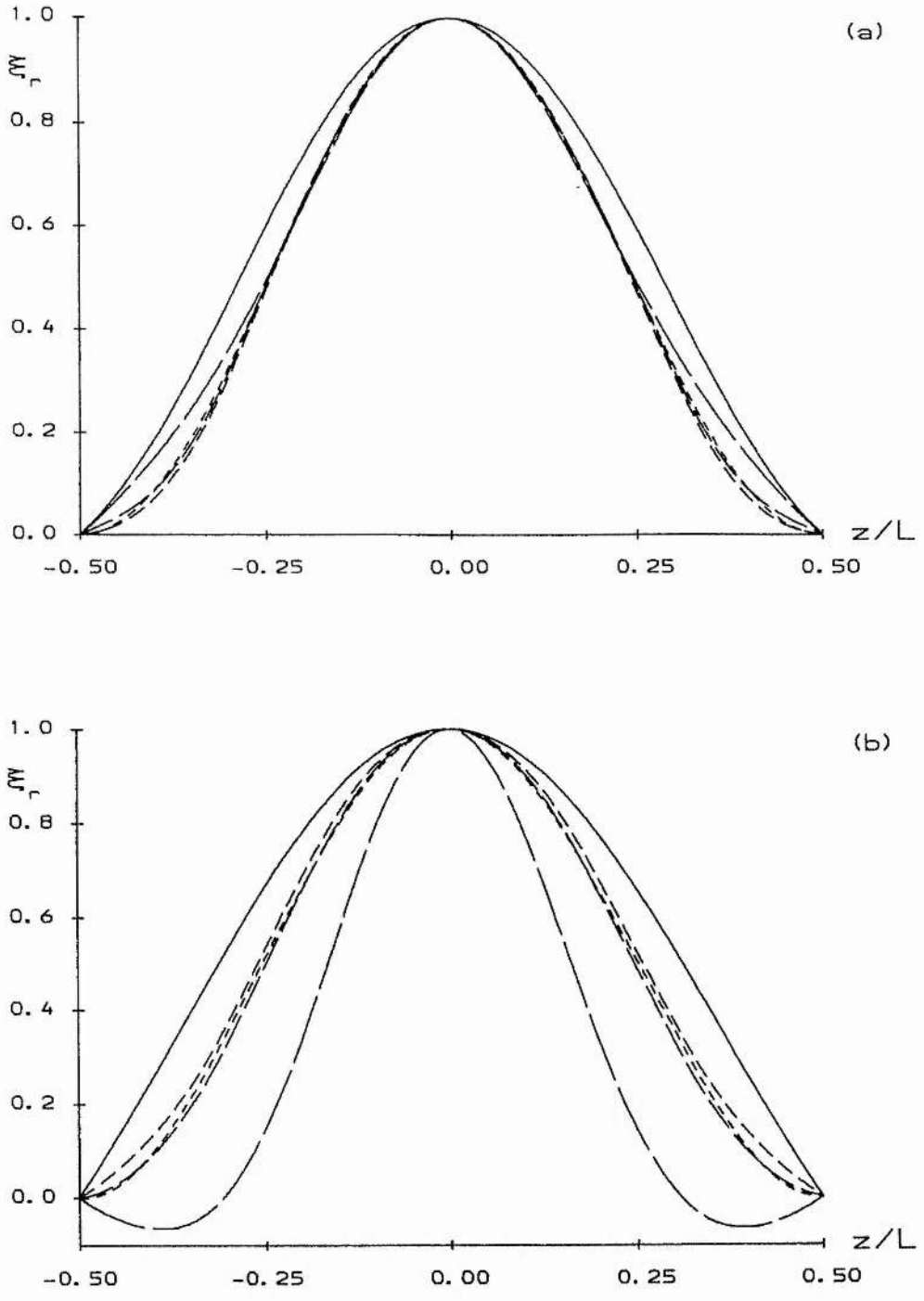

Fig. 6.6. Marginal radial eigenfunctions ξ_r versus z/L along a field line of the force-free loops (a) E1, and (b) E3. The broken lines are the eigenfunctions for the m =1,2,3,4 modes (in order of decreasing dash length). The solid curve is the eigenfunction for the localised interchange modes in the case of a slight departure ($\bar{\lambda} = 0.99$) from the force-free state.

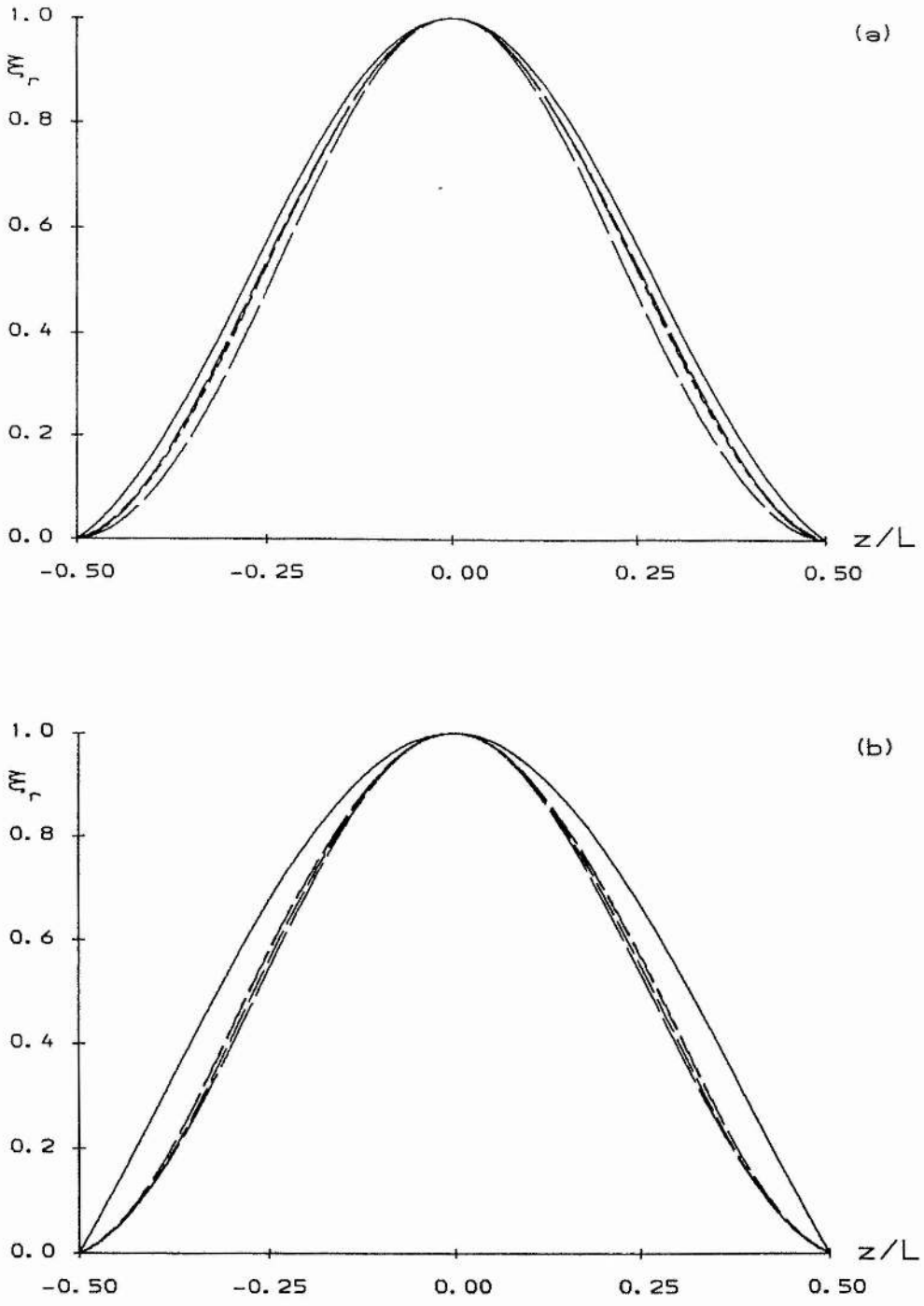

Fig. 6.7. Counterpart of Figure 6.6 when $\bar{\lambda} = 0.6$ for (a) E1, and (b) E3.

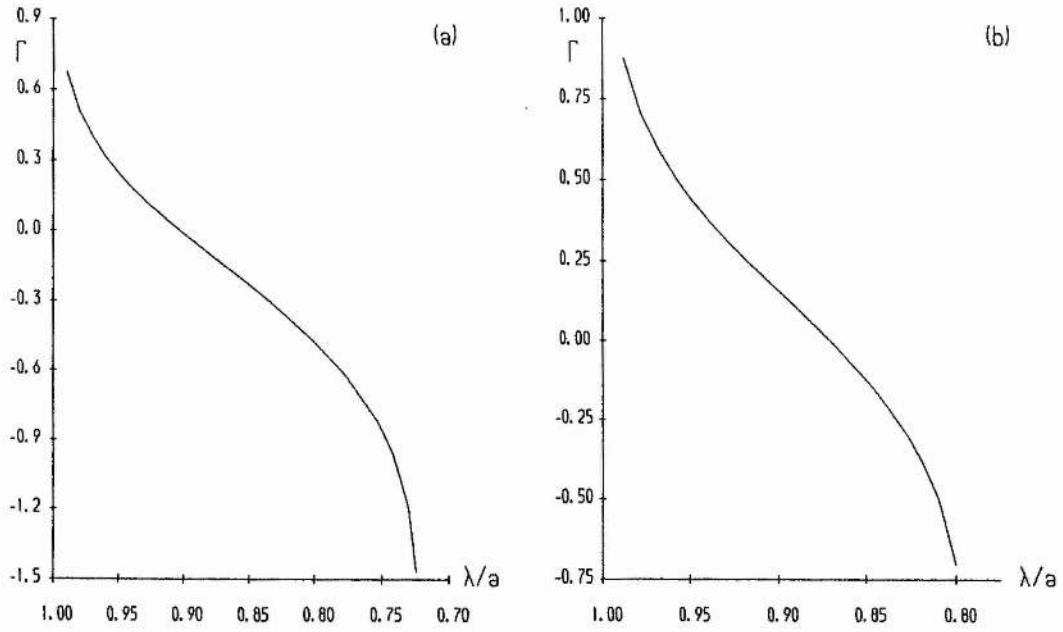

Fig. 6.8. Growth rate Γ versus $\bar{\lambda}$ of the $m = 1$ kink mode at the critical loop length for localised interchange modes for (a) E1, and (b) E3.

Finally, the growth rates of the $m = 1$ kink mode were calculated for the loop length at which the tube becomes unstable to localised interchange modes. They are presented in Figure 6.8 for (a) E1 and (b) E3. It follows that violation of the extended Suydam criterion implies a fast growing global instability.

6.4. Summary

The aim of this Chapter was to compare the stability properties of low-m modes to those of localised interchange modes ($m \to \infty$ in the limit), in a line-tied 1-D loop geometry. To study the former modes, a tractable procedure, based on a normal mode analysis, was presented. It involves the numerical integration of a set of coupled ordinary differential equations, and a scan of the perturbation parameters m and $\bar{k}_0$. Although this is not a challenging numerical problem, it remains a time-consuming task. Localised interchange modes were investigated using the extended Suydam criterion developed in Chapter 2. This is a purely analytical test, requiring only a fraction of the time needed to study low-m modes.

Both tests were applied to two classes of loop equilibria. It was shown that the local analysis based on the extended Suydam criterion, yields a necessary condition for stability to a potentially fatal $m = 1$ kink mode in line-tied coronal loops. This

result is the counterpart of what Goedbloed and Sakanaka (1974) found for an infinite loop. Moreover, the local analysis gives a good indication of the radius where the instability is driven and the shape of the perturbation. The severity of the global $m = 1$ kink mode was assessed for loop lengths that are marginally stable to localised perturbations. Contrary to what Foote and Craig (1990), who normalise Γ to the Alfvén travel time *across* the loop, argue, it appears that appreciable growth rates result when the appropriate normalisation is used. These findings confer a new significance on the investigation of localised interchange modes.

7

Discussion

7.1. Resumé

We studied the linear stability analysis of line-tied symmetric magnetohydrostatic equilibria within the framework of ideal MHD, aimed at its application to the solar corona.

We devised an easy-to-use stability procedure based on the energy principle of Bernstein *et al.* (1958). It allows one to determine necessary conditions for stability to localised perturbations and sufficient conditions for stability to all coronal displacements satisfying the rigid plate boundary conditions at the photosphere. For laminated configurations both conditions coincide. The tests are purely analytical when applied to 1-D equilibria, both cylindrically symmetric arcades and loops (De Bruyne and Hood, 1989a) and plane plasma layers in a perpendicular gravitational field. The necessary condition for stability serves as an extended Suydam criterion (Suydam, 1958) in which the stabilising effect of line-tying has been incorporated. For 2-D equilibria the tests require the numerical integration of two sets of ordinary differential equations along the field lines. They yield tight bounds on the equilibrium parameters of arcades (De Bruyne and Hood, 1989b) and prominences (De Bruyne and Hood, 1989c).

We investigated the relationship between global and localised modes for coronal loops (De Bruyne, Velli, and Hood, 1990a), using a general normal mode method developed by Velli, Einaudi, and Hood (1990a). This revealed the real significance of the study of localised interchange modes and the associated extended Suydam criterion (De Bruyne, Velli, and Hood, 1990b).

7.2. Suggestions for Future Work

Powerful as the methods developed in this thesis may be, they are based on a host

of assumptions which need to be relaxed if we are ever to gain full insight into the complex behaviour of the solar corona.

Structures on the Sun are not of infinite extent and do not have such a degree of symmetry that variations in the physical quantities in one space direction can be completely neglected. To study more realistic configurations it will therefore be necessary to develop methods that can cope with 3-D equilibria. Such equilibria themselves are hard to come by, especially in a closed analytical form. They have to satisfy a local compatibility relation (Low, 1980) imposing constraints on the field line geometry and field strength distribution. Examples of 3-D magnetohydrostatic equilibria in the astrophysical literature are a sequence of force-free fields simulating the growth of a pair of sunspots on the photosphere (Low, 1982a), a discrete bipolar plasma loop (Low, 1982b), quiescent prominence models (Low, 1984a; Wu and Low, 1987; Démoulin, Priest, and Anzer, 1989), a configuration of low-lying cool plasma loops (Low, 1985a), a prototype of the large-scale corona (Bogdan and Low, 1986), coronal arcades (Low, 1988a; Arendt and Schindler, 1988), and magnetic fields over an active region (Low and Lou, 1990). The few that have been investigated for stability, using the energy principle, turned out to be completely stable (Low, 1982b, 1988a,b), which puts a question mark on their scope. General theorems applicable to wide classes of equilibria are a very powerful tool in stability analysis, and deserve further investigation. Most theorems concern force-free fields (Woltjer, 1958a,b, 1959; Molodensky, 1974, 1975, 1976; Aly, 1990a,b), although there is the occasional exception (Zweibel, 1982). A longstanding problem that urgently needs attention is that of the stability of force-free arcades in which all field lines have both footpoints rooted in the photosphere.

We assumed the gravitational potential ϕ to be externally applied, as a result of which it is not perturbed by coronal displacements. Although this is a reasonable assumption in coronal stability analyses, it no longer holds for, e.g., the study of global stellar pulsations (Cox, 1980). The perturbed gravitational potential ϕ^1 was incorporated in the energy integral by Kovetz (1966). Note that neglecting ϕ^1, which is known as the Cowling approximation, leads to an overestimation of the stability of the system (Moss and Tayler, 1969). Another effect, important for some astrophysical applications, that can be included in the energy integral and leaves the force operator $\mathbf{F}$ self-adjoint, is that of cosmic ray pressure (Zweibel and Kulsrud, 1975).

The assumption of a static equilibrium breaks down when the plasma speed v is comparable to, or exceeds, the sound speed $c_s = \sqrt{\gamma p/\rho}$, the Alfvén speed $v_A = B/\sqrt{\mu\rho}$, or the gravitational free-fall speed $v_g = \sqrt{2g\ell}$, where ℓ is a charac-

teristic length scale. Typical coronal values are $c_s = 2 \times 10^5$ m/s, $v_A = 10^6$ m/s, and $v_g = 10^5$ m/s, while the sound and Alfvén speeds in prominences are roughly an order of magnitude smaller. Since plasma speeds in the lower corona are often below 10^4 m/s (Priest, 1981; Schmieder, 1989), many constituents of it can be approximated as being in static equilibrium. However, coronal rain and surges are supersonic phenomena, while higher up in the corona the solar wind becomes increasingly important. Furthermore, many astronomical objects, such as extragalactic jets (Ferrari, 1985), exhibit substantial plasma motions. These can give rise to Kelvin-Helmholtz instabilities, driven by an unstable distribution of the velocity field (Helmholtz, 1868; Thomson, 1871; see also Chandrasekhar, 1961, Chapter 11). When the equilibrium is not static, the inertia term introduces a non-Hermitian operator in the linearised equation of motion (Frieman and Rotenberg, 1960) and a general energy principle does not exist. This stiffens the stability analysis considerably. Although sufficient conditions for stability using energy integrals have been derived (Frieman and Rotenberg, 1960; Lynden-Bell and Ostriker, 1967; Adam, 1978; Chun and Hameiri, 1990), most investigations are based on a normal mode analysis. Examples are the Suydam-like necessary condition for stability by Bondeson, Iacono, and Bhattacharjee (1987), and the analyses of stability properties of jets by Pietrini and Torricelli-Ciamponi (1989) and Corbelli and Torricelli-Ciamponi (1990). An extension of the method developed by Velli, Einaudi, and Hood (1990a) could provide a stability procedure for line-tied stationary equilibria. Analytical studies of the full time-dependent problem pose a formidable challenge that is rarely taken up (but see, for instance, Berge, 1969, and Eckhoff, 1987).

The ideal induction equation (1.2.4) is the perfectly conducting limit of the more general equation

$$\frac{\partial \mathbf{B}}{\partial t} = \nabla \times (\mathbf{v} \times \mathbf{B}) + \eta \nabla^2 \mathbf{B}, \tag{7.2.1}$$

where the magnetic diffusivity η is assumed to be uniform, and the contributions from the battery effect, the Hall effect, and the effect of electron enertia in Ohm's law have been omitted. The extra term, responsible for the diffusion of the magnetic field through the plasma, is often neglected compared to the advection term because the magnetic Reynolds number

$$R_m = \frac{\ell v}{\eta}, \tag{7.2.2}$$

is of the order of 10^{12} and 10^8 for typical coronal and prominence values, respectively. However, when the magnetic and velocity fields are decoupled, i.e., $\nabla \times (\mathbf{v} \times \mathbf{B}) = \mathbf{0}$, or the length scale for diffusion becomes small, the assumption of the field lines being frozen into the plasma ceases to be valid and the magnetic field can change its

topology. This process of magnetic reconnection, whereby magnetic energy can be released on a short time scale, is likely to be a crucial feature in the clarification of the solar flare phenomenon and coronal heating. By allowing the field to access lower energy states, it introduces a new class of instabilities, the resistive instabilities (see, for instance, Bateman, 1978, Chapter 10), whose investigation began with a notable paper by Furth, Killeen, and Rosenbluth (1963). Energy principles for 2-D resistive instabilities were constructed by Tasso (1975, 1977) and Schindler, Birn, and Janicke (1983). Chu *et al.* (1989, 1990) devised an energy principle that yields a sufficient condition for stability to tearing modes, which tend to break the plasma into magnetic islands. Their effect on line-tied configurations was studied by, for example, Mok and Van Hoven (1982) and Velli and Hood (1989). Analysing the $m = 1$ resistive kink mode in coronal loops, Velli, Hood, and Einaudi (1988) found that line-tying is a major stabilising mechanism, as it removes the existence of mode rational surfaces. However, the importance of line-tying in prohibiting tearing modes remains an issue of debate (Hassam, 1990). Resistive ballooning modes have drawn a lot of attention too, both in fusion research (Pegoraro and Schep, 1981; Strauss, 1981; Conner and Hastie, 1985; Grassie and Krech, 1990) and astrophysics (Velli and Hood, 1986, 1987; Otani and Strauss, 1988). Their possible relevance to coronal heating was pointed out by Strauss (1989) and certainly deserves further attention. Although the approach of Velli, Einaudi, and Hood (1990a) offers interesting perspectives, it seems likely that resistive instabilities in more realistic configurations will have to be investigated by numerical means (see, for instance, Finan and Killeen, 1981; Schnack *et al.*, 1990).

The momentum equation (1.2.1) is the inviscid form of the equation

$$\rho \frac{d\mathbf{v}}{dt} = -\nabla p + \mathbf{j} \times \mathbf{B} - \rho \nabla \phi - \nabla \cdot \mathbf{\Pi}, \tag{7.2.3}$$

where $\mathbf{\Pi}$ is the viscous stress tensor (Braginskii, 1965) expressing the non-isotropy of the pressure distribution. The ratio of the size of the inertial term to the viscous term is given by the Reynolds number

$$R = \frac{\ell v}{\nu}, \tag{7.2.4}$$

with ν the coefficient of kinematic viscosity. For typical coronal and prominence values, R is of the order of 10 and 10^8, respectively. Hence, viscosity could well be the main dissipative effect in the solar corona and might therefore play an important role in coronal heating. A visco-resistive energy principle for incompressible slab equilibria was constructed by Barston (1969). Van der Linden, Goossens and Hood (1988) analysed the effect of viscosity on resistive ballooning modes in a solar context, and found that perpendicular viscosity could lead to completely stable resistive modes. Similar results were obtained by Spies (1988) in an analytical study of the Z-pinch.

The influence of finite resistivity and viscosity on flow equilibria was examined by Einaudi and Rubini (1986, 1989) using a finite difference scheme, while Cox (1990) considered visco-resistive damping of sausage and kink modes in a static Z-pinch using a linear initial value code. It would be interesting to see whether the combined effect of line-tying and viscosity could prove to be the main reason for the observed longevity of coronal structures.

Taking account of parallel thermal conduction, the adiabatic energy equation (1.2.3) transform into

$$\frac{dp}{dt} - c_s^2 \frac{d\rho}{dt} = (\gamma - 1) B \frac{\partial}{\partial s} \left(\frac{\kappa_\parallel}{B} \frac{\partial T}{\partial s} \right), \tag{7.2.5}$$

where $\kappa_\parallel$ is the parallel thermal conductivity. Processes are approximately isentropic when the Alfvén transit time $\tau_A = \ell / v_A$ and the sound transit time $\tau_s = \ell / c_s$ are smaller than the conductive transit time

$$\tau_c = \frac{\ell^2 c_s^2 \rho}{(\gamma - 1) \kappa_\parallel T} \, . \tag{7.2.6}$$

For typical coronal values these are roughly 20, 100, and 200 s, respectively, while for prominence values they are of the order of 200, 2000, and 10^{10} s, respectively. Generally speaking, thermal conduction has a stabilising effect on an equilibrium, as it smooths out any local temperature gradients which could provide a source of free energy. However, introducing a radiative loss function in the energy equation (7.2.5) opens up the prospect of a new class of instabilities, namely the thermal instabilities (see, for instance, Sparks and Van Hoven, 1988). Where the loss function increases with decreasing temperature, a radiative run-away effect can occur, giving rise to thermal condensations. These are likely to be essential in the process of prominence formation (see, for instance, Hood and Anzer, 1988, and Hood, 1989). The interplay of resistivity, conduction, radiation, and line-tying poses one of the toughest challenges to solar coronal research. Analytically, progress can be made by studying localised modes (Hood, Van der Linden, and Goossens, 1989; Cargill and Hood, 1989, 1990; Hood *et al.*, 1990). Numerically, advanced computational physics and CRAY-size mainframes are essential to cope with the vast range of space and time scales inherent in these problems (see, for instance, Kerner, 1990; Sparks, Van Hoven, and Schnack, 1990).

A major drawback of marginal linear stability analyses using the Bernstein *et al.* (1958) energy principle is the total lack of information about the growth rates of the instabilities found. It is not inconceivable that an equilibrium is labelled unstable while it could actually persist for days or weeks, simply because the instabilities take forever to develop. What one really needs is a stability technique that does

not establish whether an equilibrium is absolutely stable, but whether it is stable on a time scale relevant for modelling a coronal structure. A practical stability concept, that of σ-stability, was introduced by Goedbloed and Sakanaka (1974). An equilibrium is said to be σ-stable if no instabilities with growth faster than $\exp(\sigma t)$ exist. They devised a modified energy principle by means of which an equilibrium can be tested for σ-stability. In an accompanying paper (Sakanaka and Goedbloed, 1974) it was employed to study the stability of a range of screw pinches. Spies (1974) used it to obtain lower and upper bounds for the maximum growth rate in toroidal configurations. Another advantage of a σ-stability analysis is the fact that it avoids the difficulties associated with a stable continuous spectrum reaching to the point of marginal stability, $\omega^2 = 0$ (for a discussion of continuous spectra, see, for instance, Goedbloed, 1983). To our knowledge, this stability concept has not yet been applied to coronal equilibria, despite its obvious relevance.

Although the question of potential instability of a system can be addressed by linear theory, the question of what happens when a linear instability actually occurs can be answered only by nonlinear analysis. For example, a 1-D loop that becomes unstable may exhibit a deviation from its initial state that grows faster that exponential (Friedrichs, 1960). This is known as an explosive instability. On the other hand, the loop may buckle into a new, possibly 3-D, equilibrium that is stable (Yeh, 1973). Then the instability is said to saturate. Some analytical results on nonlinear evolution are available from fusion research. Pao (1978), Nakajima (1990) and Nakajima and Hamaguchi (1990) studied the evolution of the mode amplitude near the threshold of linear instability, using a perturbation expansion. Mondt and Weiland (1985) investigated the explosive behaviour of ballooning modes in screw pinches. Often, however, numerical techniques are required. One of the key pieces in the solar flare puzzle, the nonlinear behaviour of a twisted loop, has only been re-addressed recently (Zaidman and Tajima, 1989; Craig and Sneyd, 1990; Mikić, 1990), after its investigation was started off by Sakurai (1976) in the context of erupting prominences.

In summary, although solar coronal stability theory has gone a long way since the early investigations by Lundquist, a lot more needs to be done before we can claim to have unravelled the enigma.

Appendix A : Coordinate Systems and Variables

A.1. Cylindrical Geometry

Polar coordinates $(r, \theta, z) \rightarrow$ curvilinear coordinates (r, s, n), with $r\,dr\,d\theta\,dz = dr\,ds\,dn$.
The metric is defined by

$$(dl)^2 = (dr)^2 + r^2(d\theta)^2 + (dz)^2.$$

Other definitions are

$$\mathbf{B} = (0, B_\theta(r), B_z(r)) = B_\theta \mathbf{e}_\theta + B_z \mathbf{e}_z, \qquad \phi = 0,$$

$$\xi_r = \mathbf{e}_r \cdot \boldsymbol{\xi}, \qquad \xi_\parallel = \mathbf{B} \cdot \boldsymbol{\xi}, \qquad \zeta = (\mathbf{e}_r \times \mathbf{B}) \cdot \boldsymbol{\xi},$$

$$\frac{\partial}{\partial r} = \mathbf{e}_r \cdot \nabla\,, \qquad B\frac{\partial}{\partial s} = \mathbf{B} \cdot \nabla\,, \qquad B\frac{\partial}{\partial n} = (\mathbf{e}_r \times \mathbf{B}) \cdot \nabla\,,$$

$$\boldsymbol{\xi} = \xi_r \mathbf{e}_r + \xi_\parallel \frac{\mathbf{B}}{B} + \zeta \frac{\mathbf{e}_r \times \mathbf{B}}{B}\,,$$

$$\nabla \cdot \boldsymbol{\xi} = \frac{1}{r}\frac{\partial}{\partial r}(r\xi_r) + \frac{1}{B}\frac{\partial \xi_\parallel}{\partial s} + \frac{1}{B}\frac{\partial \zeta}{\partial n}\,.$$

A.2. Slab Geometry

Cartesian coordinates $(x, y, z) \rightarrow$ curvilinear coordinates (z, s, n), with $dx\,dy\,dz = dz\,ds\,dn$.
The metric is defined by

$$(dl)^2 = (dx)^2 + (dy)^2 + (dz)^2.$$

Other definitions are

$$\mathbf{B} = (B_x(z), B_y(z), 0) = B_x \mathbf{e}_x + B_y \mathbf{e}_y, \qquad \phi = gz,$$

$$\xi_z = \mathbf{e}_z \cdot \boldsymbol{\xi}, \qquad \xi_\parallel = \mathbf{B} \cdot \boldsymbol{\xi}, \qquad \zeta = (\mathbf{e}_z \times \mathbf{B}) \cdot \boldsymbol{\xi},$$

$$\frac{\partial}{\partial z} = \mathbf{e}_z \cdot \nabla\,, \qquad B\frac{\partial}{\partial s} = \mathbf{B} \cdot \nabla\,, \qquad B\frac{\partial}{\partial n} = (\mathbf{e}_z \times \mathbf{B}) \cdot \nabla\,,$$

$$\boldsymbol{\xi} = \xi_z \mathbf{e}_z + \xi_\parallel \frac{\mathbf{B}}{B} + \zeta \frac{\mathbf{e}_z \times \mathbf{B}}{B}\,,$$

$$\nabla \cdot \boldsymbol{\xi} = \frac{\partial \xi_z}{\partial z} + \frac{1}{B}\frac{\partial \xi_\parallel}{\partial s} + \frac{1}{B}\frac{\partial \zeta}{\partial n}\,.$$

A.3. 2-D Cartesian Geometry

Cartesian coordinates $(x, y, z) \rightarrow$ curvilinear coordinates (a, s, n), with $dx\,dy\,dz = da\,ds\,dn$.

The metric is defined by

$$(dl)^2 = (dx)^2 + (dy)^2 + (dz)^2.$$

Other definitions are

$$\mathbf{B} = (B_x(x,z), B_y(x,z), B_z(x,z)) = \nabla A \times \mathbf{e}_y + B_y \mathbf{e}_y,$$

$$\mathbf{B}_p = \nabla A \times \mathbf{e}_y, \qquad \phi = gz,$$

$$\xi_A = B_p \tilde{\xi}_A = \frac{\nabla A}{B_p} \cdot \boldsymbol{\xi}, \qquad \xi_\parallel = B\tilde{\xi}_\parallel = \frac{\mathbf{B}}{B} \cdot \boldsymbol{\xi}, \qquad \xi_n = BB_p\tilde{\xi}_n = \frac{\nabla A \times \mathbf{B}}{BB_p} \cdot \boldsymbol{\xi},$$

$$B_p \frac{\partial}{\partial a} = \nabla A \cdot \nabla\,, \qquad B\frac{\partial}{\partial s} = \mathbf{B} \cdot \nabla\,, \qquad BB_p \frac{\partial}{\partial n} = (\nabla A \times \mathbf{B}) \cdot \nabla\,,$$

$$\boldsymbol{\xi} = \tilde{\xi}_A \nabla A + \tilde{\xi}_\parallel \mathbf{B} + \tilde{\xi}_n \nabla A \times \mathbf{B},$$

$$\nabla \cdot \boldsymbol{\xi} = B_p \frac{\partial \tilde{\xi}_A}{\partial a} + B\frac{\partial \tilde{\xi}_\parallel}{\partial s} + BB_p \frac{\partial \tilde{\xi}_n}{\partial n} + \nabla^2 A\, \tilde{\xi}_A.$$

A.4. 2-D Arbitrary Geometry

Natural orthogonal coordinate basis $(q^1, q^2, q^3) \rightarrow$ curvilinear coordinates (a, s, n), with $dq^1\,dq^2\,dq^3 = da\,ds\,dn$.

The metric is defined by

$$(dl)^2 = g_{ij} dq^i dq^j,$$

with summation over repeated indices. Other definitions are

$$\mathbf{B} = (B_1(q^1,q^2), B_2(q^1,q^2), B_3(q^1,q^2)) = \nabla A \times \mathbf{g}^3 + B^3 \mathbf{g}_3,$$

$$\mathbf{B}_p = \nabla A \times \mathbf{g}^3, \qquad \phi = \phi(q^1, q^2),$$

$$\xi_A = B_p \tilde{\xi}_A = \frac{\nabla A}{B_p} \cdot \boldsymbol{\xi}, \qquad \xi_\parallel = B\tilde{\xi}_\parallel = \frac{\mathbf{B}}{B} \cdot \boldsymbol{\xi}, \qquad \xi_n = BB_p\tilde{\xi}_n = \frac{\nabla A \times \mathbf{B}}{g_{33} BB_p} \cdot \boldsymbol{\xi},$$

$$B_p \frac{\partial}{\partial a} = \frac{\nabla A}{g_{33}} \cdot \nabla\,, \qquad B\frac{\partial}{\partial s} = \mathbf{B} \cdot \nabla\,, \qquad BB_p \frac{\partial}{\partial n} = (\nabla A \times \mathbf{B}) \cdot \nabla\,,$$

$$\boldsymbol{\xi} = \tilde{\xi}_A \frac{\nabla A}{g_{33}} + \tilde{\xi}_\parallel \mathbf{B} + \tilde{\xi}_n \nabla A \times \mathbf{B},$$

$$\nabla \cdot \boldsymbol{\xi} = B_p \frac{\partial \tilde{\xi}_A}{\partial a} + B\frac{\partial \tilde{\xi}_\parallel}{\partial s} + BB_p \frac{\partial \tilde{\xi}_n}{\partial n} + \nabla \cdot \left(\frac{\nabla A}{g_{33}}\right) \tilde{\xi}_A.$$

Appendix B : An Expression for δW in Line-Tied Cylindrical Geometry

The aim is to rearrange δW in the form (1.4.1). Consider as a starting point Equation (3.4) of Hood (1984) for the perturbed potential energy integral. Taking into account compressibility and using the notation of Appendix A.1, this reads

$$\delta W = \frac{1}{2\mu}\int\left\{B^2\left[\frac{\partial \xi_r}{\partial s}\right]^2 - \frac{2B_\theta}{r^2}(rB_\theta)'\xi_r^2 + \left[\frac{\partial \zeta}{\partial z} + rB_\theta\frac{\partial}{\partial r}\left(\frac{\xi_r}{r}\right)\right]^2 + \right.$$
$$\left. + \left[\frac{1}{r}\frac{\partial \zeta}{\partial \theta} - \frac{B_z}{r}\frac{\partial}{\partial r}(r\xi_r)\right]^2 + \gamma\mu p(\nabla\cdot\boldsymbol{\xi})^2\right\} r\,dr\,d\theta\,dz.$$

Introducing the following notations

$$\tilde{C} = \frac{\partial \xi_\parallel}{\partial s} + \frac{2B_\theta^2}{rB}\xi_r,$$
$$\tilde{D} = \frac{\partial \zeta}{\partial s} - \frac{2B_\theta B_z}{rB}\xi_r,$$
$$\tilde{F} = \frac{B}{B_\theta}\left[\frac{\partial \zeta}{\partial z} + rB_\theta\frac{\partial}{\partial r}\left(\frac{\xi_r}{r}\right)\right] - \frac{B_z}{B_\theta}\tilde{D},$$

and using the transformations

$$\left[\frac{\partial \zeta}{\partial z} + rB_\theta\frac{\partial}{\partial r}\left(\frac{\xi_r}{r}\right)\right]^2 + \left[\frac{1}{r}\frac{\partial \zeta}{\partial \theta} - \frac{B_z}{r}\frac{\partial}{\partial r}(r\xi_r)\right]^2 = \tilde{D}^2 + \tilde{F}^2,$$
$$\nabla\cdot\boldsymbol{\xi} = \frac{1}{B}(\tilde{C} + \tilde{F}),$$
$$\tilde{F}^2 + \frac{\gamma\mu p}{B^2}(\tilde{C} + \tilde{F})^2 = \frac{\gamma\mu p}{B^2 + \gamma\mu p}\tilde{C}^2 + $$
$$+ \frac{B^2 + \gamma\mu p}{B^2}\left[\tilde{F} + \frac{\gamma\mu p}{B^2 + \gamma\mu p}\tilde{C}\right]^2,$$
$$\frac{B}{B_\theta}\frac{\partial \zeta}{\partial z} - \frac{B_z}{B_\theta}\frac{\partial \zeta}{\partial s} = \frac{\partial \zeta}{\partial n},$$
$$\frac{2B_z^2}{rB}\xi_r + \frac{2B_\theta^2}{rB}\frac{\gamma\mu p}{B^2 + \gamma\mu p}\xi_r = 2\frac{B_z^2 + \gamma\mu p}{B^2 + \gamma\mu p}B\frac{\xi_r}{r},$$

one arrives at

$$\delta W = \frac{1}{2\mu}(\mathcal{I} + \mathcal{J}),$$

where

$$\mathcal{I} = \int \left\{ B^2 \left[\frac{\partial \xi_r}{\partial s} \right]^2 - \frac{2B_\theta}{r^2}(rB_\theta)' \xi_r^2 + \frac{\gamma \mu p}{B^2 + \gamma \mu p} \left[\frac{\partial \xi_\parallel}{\partial s} + \frac{2B_\theta^2}{rB} \xi_r \right]^2 + \right.$$
$$\left. + \left[\frac{\partial \zeta}{\partial s} - \frac{2B_\theta B_z}{rB} \xi_r \right]^2 \right\} r \, dr \, d\theta \, dz$$

and

$$\mathcal{J} = \int \left\{ \frac{B^2 + \gamma \mu p}{B^2} \left[rB \frac{\partial}{\partial r} \left(\frac{\xi_r}{r} \right) + \frac{\partial \zeta}{\partial n} + \frac{\gamma \mu p}{B^2 + \gamma \mu p} \frac{\partial \xi_\parallel}{\partial s} + \right. \right.$$
$$\left. \left. + 2 \frac{B_z^2 + \gamma \mu p}{B^2 + \gamma \mu p} B \frac{\xi_r}{r} \right]^2 \right\} r \, dr \, d\theta \, dz.$$

Appendix C : An Expression for δW in Line-Tied Slab Geometry

As in Appendix B, the aim is to rearrange the perturbed potential energy integral in a form (1.4.1). Using variables and derivatives defined in Appendix A.2 and applying the rigid plate boundary conditions (1.4.2), expression (2.3.4) for δW is readily transformed into

$$\delta W = \frac{1}{2\mu}\int\Bigg\{B^2\left[\frac{\partial \xi_z}{\partial s}\right]^2 - \mu\rho' g\xi_z^2 + \left[\frac{\partial \zeta}{\partial y} + B_x\xi_z'\right]^2 + \left[\frac{\partial \zeta}{\partial x} - B_y\xi_z'\right]^2 - \\ -2\mu\rho g\xi_z(\nabla\cdot\boldsymbol{\xi}) + \gamma\mu p(\nabla\cdot\boldsymbol{\xi})^2\Bigg\}\,dx\,dy\,dz.$$

Introducing the following notations

$$N^2 = -g\left(\frac{g}{c_s^2} + \frac{\rho'}{\rho}\right),$$

$$\tilde{C} = \frac{\partial \xi_{\parallel}}{\partial s},$$

$$\tilde{D} = \frac{\partial \zeta}{\partial s},$$

$$\tilde{F} = \frac{B}{B_x}\left[\frac{\partial \zeta}{\partial y} + B_x\xi_z'\right] - \frac{B_y}{B_x}\tilde{D},$$

$$\tilde{G} = \hat{\beta}\tilde{C}^2 - 2\frac{g}{v_A^2}B\xi_z\tilde{C} - \frac{B^2}{B^2+\gamma\mu p}\left[\hat{\beta}\tilde{C} - \frac{g}{v_A^2}B\xi_z\right]^2,$$

and using the transformations

$$\left[\frac{\partial \zeta}{\partial y} + B_x\xi_z'\right]^2 + \left[\frac{\partial \zeta}{\partial x} - B_y\xi_z'\right]^2 = \tilde{D}^2 + \tilde{F}^2,$$

$$(\nabla\cdot\boldsymbol{\xi}) = \frac{1}{B}(\tilde{C}+\tilde{F}),$$

$$\tilde{F}^2 - 2\frac{g}{v_A^2}B\xi_z(\tilde{C}+\tilde{F}) + \hat{\beta}(\tilde{C}+\tilde{F})^2 = \tilde{G} + \frac{B^2+\gamma\mu p}{B^2}\times \\ \times\left[\tilde{F} + \frac{\gamma\mu p}{B^2+\gamma\mu p}\left(\tilde{C} - \frac{g}{c_s^2}B\xi_z\right)\right]^2,$$

$$-\mu\rho' g\xi_z^2 + \tilde{G} = \mu\rho N^2\xi_z^2 + \frac{\gamma\mu p}{B^2+\gamma\mu p}\left[\tilde{C} - \frac{g}{c_s^2}B\xi_z\right]^2,$$

$$\frac{B}{B_x}\frac{\partial\zeta}{\partial y} - \frac{B_y}{B_x}\frac{\partial\zeta}{\partial s} = \frac{\partial\zeta}{\partial n},$$

one arrives at

$$\delta W = \frac{1}{2\mu}(\mathcal{I} + \mathcal{J}),$$

where

$$\mathcal{I} = \int\left\{B^2\left[\frac{\partial\xi_z}{\partial s}\right]^2 + \mu\rho N^2\xi_z^2 + \frac{\gamma\mu p}{B^2+\gamma\mu p}\left[\frac{\partial\xi_\parallel}{\partial s} - \frac{g}{c_s^2}B\xi_z\right]^2 + \left[\frac{\partial\zeta}{\partial s}\right]^2\right\}dx\,dy\,dz$$

and

$$\mathcal{J} = \int\left\{\frac{B^2+\gamma\mu p}{B^2}\left[B\xi_z' + \frac{\partial\zeta}{\partial n} + \frac{\gamma\mu p}{B^2+\gamma\mu p}\left(\frac{\partial\xi_\parallel}{\partial s} - \frac{g}{c_s^2}B\xi_z\right)\right]^2\right\}dx\,dy\,dz.$$

Appendix D : An Expression for δW in Line-Tied 2-D Cartesian Geometry

To write the energy integral δW in a form (1.4.1), consider as a starting point Equation (31) of Schindler, Birn, and Janicke (1983), which in our coordinate system reads

$$\delta W = \frac{1}{2\mu}\int\left\{\frac{1}{B_p^2}\left[\mathbf{B}\cdot\nabla A_1\right]^2 + VA_1^2 + \left[-B_y\nabla\cdot\boldsymbol{\xi}_p + \mathbf{B}_p\cdot\nabla\xi_y\right]^2 + \right.$$
$$+\left[-\frac{1}{B_p}\left(\nabla A\cdot\nabla A_1 + JA_1\right) - B_p\frac{\partial\xi_y}{\partial y} + B_y\frac{\partial\xi_{\|p}}{\partial y}\right]^2 + \qquad \text{(D.1)}$$
$$\left.+\left(\gamma\mu p + \frac{\mu\rho^2}{\partial\rho/\partial\phi}\right)\left[\nabla\cdot\boldsymbol{\xi}\right]^2 - \mu\frac{\partial\rho}{\partial\phi}\left[\boldsymbol{\xi}\cdot\nabla\phi + \frac{\rho}{\partial\rho/\partial\phi}\nabla\cdot\boldsymbol{\xi}\right]^2\right\}\,d\mathcal{V},$$

with

$$V = \nabla\cdot\left(\frac{J\nabla A}{B_p^2}\right) - \frac{J^2}{B_p^2} - \frac{\partial J}{\partial A}\,.$$

The following notations have been used :

$$\boldsymbol{\xi} = \boldsymbol{\xi}_p + \xi_y\mathbf{e}_y,$$
$$\xi_{\|p} = \frac{\boldsymbol{\xi}_p\cdot\mathbf{B}_p}{B_p}\,,$$
$$A_1 = \boldsymbol{\xi}_p\cdot\nabla A.$$

Note that $\partial/\partial A$ stands for the derivative with respect to A while ϕ is kept constant, and likewise $\partial/\partial\phi$ stands for the derivative with respect to ϕ while A is kept constant. Changing variables according to Appendix A.3, introducing the notations

$$\tilde{A} = \left(\frac{\rho}{\gamma p} + \frac{1}{\rho}\frac{\partial\rho}{\partial\phi}\right),$$
$$\tilde{\xi}_\phi = \nabla\phi\cdot\boldsymbol{\xi},$$
$$\tilde{F} = B_p\frac{\partial\tilde{\xi}_A}{\partial a} + BB_p\frac{\partial\tilde{\xi}_n}{\partial n}\,,$$

and using the transformations

$$
\begin{aligned}
A_1 &= B_p \xi_A, \\
\frac{\partial J}{\partial A} &= \frac{1}{B_p}\frac{\partial J}{\partial a} - \frac{1}{B_p}\frac{\partial \phi}{\partial a}\frac{\partial J}{\partial \phi}, \\
V A_1^2 &= -\Big(2J\Big(J + \frac{\partial B_p}{\partial a}\Big) - B_p \frac{\partial \phi}{\partial a}\frac{\partial J}{\partial \phi}\Big)\xi_A^2, \\
-B_y \nabla \cdot \boldsymbol{\xi}_p + \mathbf{B}_p \cdot \nabla \xi_y &= -B_y \tilde{F} - B_p \frac{\partial \xi_n}{\partial s} - B\frac{\partial}{\partial s}\Big(\frac{B_p}{B}\Big)\xi_n + B_y J \tilde{\xi}_A, \\
\frac{\nabla A \cdot \nabla A_1 + J A_1}{-B_p} - B_p \frac{\partial \xi_y}{\partial y} + B_y \frac{\partial \xi_{\|p}}{\partial y} &= -B_p \tilde{F} + B_y \frac{\partial \xi_n}{\partial s} - B_p \frac{\partial (B B_p)}{\partial n}\tilde{\xi}_n - \\
&\quad - \frac{\partial B_p^2}{\partial a}\tilde{\xi}_A - B_p J \tilde{\xi}_A, \\
\gamma \mu p + \frac{\mu \rho^2}{\partial \rho / \partial \phi} &= \frac{\mu \rho^2 c_s^2}{\partial \rho / \partial \phi}\tilde{A}, \\
\nabla \cdot \boldsymbol{\xi} &= \tilde{F} + B\frac{\partial \tilde{\xi}_\|}{\partial s} - J\tilde{\xi}_A,
\end{aligned}
$$

noting that for an equilibrium quantity h, $B_y \partial h/\partial s = B_p \partial h/\partial n$, one arrives at

$$
\begin{aligned}
\delta W = \frac{1}{2\mu}\int \Bigg\{ & \frac{B^2}{B_p^2}\Big[\frac{\partial}{\partial s}(B_p \xi_A)\Big]^2 - \Big(2J\Big(J + \frac{\partial B_p}{\partial a}\Big) - B_p \frac{\partial \phi}{\partial a}\frac{\partial J}{\partial \phi}\Big)\xi_A^2 + \\
& + \Big[-B_y \tilde{F} - B_p \frac{\partial \xi_n}{\partial s} - B\frac{\partial}{\partial s}\Big(\frac{B_p}{B}\Big)\xi_n + B_y J \tilde{\xi}_A\Big]^2 + \\
& + \Big[-B_p \tilde{F} + B_y \frac{\partial \xi_n}{\partial s} - B_p \frac{\partial (B B_p)}{\partial n}\tilde{\xi}_n - \frac{\partial B_p^2}{\partial a}\tilde{\xi}_A - B_p J \tilde{\xi}_A\Big]^2 + \\
& + \frac{\mu \rho^2 c_s^2}{\partial \rho / \partial \phi}\tilde{A}\Big[\tilde{F} + B\frac{\partial \tilde{\xi}_\|}{\partial s} - J\tilde{\xi}_A\Big]^2 - \\
& - \frac{\mu \rho^2}{\partial \rho / \partial \phi}\Big[\tilde{F} + B\frac{\partial \tilde{\xi}_\|}{\partial s} - J\tilde{\xi}_A + \frac{\partial \rho / \partial \phi}{\rho}\tilde{\xi}_\phi\Big]^2\Bigg\}\, d\mathcal{V}.
\end{aligned}
$$

The last four terms of the integrand, i.e., those that hold the derivatives of the displacement across the field (contained in $\tilde{F}$), can be re-arranged by writing them as

$$
\begin{aligned}
(\alpha_1 \tilde{F} + a_1)^2 + (\alpha_2 \tilde{F} + a_2)^2 + \alpha_3(\tilde{F} + a_3)^2 + \alpha_4(\tilde{F} + a_4)^2 = \\
= (\alpha_1^2 + \alpha_2^2 + \alpha_3 + \alpha_4)\Big[\tilde{F} + \frac{\alpha_1 a_1 + \alpha_2 a_2 + \alpha_3 a_3 + \alpha_4 a_4}{\alpha_1^2 + \alpha_2^2 + \alpha_3 + \alpha_4}\Big]^2 + \\
+ a_1^2 + a_2^2 + \alpha_3 a_3^2 + \alpha_4 a_4^2 - \frac{(\alpha_1 a_1 + \alpha_2 a_2 + \alpha_3 a_3 + \alpha_4 a_4)^2}{\alpha_1^2 + \alpha_2^2 + \alpha_3 + \alpha_4},
\end{aligned}
$$

where

$$\alpha_1 = -B_y,$$

$$\alpha_2 = -B_p,$$

$$\alpha_3 = \frac{\mu\rho^2 c_s^2}{\partial\rho/\partial\phi}\tilde{A},$$

$$\alpha_4 = -\frac{\mu\rho^2}{\partial\rho/\partial\phi},$$

$$a_1 = -B_p\frac{\partial\xi_n}{\partial s} - B\frac{\partial}{\partial s}\Big(\frac{B_p}{B}\Big)\xi_n + B_y J\tilde{\xi}_A,$$

$$a_2 = B_y\frac{\partial\xi_n}{\partial s} - B_p\frac{\partial(BB_p)}{\partial n}\tilde{\xi}_n - \frac{\partial B_p^2}{\partial a}\tilde{\xi}_A - B_p J\tilde{\xi}_A,$$

$$a_3 = B\frac{\partial\tilde{\xi}_\parallel}{\partial s} - J\tilde{\xi}_A,$$

$$a_4 = B\frac{\partial\tilde{\xi}_\parallel}{\partial s} - J\tilde{\xi}_A + \frac{\partial\rho/\partial\phi}{\rho}\tilde{\xi}_\phi.$$

Now making use of the formulae

$$\alpha_1^2 + \alpha_2^2 + \alpha_3 + \alpha_4 = B^2 + \gamma\mu p,$$

$$\alpha_1 a_1 + \alpha_2 a_2 + \alpha_3 a_3 + \alpha_4 a_4 = -(B^2 + \gamma\mu p)J\tilde{\xi}_A + \gamma\mu p\Big(B\frac{\partial\tilde{\xi}_\parallel}{\partial s} - \frac{\tilde{\xi}_\phi}{c_s^2}\Big) + \\ + 2B_p\Big(\Big(J + \frac{\partial B_p}{\partial a}\Big)\xi_A + \frac{\partial B_p}{\partial n}\xi_n\Big),$$

and completing the squares in $\partial\tilde{\xi}_\parallel/\partial s$ and $\partial\xi_n/\partial s$, δW finally takes the form

$$\delta W = \frac{1}{2\mu}\int\Big\{\frac{B^2}{B_p^2}\Big[\frac{\partial}{\partial s}(B_p\xi_A)\Big]^2 - \Big(2J\Big(J + \frac{\partial B_p}{\partial a}\Big) - B_p\frac{\partial\phi}{\partial a}\frac{\partial J}{\partial\phi}\Big)\xi_A^2 - \mu\rho\tilde{A}\tilde{\xi}_\phi^2 + \\ + \frac{\gamma\mu p}{B^2 + \gamma\mu p}\Big[B\Big(B\frac{\partial\tilde{\xi}_\parallel}{\partial s} - \frac{\tilde{\xi}_\phi}{c_s^2}\Big) - 2\frac{B_p}{B}\Big(\Big(J + \frac{\partial B_p}{\partial a}\Big)\xi_A + \frac{\partial B_p}{\partial n}\xi_n\Big)\Big]^2 + \\ + \Big[B\frac{\partial\xi_n}{\partial s} - \frac{B_y}{B}\Big(2\Big(J + \frac{\partial B_p}{\partial a}\Big)\xi_A + \frac{\partial B_p}{\partial n}\xi_n\Big)\Big]^2 + \\ + (B^2 + \gamma\mu p)\Big[B_p\frac{\partial\tilde{\xi}_A}{\partial a} + BB_p\frac{\partial\tilde{\xi}_n}{\partial n} - J\tilde{\xi}_A + \frac{\gamma\mu p}{B^2 + \gamma\mu p}\Big(B\frac{\partial\tilde{\xi}_\parallel}{\partial s} - \frac{\tilde{\xi}_\phi}{c_s^2}\Big) + \\ + \frac{2B_p}{B^2 + \gamma\mu p}\Big(\Big(J + \frac{\partial B_p}{\partial a}\Big)\xi_A + \frac{\partial B_p}{\partial n}\xi_n\Big)\Big]^2\Big\}\,d\mathcal{V}.$$

Appendix E : The Effect of Gravity on the Stability of Equilibrium (3.4.8)

In the systems (3.3.8) and (3.3.11) for isothermal atmospheres the numerical value for the gravitational acceleration g enters the equations via the pressure scale height

$$H = \frac{\mathcal{R}T}{\tilde{\mu}g} .$$

Hence it influences the value for the dimensionless parameter

$$\bar{k} = \frac{\pi H}{L}$$

of equilibrium (3.4.8). We want to asses the effect of gravity on the stability in the simple case of a shearless field with no background plasma pressure and $\gamma = 5/3$, by calculating the value of

$$\frac{2\mu p}{B_z^2} = \frac{\beta_{1,2}}{\bar{k}^2} \operatorname{cotg}^2 \bar{k}\bar{x}\ \mathrm{e}^{-z}$$

(from Equation (3.4.8)), a crude estimate of the plasma beta $2\mu p/B^2$.

Recalling that *the* stability curve (when $\lambda = 0$ necessary and sufficient conditions coincide) originates at the 'island point' ($A = 1.0, 2\beta^{1/2} = j'_{2k,1}$) we find that

$$\bar{k} = 5 \qquad y'_{10,1} \approx 11.8 \qquad \frac{\beta_{1,2}}{\bar{k}^2} \approx 1.39$$

$$\bar{k} = 1 \qquad y'_{2,1} \approx 3.05 \qquad \frac{\beta_{1,2}}{\bar{k}^2} \approx 2.33$$

$$\bar{k} = \tfrac{1}{2} \qquad y'_{\frac{1}{2},1} \approx 1.17 \qquad \frac{\beta_{1,2}}{\bar{k}^2} \approx 5.48$$

and hence that the critical plasma beta, i.e., the value of the plasma beta for which the equilibrium becomes unstable, increases as g increases. This means that gravity plays a stabilising role in this field. This should not be too surprising since, for isothermal equilibria, the modified Brunt-Väisälä frequency is always non-negative and so implies a stable stratification. Thus an increase in the value of g will increase a positive contribution in the potential energy integral, making the system more stable.

Appendix F : An Expression for δW in Line-Tied 2-D Arbitrary Geometry

To rewrite the perturbed potential energy integral δW in the familiar form (1.4.1), consider as a starting point Equation (13) of Hu (1987), which in our coordinate system reads

$$\delta W = \frac{1}{2\mu}\int\left\{\frac{g^{33}}{B_p^2}\left[\mathbf{B}\cdot\nabla A_1\right]^2 + VA_1^2 + g_{33}\left[-B_3\nabla\cdot\left(g^{33}\boldsymbol{\xi}_p\right) + \mathbf{B}_p\cdot\nabla\xi^3\right]^2 + \right.$$
$$+\left[-\frac{1}{B_p}\left(g^{33}\nabla A\cdot\nabla A_1 + JA_1\right) - B_p\frac{\partial\xi^3}{\partial q^3} + B^3\frac{\partial\xi_{\|p}}{\partial q^3}\right]^2 + \qquad \text{(F.1)}$$
$$\left. + \gamma\mu p\left[\nabla\cdot\boldsymbol{\xi} - \frac{\tilde{\xi}_\phi}{c_s^2}\right]^2 - \mu\rho\tilde{A}\tilde{\xi}_\phi^2\right\}\,d\mathcal{V},$$

with

$$V = \nabla\cdot\left(\frac{g^{33}J\nabla A}{B_p^2}\right) - \frac{J^2}{B_p^2} - \frac{\partial J}{\partial A} + B_3B_3'\frac{\partial g^{33}}{\partial A}\ .$$

The following notations have been used :

$$\boldsymbol{\xi} = \boldsymbol{\xi}_p + \xi^3\mathbf{g}_3,$$
$$\xi_{\|p} = \frac{\boldsymbol{\xi}_p\cdot\mathbf{B}_p}{B_p},$$
$$A_1 = \boldsymbol{\xi}_p\cdot\nabla A,$$
$$\tilde{A} = \left(\frac{\rho}{\gamma p} + \frac{1}{\rho}\frac{\partial\rho}{\partial\phi}\right),$$
$$\tilde{\xi}_\phi = \nabla\phi\cdot\boldsymbol{\xi}.$$

Note that, as opposed to an upper index 3, an upper index 2 stands for an exponent. Also, $\partial/\partial A$ stands for the derivative with respect to A while ϕ is kept constant, and likewise $\partial/\partial\phi$ stands for the derivative with respect to ϕ while A is kept constant. Expression (F.1) reduces to (D.1) when g_{33} equals unity.

Changing the variables according to Appendix A.4, introducing the notations

$$\tilde{F} = B_p \frac{\partial \tilde{\xi}_A}{\partial a} + B B_p \frac{\partial \tilde{\xi}_n}{\partial n} - J \tilde{\xi}_A,$$

$$a_1 = -B \frac{\partial}{\partial s}\left(B_p^2 \tilde{\xi}_n\right) - B_3 B_p \left(\frac{\partial g^{33}}{\partial a} \tilde{\xi}_A + B \frac{\partial g^{33}}{\partial n} \tilde{\xi}_n\right),$$

$$a_2 = -2B_p\left(J + \frac{\partial B_p}{\partial a}\right)\tilde{\xi}_A + B_3 B_p B \frac{\partial \tilde{\xi}_n}{\partial s},$$

$$a_3 = B \frac{\partial \tilde{\xi}_\parallel}{\partial s} - \frac{\tilde{\xi}_\phi}{c_s^2},$$

and using the transformations

$$A_1 = B_p \xi_A,$$

$$\frac{\partial J}{\partial A} = \frac{1}{B_p}\frac{\partial J}{\partial a} - \frac{1}{B_p}\frac{\partial \phi}{\partial a}\frac{\partial J}{\partial \phi},$$

$$V = -\frac{2J}{B_p^2}\left(J + \frac{\partial B_p}{\partial a}\right) - \frac{\mu}{B_p}\frac{\partial \rho}{\partial A}\frac{\partial \phi}{\partial a} + \frac{B_3 B_3'}{B_p}\frac{\partial g^{33}}{\partial a},$$

$$-B_3 \nabla \cdot (g^{33} \boldsymbol{\xi}_p) + \mathbf{B}_p \cdot \nabla \xi^3 = -B^3 \tilde{F} + a_1,$$

$$-\frac{1}{B_p}(g^{33} \nabla A \cdot \nabla A_1 + J A_1) - B_p \frac{\partial \xi^3}{\partial q^3} + B^3 \frac{\partial \xi_{\parallel p}}{\partial q^3} = -B_p \tilde{F} + a_2,$$

$$\nabla \cdot \boldsymbol{\xi} - \frac{\tilde{\xi}_\phi}{c_s^2} = \tilde{F} + a_3,$$

noting that for an equilibrium quantity h, $B_3 \partial h/\partial s = B_p \partial h/\partial n$, one can rewrite the third, fourth, and fifth term in the integrand of Equation (F.1) as

$$g_{33}(-B^3 \tilde{F} + a_1)^2 + (-B_p \tilde{F} + a_2)^2 + \gamma \mu p (\tilde{F} + a_3)^2 =$$

$$= (B^2 + \gamma \mu p)\left[\tilde{F} + \frac{-B_3 a_1 - B_p a_2 + \gamma \mu p\, a_3}{B^2 + \gamma \mu p}\right]^2 +$$

$$+ g_{33} a_1^2 + a_2^2 + \gamma \mu p\, a_3^2 - \frac{(-B_3 a_1 - B_p a_2 + \gamma \mu p\, a_3)^2}{B^2 + \gamma \mu p}.$$

Now making use of the formulae

$$-B_3 a_1 - B_p a_2 + \gamma \mu p\, a_3 = \gamma \mu p\left(B \frac{\partial \tilde{\xi}_\parallel}{\partial s} - \frac{\tilde{\xi}_\phi}{c_s^2}\right) + \left(2\mu \frac{\partial p}{\partial A} B_p + \frac{\partial B^2}{\partial a}\right)\xi_A + \frac{\partial B^2}{\partial n}\xi_n,$$

$$2B^3\left(J + \frac{\partial B_p}{\partial a}\right) - B_3 B_p \frac{\partial g^{33}}{\partial a} = \frac{B^3}{B_p}\left(2\mu \frac{\partial p}{\partial A} B_p + g^{33}\frac{\partial}{\partial a}(g_{33} B^2)\right),$$

and completing the squares in $\partial \tilde{\xi}_\parallel/\partial s$ and $\partial \tilde{\xi}_n/\partial s$, δW finally takes the form

$$\delta W = \frac{1}{2\mu}(\mathcal{I} + \mathcal{J}),$$

where

$$\mathcal{I} = \int \Bigg\{ \frac{g^{33}B^2}{B_p^2}\left[\frac{\partial}{\partial s}(B_p^2\tilde{\xi}_A)\right]^2 - \left(2J\left(J + \frac{\partial B_p}{\partial a}\right) + \mu\frac{\partial \rho}{\partial A}B_p\frac{\partial \phi}{\partial a} - B_3 B_3' B_p \frac{\partial g^{33}}{\partial a}\right)\xi_A^2 -$$

$$-\mu\rho\tilde{A}\tilde{\xi}_\phi^2 + \frac{\gamma\mu p}{B^2+\gamma\mu p}\left[B\left(B\frac{\partial \tilde{\xi}_\parallel}{\partial s} - \frac{\tilde{\xi}_\phi}{c_s^2}\right) - \frac{1}{B}\left(\left(2\mu\frac{\partial p}{\partial A}B_p + \frac{\partial B^2}{\partial a}\right)\xi_A + \frac{\partial B^2}{\partial n}\xi_n\right)\right]^2 +$$

$$+ g_{33}\left[B_p\frac{\partial}{\partial s}(B^2\tilde{\xi}_n) - \frac{B^3}{BB_p}\left(2\mu\frac{\partial p}{\partial A}B_p + g^{33}\frac{\partial}{\partial a}\left(g_{33}B^2\right)\right)\xi_A\right]^2 \Bigg\}\, d\mathcal{V}$$

and

$$\mathcal{J} = \int \Bigg\{ (B^2+\gamma\mu p)\left[B_p\frac{\partial \tilde{\xi}_A}{\partial a} + BB_p\frac{\partial \tilde{\xi}_n}{\partial n} - J\tilde{\xi}_A + \frac{\gamma\mu p}{B^2+\gamma\mu p}\left(B\frac{\partial \tilde{\xi}_\parallel}{\partial s} - \frac{\tilde{\xi}_\phi}{c_s^2}\right) + \right.$$

$$\left. + \frac{1}{B^2+\gamma\mu p}\left(\left(2\mu\frac{\partial p}{\partial A}B_p + \frac{\partial B^2}{\partial a}\right)\xi_A + \frac{\partial B^2}{\partial n}\xi_n\right)\right]^2 \Bigg\}\, d\mathcal{V}.$$

Appendix G : Derivation of the Auxiliary Equation in System (5.3.5)

Starting off with

$$\begin{aligned}\nabla \times (S\mathbf{g}^3) &= \nabla S \times \mathbf{g}^3 \\ &= \frac{\nabla A \cdot \nabla S}{|\nabla A|^2}\nabla A \times \mathbf{g}^3 + \frac{\mathbf{B}_p \cdot \nabla S}{B_p^2}\mathbf{B}_p \times \mathbf{g}^3 \\ &= \frac{\nabla A \cdot \nabla S}{g_{33}B_p^2}\mathbf{B}_p - \frac{\mathbf{B}_p \cdot \nabla S}{g_{33}B_p^2}\nabla A,\end{aligned}$$

where S is defined by Equation (5.3.2), and taking the divergence yields

$$\nabla \cdot \nabla \times (S\mathbf{g}^3) = 0 = \nabla \cdot \left(\frac{\nabla A \cdot \nabla S}{g_{33}B_p^2}\mathbf{B}_p\right) - \nabla \cdot \left(\frac{\mathbf{B}_p \cdot \nabla S}{g_{33}B_p^2}\nabla A\right).$$

So,

$$\mathbf{B}_p \cdot \nabla \left(\frac{\nabla A \cdot \nabla S}{g_{33}B_p^2}\right) = -\nabla \cdot \left(\frac{B^3}{g_{33}B_p^2}\nabla A\right),$$

since $\nabla \cdot \mathbf{B}_p = 0$ and $\mathbf{B} \cdot \nabla S = 0 = B^3 + \mathbf{B}_p \cdot \nabla S$. Therefore,

$$\mathbf{B} \cdot \nabla \left(\frac{\nabla A \cdot \nabla S}{g_{33}B_p^2}\right) = -\frac{B^3}{B_p^2}\nabla \cdot \left(\frac{\nabla A}{g_{33}}\right) - \frac{\nabla A}{g_{33}} \cdot \nabla \left(\frac{g^{33}B_3}{B_p^2}\right),$$

i.e.,

$$\mathbf{B} \cdot \nabla \left(\frac{\nabla A \cdot \nabla S}{g_{33}B_p^2}\right) = -g^{33}\frac{dB_3}{dA} + \frac{B^3}{B_p^2}\left(J + 2\frac{\partial B_p}{\partial a} - g_{33}B_p\frac{\partial g^{33}}{\partial a}\right).$$

Use of the definitions

$$B\frac{\partial}{\partial s} = \mathbf{B} \cdot \nabla \quad \text{and} \quad y_5 = \frac{\nabla A \cdot \nabla S}{g_{33}B_p^2}$$

then results in the desired equation.

Appendix H : Normal Mode Analysis in Line-Tied 1-D Loop Geometry

H.1. Non-Force-Free Case

The aim is to derive the system of ordinary differential equations and corresponding boundary conditions for the radial displacement, constituting the eigenvalue problem governing the stability of a line-tied 1-D loop. We recall the components (6.2.3) of the linearised momentum equation,

$$-\mu\rho\omega^2\xi_r = B^2\frac{\partial^2\xi_r}{\partial s^2} + \frac{\partial}{\partial r}\left(\frac{B^2}{r}\frac{\partial}{\partial r}(r\xi_r)\right) - \frac{\partial}{\partial r}\left(\frac{B_\theta^2}{r^2}\right)r\xi_r + \\ + \frac{\partial}{\partial r}\left(B\frac{\partial\zeta}{\partial n}\right) + 2\frac{B_\theta}{r}\frac{\partial\zeta}{\partial z} + \frac{\partial}{\partial r}\left(\gamma\mu p\nabla\cdot\boldsymbol{\xi}\right), \tag{H.1a}$$

$$-\mu\rho\omega^2\xi_\parallel = B\frac{\partial}{\partial s}\left(\gamma\mu p\nabla\cdot\boldsymbol{\xi}\right), \tag{H.1b}$$

$$-\mu\rho\omega^2\zeta = B^2\frac{\partial^2\zeta}{\partial s^2} + B^2\frac{\partial^2\zeta}{\partial n^2} + \frac{B^3}{r}\frac{\partial}{\partial n}\left(\frac{\partial}{\partial r}(r\xi_r)\right) - \\ - 2\frac{B^2B_\theta}{r}\frac{\partial\xi_r}{\partial z} + B\frac{\partial}{\partial n}\left(\gamma\mu p\nabla\cdot\boldsymbol{\xi}\right), \tag{H.1c}$$

the Fourier decomposition (6.2.4) of the displacement vector $\boldsymbol{\xi}$,

$$\begin{aligned}
\xi_r(\mathbf{r}) &= \mathrm{Re}\sum_{m=-\infty}^{+\infty}\sum_{n=-\infty}^{+\infty}\xi_{nm}(r)\,\exp[i(m\theta + n\pi(\frac{2z}{L}+1))], \\
\xi_\parallel(\mathbf{r}) &= \mathrm{Re}\sum_{m=-\infty}^{+\infty}\sum_{n=-\infty}^{+\infty}\eta_{nm}(r)\,\exp[i(m\theta + n\pi(\frac{2z}{L}+1)+\frac{\pi}{2})], \\
\zeta(\mathbf{r}) &= \mathrm{Re}\sum_{m=-\infty}^{+\infty}\sum_{n=-\infty}^{+\infty}\zeta_{nm}(r)\,\exp[i(m\theta + n\pi(\frac{2z}{L}+1)+\frac{\pi}{2})],
\end{aligned} \tag{H.2}$$

and the rigid plate boundary conditions (6.2.5),

$$\forall r, m: \sum_{n=-\infty}^{+\infty}\xi_{nm}(r) = 0, \tag{H.3a}$$

$$\forall r, m: \sum_{n=-\infty}^{+\infty}\eta_{nm}(r) = 0, \tag{H.3b}$$

$$\forall r, m: \sum_{n=-\infty}^{+\infty}\zeta_{nm}(r) = 0. \tag{H.3c}$$

Note that the Fourier expansion (H.2) should not be used for the derivatives of the displacement vector in Equations (H.1), as the derivative of a Fourier series does not necessarily equal the Fourier series of a derivative.

To obtain the equations governing the radial dependence of the Fourier amplitudes of the displacement vector $\boldsymbol{\xi}$, Equations (H.1) are multiplied by the appropriate phase factors ($\exp[-i(m\theta + n\pi(\frac{2z}{L}+1))]$ for (H.1a), and $\exp[-i(m\theta + n\pi(\frac{2z}{L}+1)+\frac{\pi}{2})]$ for (H.1b) and (H.1c)), and integrated in θ and z. Due to the orthogonality property of the Fourier expansion functions, this will isolate one Fourier component. Upon integration by parts, terms involving second derivatives with respect to z will yield unknown surface contributions, because of what was mentioned at the end of the previous paragraph. These surface contributions will allow the constraints (H.3) to be satisfied.

To carry out the analysis outlined above, the following notations are introduced :

$$k_n = \frac{2n\pi}{L}\,, \qquad f_{nm}(r) = \frac{m}{r}B_\theta + k_n B_z, \qquad g_{nm}(r) = k_n B_\theta - \frac{m}{r}B_z,$$

$$\lambda_r(r) = \frac{1}{2\pi L}\left[\int_{-\pi}^{\pi} \frac{\partial \xi_r}{\partial z}\exp[-im\theta]d\theta\right]_{-L/2}^{L/2},$$

$$\lambda_\parallel(r) = \frac{1}{2\pi L}\left[\int_{-\pi}^{\pi} \frac{\partial \xi_\parallel}{\partial z}\exp[-i(m\theta+\frac{\pi}{2})]d\theta\right]_{-L/2}^{L/2},$$

$$\lambda_\perp(r) = \frac{1}{2\pi L}\left[\int_{-\pi}^{\pi} \frac{\partial \zeta}{\partial z}\exp[-i(m\theta+\frac{\pi}{2})]d\theta\right]_{-L/2}^{L/2}.$$

The appearance of the surface contributions $\lambda_r, \lambda_\parallel$, and $\lambda_\perp$ will now be illustrated by means of an example. Multiplying Equation (H.1b) by the phase factor $\exp[-i(m\theta + n\pi(\frac{2z}{L}+1)+\frac{\pi}{2})]$ and integrating in θ and z, one of the terms of the right hand side contains the factor

$$I_1 = \int_{-L/2}^{L/2}\int_{-\pi}^{\pi} \frac{\partial^2 \xi_\parallel}{\partial z^2}\exp[-i(m\theta + n\pi(\frac{2z}{L}+1)+\frac{\pi}{2})]d\theta dz.$$

This integral can be integrated by parts as follows :

$$\begin{aligned} I_1 &= \left[\int_{-\pi}^{\pi} \frac{\partial \xi_\parallel}{\partial z}\exp[-i(m\theta+\frac{\pi}{2})]d\theta\right]_{-L/2}^{L/2} + \\ &\quad + ik_n\int_{-L/2}^{L/2}\left(\int_{-\pi}^{\pi} \frac{\partial \xi_\parallel}{\partial z}\exp[-i(m\theta+\frac{\pi}{2})]d\theta\right)\exp[-in\pi(\frac{2z}{L}+1)]dz \\ &= 2\pi L\lambda_\parallel + ik_n\underbrace{\left[\int_{-\pi}^{\pi}\xi_\parallel\exp[-i(m\theta+\frac{\pi}{2})]d\theta\right]_{-L/2}^{L/2}}_{0} - \\ &\quad - k_n^2\underbrace{\int_{-L/2}^{L/2}\int_{-\pi}^{\pi}\xi_\parallel\exp[-i(m\theta+n\pi(\frac{2z}{L}+1)+\frac{\pi}{2})]d\theta dz}_{2\pi L\eta_{nm}}. \end{aligned}$$

One therefore arrives at

$$I_1 = 2\pi L\,(\lambda_{\|} - k_n^2 \eta_{nm})\,.$$

The rigid plate boundary conditions (1.4.2) and the orthogonality property of the Fourier expansion functions were used to evaluate the last two integrals. Similar manipulations are performed on Equations (H.1a) and (H.1c).

This transforms the parallel and perpendicular components of the perturbed equation of motion (H.1) into the matrix equation

$$A_{nm}\,\Xi_{nm} + B_{nm}\frac{(r\xi_{nm})'}{r} + C_n(r\xi_{nm}) + D\Lambda_m = \mathbf{0},$$

where

$$\Xi_{nm} = \begin{pmatrix} \eta_{nm} \\ \zeta_{nm} \end{pmatrix}, \qquad \Lambda_m = \begin{pmatrix} \lambda_{\|} \\ \lambda_{\perp} \end{pmatrix}, \qquad \mathbf{0} = \begin{pmatrix} 0 \\ 0 \end{pmatrix},$$

$$A_{nm} = \begin{pmatrix} -\mu\rho\omega^2 + \hat{\beta} f_{nm}^2 & \hat{\beta} f_{nm} g_{nm} \\ \hat{\beta} f_{nm} g_{nm} & -\mu\rho\omega^2 + f_{nm}^2 + (1+\hat{\beta}) g_{nm}^2 \end{pmatrix},$$

$$B_{nm} = -B^2 \begin{pmatrix} \hat{\beta} f_{nm} \\ (1+\hat{\beta}) g_{nm} \end{pmatrix}, \qquad C_n = \frac{B^2}{r} \begin{pmatrix} 0 \\ 2\frac{B_\theta}{r} k_n \end{pmatrix},$$

$$D = -\begin{pmatrix} \hat{\beta} B_z^2 & \hat{\beta} B_\theta B_z \\ \hat{\beta} B_\theta B_z & B^2 + \hat{\beta} B_\theta^2 \end{pmatrix},$$

and primes denote derivatives with respect to r. Using the constraints (H.3b) and (H.3c), this equation can be solved for $D\Lambda_m$ and Ξ_{nm} in terms of ξ_{nm} :

$$D\Lambda_m = -E_m^{-1}\left(\sum_n F_{nm}\frac{(r\xi_{nm})'}{r} + \sum_n G_{nm}(r\xi_{nm})\right),$$

$$\Xi_{nm} = -A_{nm}^{-1}\left(B_{nm}\frac{(r\xi_{nm})'}{r} + C_n(r\xi_{nm}) + D\Lambda_m\right),$$

where

$$E_m = \sum_n A_{nm}^{-1}, \qquad F_{nm} = A_{nm}^{-1} B_{nm}, \qquad G_{nm} = A_{nm}^{-1} C_n.$$

The radial component of the perturbed equation of motion then reads

$$-\left((B^2 + \gamma\mu p)\frac{(r\xi_{nm})'}{r}\right)' + (-\mu\rho\omega^2 + f_{nm}^2)\xi_{nm} + \left(\frac{B_\theta^2}{r^2}\right)' r\xi_{nm} + \\ + (H_{nm}\,\Xi_{nm})' + K_n \Xi_{nm} - B_z^2 \lambda_r = 0,$$

where

$$B_{nm} = -B^2 H_{nm}^{\mathrm{T}}, \qquad C_n = \frac{B^2}{r} K_n^{\mathrm{T}}.$$

For fixed m, this is the n^{th} equation of an infinite set of second order ordinary differential equations for ξ_n, coupled through the constraint (H.3a). Truncating the system to N harmonics, eliminating λ_r by substracting the N^{th} equation from the remaining $N-1$, and using the constraint (H.3a) to write ξ_N in terms of $\xi_n, n = 1, \ldots, N-1$, then results in a system of $(N-1)$ differential equations that can be written in the

form

$$(\mathcal{U}\mathbf{y}')' + \mathcal{V}\mathbf{y}' + \mathcal{W}\mathbf{y} = \mathbf{0}, \tag{H.4}$$

where $\mathbf{y}(r) = r(\xi_1, \ldots, \xi_{N-1})^{\mathrm{T}}$, and $\mathcal{U}, \mathcal{V}, \mathcal{W}$ are $(N-1) \times (N-1)$ matrices with elements

$$\mathcal{U}_{ij} = -(1+\delta_{ij})\frac{B^2+\gamma\mu p}{r} - \frac{H_i F_i}{r}\delta_{ij} - \frac{H_N F_N}{r} + \\ + (H_i A_i^{-1} - H_N A_N^{-1})E^{-1}\frac{F_j - F_N}{r}, \tag{H.5a}$$

$$\mathcal{V}_{ij} = (H_i A_i^{-1} - H_N A_N^{-1})E^{-1}(G_j - G_N) + \\ + (K_i A_i^{-1} - K_N A_N^{-1})E^{-1}\frac{F_j - F_N}{r}, \tag{H.5b}$$

$$\mathcal{W}_{ij} = \frac{-\mu\rho\omega^2 + f_i^2}{r}\delta_{ij} + \frac{-\mu\rho\omega^2 + f_N^2}{r} + (1+\delta_{ij})\left(\frac{B_\theta^2}{r^2}\right)' - \\ - K_i G_i \delta_{ij} - K_N G_N + (K_i A_i^{-1} - K_N A_N^{-1})E^{-1}(G_j - G_N) - \\ - [H_i G_i \delta_{ij} + H_N G_N - (H_i A_i^{-1} - H_N A_N^{-1})E^{-1}(G_j - G_N)]'. \tag{H.5c}$$

Note that $\mathcal{U}_{ji} = \mathcal{U}_{ij}$ and $\mathcal{V}_{ji} = -\mathcal{V}_{ij}$. The corresponding boundary conditions in the radial direction are (see, for instance, Hood and Priest, 1981)

$$y_i = 0 \qquad \text{at} \quad r = 0 \quad \text{and} \quad r = \infty, \qquad i = 1, \ldots, N-1. \tag{H.6}$$

H.2. Force-Free Case

When $p \equiv 0$, the right hand side of the perturbed momentum equation (1.3.9) with $\nabla\phi = \mathbf{0}$ is independent of $\xi_\parallel$, which may therefore be set equal to zero without loss of generality. The radial and perpendicular components of Equation (1.3.9) may then be written as

$$-\mu\rho\omega^2\xi_r = B^2\frac{\partial^2\xi_r}{\partial s^2} + \frac{\partial}{\partial r}\left(\frac{B^2}{r}\frac{\partial}{\partial r}(r\xi_r)\right) - \frac{\partial}{\partial r}\left(\frac{B_\theta^2}{r^2}\right)r\xi_r \\ + \frac{\partial}{\partial r}\left(B\frac{\partial\zeta}{\partial n}\right) + 2\frac{B_\theta}{r}\frac{\partial\zeta}{\partial z}, \tag{H.7a}$$

$$-\mu\rho\omega^2\zeta = B^2\frac{\partial^2\zeta}{\partial s^2} + B^2\frac{\partial^2\zeta}{\partial n^2} + \frac{B^3}{r}\frac{\partial}{\partial n}\left(\frac{\partial}{\partial r}(r\xi_r)\right) - 2\frac{B^2 B_\theta}{r}\frac{\partial\xi_r}{\partial z}. \tag{H.7b}$$

An analysis similar to that of the previous Section may now be carried out. Equation (H.7b) is transformed into

$$\tilde{A}_{nm}\zeta_{nm} - g_{nm}\frac{(r\xi_{nm})'}{r} + 2\frac{B_\theta}{r}k_n\xi_{nm} - \lambda_\perp = 0,$$

where

$$\tilde{A}_{nm} = \frac{-\mu\rho\omega^2 + f_{nm}^2 + g_{nm}^2}{B^2}.$$

Using the constraint (H.3c), this equation can be solved for $\lambda_\perp$ and ζ_{nm} in terms of

the radial Fourier component ξ_{nm} :

$$\lambda_\perp = -\frac{1}{\tilde{E}_m}\left(\sum_n \frac{g_{nm}}{\tilde{A}_{nm}}\frac{(r\xi_{nm})'}{r} - \sum_n \frac{1}{\tilde{A}_{nm}} 2\frac{B_\theta}{r} k_n \xi_{nm}\right),$$

$$\zeta_{nm} = \frac{1}{\tilde{A}_{nm}}\left(g_{nm}\frac{(r\xi_{nm})'}{r} - 2\frac{B_\theta}{r}k_n\xi_{nm} + \lambda_\perp\right),$$

where

$$\tilde{E}_m = \sum_n \frac{1}{\tilde{A}_{nm}}\,.$$

The radial component of the perturbed equation of motion, (H.7a), then reads

$$-\left(B^2\frac{(r\xi_{nm})'}{r}\right)' + (-\mu\rho\omega^2 + f_{nm}^2)\xi_{nm} + \left(\frac{B_\theta^2}{r^2}\right)' r\xi_{nm} + (g_{nm}\zeta_{nm})' + 2\frac{B_\theta}{r}k_n\zeta_{nm} - B_z^2\lambda_r = 0.$$

Following the lines of the previous Section, this too leads to a system of $(N-1)$ differential equations of the form (H.4) with radial boundary conditions (H.6). Here, the matrix elements are

$$\mathcal{U}_{ij} = -\frac{-\mu\rho\omega^2 + f_i^2}{r\tilde{A}_i}\delta_{ij} - \frac{-\mu\rho\omega^2 + f_N^2}{r\tilde{A}_N} - \frac{1}{r\tilde{E}}\left(\frac{g_i}{\tilde{A}_i} - \frac{g_N}{\tilde{A}_N}\right)\left(\frac{g_j}{\tilde{A}_j} - \frac{g_N}{\tilde{A}_N}\right), \tag{H.8a}$$

$$\mathcal{V}_{ij} = \frac{2B_\theta}{r^2\tilde{E}}\left[\left(\frac{g_i}{\tilde{A}_i} - \frac{g_N}{\tilde{A}_N}\right)\left(\frac{k_j}{\tilde{A}_j} - \frac{k_N}{\tilde{A}_N}\right) - \left(\frac{g_j}{\tilde{A}_j} - \frac{g_N}{\tilde{A}_N}\right)\left(\frac{k_i}{\tilde{A}_i} - \frac{k_N}{\tilde{A}_N}\right)\right], \tag{H.8b}$$

$$\begin{aligned}\mathcal{W}_{ij} = {} & \frac{-\mu\rho\omega^2 + f_i^2}{r}\delta_{ij} + \frac{-\mu\rho\omega^2 + f_N^2}{r} + (1+\delta_{ij})\left(\frac{B_\theta^2}{r^2}\right)' - \\ & - \frac{4B_\theta^2}{r^3}\left[\frac{k_i^2}{\tilde{A}_i}\delta_{ij} + \frac{k_N^2}{\tilde{A}_N} - \frac{1}{\tilde{E}}\left(\frac{k_i}{\tilde{A}_i} - \frac{k_N}{\tilde{A}_N}\right)\left(\frac{k_j}{\tilde{A}_j} - \frac{k_N}{\tilde{A}_N}\right)\right] - \\ & - \left\{\frac{2B_\theta}{r^2}\left[\frac{g_i k_i}{\tilde{A}_i}\delta_{ij} + \frac{g_N k_N}{\tilde{A}_N} - \frac{1}{\tilde{E}}\left(\frac{g_i}{\tilde{A}_i} - \frac{g_N}{\tilde{A}_N}\right)\left(\frac{k_j}{\tilde{A}_j} - \frac{k_N}{\tilde{A}_N}\right)\right]\right\}'.\end{aligned} \tag{H.8c}$$

As before, $\mathcal{U}_{ji} = \mathcal{U}_{ij}$ and $\mathcal{V}_{ji} = -\mathcal{V}_{ij}$.

References

Abramowitz, M. and Stegun, I. A.: 1970, *Handbook of Mathematical Functions*, Dover Publications, New York.

Adam, J. A.: 1978, *J. Plasma Phys.* **19**, 77.

Aly, J. J.: 1990a, *Comp. Phys. Comm.* **59**, 13.

Aly, J. J.: 1990b, *Phys. Fluids B* **2**, 1928.

An, C.-H.: 1984, *Astrophys. J.* **281**, 419.

An, C.-H., Suess, S. T., and Wu, S. T.: 1989, *Astrophys. J.* **337**, 989.

Anzer, U.: 1968, *Solar Phys.* **3**, 298.

Anzer, U.: 1969, *Solar Phys.* **8**, 37.

Anzer, U.: 1989, in E. R. Priest (ed), *Dynamics and Structure of Quiescent Solar Prominences*, Kluwer Academic Publishers, Holland.

Appert, K., Gruber, R., and Vaclavik, J.: 1974, *Phys. Fluids* **17**, 1471.

Arendt, U. and Schindler, K.: 1988, *Astron. Astrophys.* **204**, 229.

Asséo, E., Cesarsky, C. J., Lachièze-Rey, M., and Pellat, R.: 1978, *Astrophys. J.* **225**, L21.

Asséo, E., Cesarsky, C. J., Lachièze-Rey, M., and Pellat, R.: 1980, *Astrophys. J.* **237**, 752.

Barnes, C. W. and Sturrock, P. A.: 1972, *Astrophys. J.* **174**, 659.

Barston, E. M.: 1969, *Phys. Fluids* **12**, 2162.

Bateman, G.: 1978, *MHD Instabilities*, MIT Press, Cambridge, Massachusetts.

Berge, G.: 1969, *Culham Report* , No CLM–R97.

Berger, M. A.: 1985, *Astrophys. J. Suppl.* **59**, 433.

Bernstein, I. B., Frieman, E. A., Kruskal, M. D., and Kulsrud, R. M.: 1958, *Proc. Roy. Soc. London* **A244**, 17.

Birn, J., Goldstein, H., and Schindler, K.: 1978, *Solar Phys.* **57**, 81.

Birn, J. and Schindler, K.: 1981, in E. R. Priest (ed), *Solar Flare Magnetohydrodynamics*, Gordon and Breach Science Publishers, New York.

Bogdan, T. J.: 1985, *Astrophys. J.* **288**, 672.

Bogdan, T. J. and Low, B. C.: 1986, *Astrophys. J.* **306**, 271.

Bondeson, A., Iacono, R., and Bhattacharjee, A.: 1987, *Phys. Fluids* **30**, 2167.

Boyd, T. J. M. and Sanderson, J. J.: 1969, *Plasma Dynamics*, Nelson, London.

Braginskii, S. I.: 1965, in M. A. Leontovich (ed), *Reviews of Plasma Physics*, Consultants Bureau, New York, **1**, 205.

Brown, A.: 1958, *Astrophys. J.* **128**, 646.

Browning, P. K.: 1988, *Phys. Rep.* **169**, 329.

Browning, P. K. and Hood, A. W.: 1989, *Solar Phys.* **124**, 271.

Cargill, P. J. and Hood, A. W.: 1989, *Solar Phys.* **124**, 101.

Cargill, P. J. and Hood, A. W.: 1990, *Solar Phys.* , submitted.

Cargill, P. J., Hood, A. W., and Migliuolo, S.: 1986, *Astrophys. J.* **309**, 402.

Chandrasekhar, S.: 1961, *Hydrodynamic and Hydromagnetic Stability*, Clarendon Press, Oxford.

Chiuderi, C. and Einaudi, G.: 1981, *Solar Phys.* **73**, 89.

Chiuderi, C., Einaudi, G., Ma, S. S., and Van Hoven, G.: 1980, *J. Plasma Phys.* **24**, 39.

Chiueh, T. and Zweibel, E. G.: 1989, *Astrophys. J.* **338**, 1158.

Chu, M. S., Chance, M. S., Greene, J. M., and Jensen, T. H.: 1989, *Phys. Fluids B* **1**, 62.

Chu, M. S., Chance, M. S., Greene, J. M., and Jensen, T. H.: 1990, *Phys. Fluids B* **2**, 97.

Chun, S. T. and Hameiri, E.: 1990, *Phys. Fluids B* **2**, 1745.

Conner, J. W. and Hastie, R. J.: 1985, *Plasma Phys. Control. Fusion* **27**, 621.

Conner, J. W., Hastie, R. J., and Taylor, J. B.: 1979, *Proc. Roy. Soc. London* **A365**, 1.

Corbelli, E. and Torricelli-Ciamponi, G.: 1990, *Phys. Fluids B* **2**, 828.

Cox, J. P.: 1980, *Theory of Stellar Pulsation*, Princeton University Press, Princeton, New Jersey.

Cox, P. M.: 1990, *Plasma Phys. Control. Fusion* **32**, 553.

Craig, I. J. D., McClymont, A. N., and Sneyd, A. D.: 1988, *Astrophys. J.* **335**, 441.

Craig, I. J. D., Robb, T. D., Sneyd, A. D., and McClymont, A. N.: 1990, *Astrophys. Space Science* **166**, 289.

Craig, I. J. D. and Sneyd, A. D.: 1990, *Astrophys. J.* **357**, 653.

De Bruyne, P. and Hood, A. W.: 1989a, *Solar Phys.* **119**, 87.

De Bruyne, P. and Hood, A. W.: 1989b, *Solar Phys.* **123**, 241.

De Bruyne, P. and Hood, A. W.: 1989c, *Hvar Obs. Bull.* **13**, 269.

De Bruyne, P., Velli, M., and Hood, A. W.: 1990a, *Comp. Phys. Comm.* **59**, 55.

De Bruyne, P., Velli, M., and Hood, A. W.: 1990b, *Publ. Debrecen Heliophys. Obs.* , in press.

Démoulin, P., Priest, E. R., and Anzer, U.: 1989, *Astron. Astrophys.* **221**, 326.

Dewar, R. L. and Glasser, A. H.: 1983, *Phys. Fluids* **26**, 3038.

Dewar, R. L., Manickam, J., Grimm, R. C., and Chance, M. S.: 1981, *Nuclear Fusion* **21**, 493.

Dungey, J. W.: 1953, *Monthly Notices Roy. Astron. Soc.* **113**, 180.

Eckhoff, K. S.: 1987, *Phys. Fluids* **30**, 3673.

Edenstrasser, J. W.: 1978, *J. Plasma Phys.* **20**, 503.

Edenstrasser, J. W.: 1980a, *J. Plasma Phys.* **24**, 299.

Edenstrasser, J. W.: 1980b, *J. Plasma Phys.* **24**, 515.

Einaudi, G. and Rubini, F.: 1986, *Phys. Fluids* **29**, 2563.

Einaudi, G. and Rubini, F.: 1989, *Phys. Fluids B* **1**, 2224.

Einaudi, G. and Van Hoven, G.: 1981, *Phys. Fluids* **24**, 1092.

Einaudi, G. and Van Hoven, G.: 1983, *Solar Phys.* **88**, 163.

Ferrari, A.: 1985, in M. R. Kundu and G. D. Holman (eds), *Unstable Current Systems and Plasma Instabilities in Astrophysics*, D. Reidel Publ. Co., Dordrecht, Holland.

Fiedler, R. A. S. and Cally, P. S.: 1990, *Solar Phys.* **126**, 69.

Finan, C. H. III and Killeen, J.: 1981, *Comp. Phys. Comm.* **24**, 441.

Finn, J. M. and Chen, J.: 1990, *Astrophys. J.* **349**, 345.

Foote, B. J. and Craig, I. J. D.: 1990, *Astrophys. J.* **350**, 437.

Foukal, P.: 1971, *Solar Phys.* **19**, 59.

Freidberg, J. P.: 1970, *Phys. Fluids* **13**, 1812.

Freidberg, J. P.: 1982, *Rev. Mod. Phys.* **54**, 801.

Freidberg, J. P.: 1987, *Ideal Magnetohydrodynamics*, Plenum Press, New York.

Friedrichs, K. O.: 1960, *Rev. Mod. Phys.* **32**, 889.

Frieman, E. and Rotenberg, M.: 1960, *Rev. Mod. Phys.* **32**, 898.

Furth, H. P., Killeen, J., and Rosenbluth, M. N.: 1963, *Phys. Fluids* **6**, 459.

Galindo Trejo, J.: 1987, *Solar Phys.* **108**, 265.

Galindo Trejo, J.: 1989a, *Geophys. Astrophys. Fluid Dyn.* **47**, 69.

Galindo Trejo, J.: 1989b, *Rev. Mexicana Astron. Astrof.* **17**, 47.

Galindo Trejo, J. and Schindler, K.: 1984, *Astrophys. J.* **277**, 422.

Gautschy, A. and Glatzel, W.: 1990, *Monthly Notices Roy. Astron. Soc.* **245**, 154.

Giachetti, R., Van Hoven, G., and Chiuderi, C.: 1977, *Solar Phys.* **55**, 371.

Goedbloed, J. P.: 1971a, *Physica* **53**, 412.

Goedbloed, J. P.: 1971b, *Physica* **53**, 501.

Goedbloed, J. P.: 1971c, *Physica* **53**, 535.

Goedbloed, J. P.: 1983, *Lecture Notes on Ideal Magnetohydrodynamics*, Rijnhuizen Report 83–145.

Goedbloed, J. P.: 1990, *Comp. Phys. Comm.* **59**, 39.

Goedbloed, J. P. and Hagebeuk, H. J. L.: 1972, *Phys. Fluids* **15**, 1090.

Goedbloed, J. P. and Sakanaka, P. H.: 1974, *Phys. Fluids* **17**, 908.

Goedbloed, J. P. and Schuurman, W.: 1972, *Plasma Phys.* **14**, 1.

Gold, T. and Hoyle, F.: 1960, *Monthly Notices Roy. Astron. Soc.* **120**, 89.

Grassie, K. and Krech, M.: 1990, *Phys. Fluids B* **2**, 536.

Gratton, J., Gratton, F. T., and González, A. G.: 1988, *Plasma Phys. Control. Fusion* **30**, 435.

Greene, J. M. and Johnson, J. L.: 1968, *Plasma Phys.* **10**, 729.

Hagyard, M. J., Gaizauskas, V., Chapman, G. A., deLoach, A. C., Gary, G. A., Jones, H. P., Karpen, J. T., Martres, M.-J., Porter, J. G., Schmieder, B., Smith, J. B. Jr., and Toomre, J.: 1986, in M. Kundu and B. Woodgate (eds), *Energetic Phenomena on the Sun*, NASA Conference Publ. 2439.

Hain, K. Von and Lüst, R.: 1958, *Z. Naturforschg.* **13a**, 936.

Hain, K. Von, Lüst, R., and Schlüter, A.: 1957, *Z. Naturforschg.* **12a**, 833.

Hassam, A. B.: 1990, *Astrophys. J.* **348**, 778.

Helmholtz, H.: 1868, *Phil. Mag. (Ser. IV)* **36**, 337.

Hirayama, T.: 1985, *Solar Phys.* **100**, 415.

Hirayama, T.: 1989, *Hvar Obs. Bull.* **13**, in press.

Hood, A. W.: 1983a, *Solar Phys.* **87**, 279.

Hood, A. W.: 1983b, *Solar Phys.* **89**, 235.

Hood, A. W.: 1984, *Geophys. Astrophys. Fluid Dyn.* **28**, 223.

Hood, A. W.: 1986a, *Solar Phys.* **103**, 329.

Hood, A. W.: 1986b, *Solar Phys.* **105**, 307.

Hood, A. W.: 1989, in E. R. Priest (ed), *Dynamics and Structure of Quiescent Solar Prominences*, Kluwer Academic Publishers, Holland.

Hood, A. W.: 1990, *Comp. Phys. Rep.* **12**, 177.

Hood, A. and Anzer, U.: 1987, *Solar Phys.* **111**, 333.

Hood, A. and Anzer, U.: 1988, *Solar Phys.* **115**, 61.

Hood, A. W. and Anzer, U.: 1990, *Solar Phys.* **126**, 117.

Hood, A. W., Cargill, P. J., Van der Linden, R. A. M., and Goossens, M.: 1990, *Solar Phys.* , submitted.

Hood, A. W. and Priest, E. R.: 1979, *Solar Phys.* **64**, 303.

Hood, A. W. and Priest, E. R.: 1980, *Solar Phys.* **66**, 113.

Hood, A. W. and Priest, E. R.: 1981, *Geophys. Astrophys. Fluid Dyn.* **17**, 297.

Hood, A. W., Van der Linden, R., and Goossens, M.: 1989, *Solar Phys.* **120**, 261.

Hu, Y. Q.: 1987, *Scientia Sinica (Ser. A)* **30**, 509.

Hu, Y. Q.: 1988, *Astrophys. J.* **331**, 402.

Hughes, D. W. and Cattaneo, F.: 1987, *Geophys. Astrophys. Fluid Dyn.* **39**, 65.

Hundhausen, J. R., Hundhausen, A. J., and Zweibel, E. G.: 1981, *J. Geophys. Res.* **86**, 11117.

Jeffrey, A. and Taniuti, T.: 1966, *Magnetohydrodynamic Stability and Thermonuclear Containment*, Academic Press, New York.

Jockers, K.: 1976, *Solar Phys.* **50**, 405.

Jockers, K.: 1978, *Solar Phys.* **56**, 37.

Kadomtsev, B. B.: 1966, in M. A. Leontovich (ed), *Reviews of Plasma Physics*, Consultants Bureau, New York, **2**, 153.

Kerner, W.: 1990, *Comp. Phys. Rep.* **12**, 135.

Kippenhahn, R. and Schlüter, A.: 1957, *Z. Astrophysik* **43**, 36.

Kirby, P.: 1985, *Culham Theor. Phys. Note* , No 85/1.

Klimchuk, J. A. and Sturrock, P. A.: 1989, *Astrophys. J.* **345**, 1034.

Klimchuk, J. A., Sturrock, P. A., and Yang, W.-H.: 1988, *Astrophys. J.* **335**, 456.

Kovetz, A.: 1966, *Astrophys. J.* **146**, 462.

Kruskal, M. and Schwarzschild, M.: 1954, *Proc. Roy. Soc. London* **A223**, 348.

Kuijpers, J.: 1989, in M. A. Dubois (ed), *Proc. Ninth Cargese Workshop on Plasma Turbulence*, Les Editions de Physique, France.

Kuperus, M. and Raadu, M.: 1974, *Astron. Astrophys.* **31**, 189.

Laval, G., Mercier, C., and Pellat, R.: 1965, *Nuclear Fusion* **5**, 156.

Lentini, M. and Pereyra, V.: 1977, *SIAM J. Numer. Anal.* **14**, 91.

Lerche, I. and Low, B. C.: 1980, *Solar Phys.* **67**, 229.

Leroy, J. L.: 1989, in E. R. Priest (ed), *Dynamics and Structure of Quiescent Solar Prominences*, Kluwer Academic Publishers, Holland.

Leroy, J. L., Bommier, V., and Sahal-Bréchot, S.: 1983, *Solar Phys.* **83**, 135.

Lothian, R. M. and Hood, A. W.: 1989, *Solar Phys.* **122**, 227.

Low, B. C.: 1975a, *Astrophys. J.* **197**, 251.

Low, B. C.: 1975b, *Astrophys. J.* **198**, 211.

Low, B. C.: 1977a, *Astrophys. J.* **212**, 234.
Low, B. C.: 1977b, *Astrophys. J.* **217**, 988.
Low, B. C.: 1980, *Solar Phys.* **65**, 147.
Low, B. C.: 1981a, *Astrophys. J.* **246**, 538.
Low, B. C.: 1981b, *Astrophys. J.* **251**, 352.
Low, B. C.: 1982a, *Solar Phys.* **77**, 43.
Low, B. C.: 1982b, *Astrophys. J.* **263**, 952.
Low, B. C.: 1984a, *Astrophys. J.* **277**, 415.
Low, B. C.: 1984b, *Astrophys. J.* **286**, 772.
Low, B. C.: 1985a, *Astrophys. J.* **293**, 31.
Low, B. C.: 1985b, *Solar Phys.* **100**, 309.
Low, B. C.: 1988a, *Solar Phys.* **115**, 269.
Low, B. C.: 1988b, *Astrophys. J.* **330**, 992.
Low, B. C., Hundhausen, A. J., and Zweibel, E. G.: 1983, *Phys. Fluids* **26**, 2731.
Low, B. C. and Lou, Y. Q.: 1990, *Astrophys. J.* **352**, 343.
Lowder, R. S. and Thomassen, K. I.: 1973, *Phys. Fluids* **16**, 1497.
Lundquist, S.: 1951, *Phys. Rev. (Ser. II)* **83**, 307.
Lynden-Bell, D. and Ostriker, J. P.: 1967, *Monthly Notices Roy. Astron. Soc.* **136**, 293.
Melville, J. P., Hood, A. W., and Priest, E. R.: 1983, *Solar Phys.* **87**, 301.
Melville, J. P., Hood, A. W., and Priest, E. R.: 1984, *Solar Phys.* **92**, 15.
Melville, J. P., Hood, A. W., and Priest, E. R.: 1986, *Solar Phys.* **105**, 291.
Melville, J. P., Hood, A. W., and Priest, E. R.: 1987, *Geophys. Astrophys. Fluid Dyn.* **39**, 83.
Menzel, D. H.: 1951, in *Proc. of Conferences on Dynamics of Ionised Media*, University College, London.
Mercier, C.: 1960, *Nuclear Fusion* **1**, 47.
Migliuolo, S.: 1982, *J. Geophys. Res.* **87**, 8057.
Migliuolo, S. and Cargill, P. J.: 1983, *Astrophys. J.* **271**, 820.
Migliuolo, S., Cargill, P. J., and Hood, A. W.: 1984, *Astrophys. J.* **281**, 413.
Mikić, Z.: 1990, *Phys. Fluids B* **2**, 1450.
Mikić, Z., Barnes, D. C., and Schnack, D. D.: 1988, *Astrophys. J.* **328**, 830.
Mikić, Z., Schnack, D. D., and Van Hoven, G.: 1990, *Astrophys. J.* , submitted.
Mok, Y. and Van Hoven, G.: 1982, *Phys. Fluids* **25**, 636.
Molodensky, M. M.: 1974, *Solar Phys.* **39**, 393.
Molodensky, M. M.: 1975, *Solar Phys.* **43**, 311.

Molodensky, M. M.: 1976, *Solar Phys.* **49**, 279.

Mondt, J. P. and Weiland, J.: 1985, *J. Plasma Phys.* **34**, 143.

Moss, D. L. and Tayler, R. J.: 1969, *Monthly Notices Roy. Astron. Soc.* **145**, 217.

Nakajima, N.: 1990, *Phys. Fluids B* **2**, 1170.

Nakajima, N. and Hamaguchi, S.: 1990, *Phys. Fluids B* **2**, 1184.

Newcomb, W. A.: 1960, *Ann. Phys.* **10**, 232.

Newcomb, W. A.: 1961, *Phys. Fluids* **4**, 391.

Otani, N. F. and Strauss, H. R.: 1988, *Astrophys. J.* **325**, 468.

Pao, Y.: 1978, *Phys. Fluids* **21**, 765.

Parker, E. N.: 1979, *Cosmical Magnetic Fields*, Clarendon Press, Oxford.

Pegoraro, F. and Schep, T. J.: 1981, *Phys. Fluids* **24**, 478.

Pietrini, P. and Torricelli-Ciamponi, G.: 1989, *Phys. Fluids B* **1**, 923.

Press, W. H., Flannery, B. P., Teukolsky, S. A., and Vetterling, W. T.: 1987, *Numerical Recipes*, Cambridge University Press, Cambridge.

Priest, E. R.: 1981, in F. Q. Orrall (ed), *Solar Active Regions*, Colorado Associated University Press.

Priest, E. R.: 1982, *Solar Magnetohydrodynamics*, D. Reidel Publ. Co., Dordrecht, Holland.

Priest, E. R. (ed): 1989, *Dynamics and Structure of Quiescent Solar Prominences*, Kluwer Academic Publishers, Dordrecht, Holland.

Priest, E. R., Hood, A. W., and Anzer, U.: 1989, *Astrophys. J.* **344**, 1010.

Raadu, M. A.: 1972, *Solar Phys.* **22**, 425.

Ray, A. and Van Hoven, G.: 1982, *Solar Phys.* **79**, 353.

Rayleigh, Lord: 1883, *Proc. London Math. Soc. (Ser. I)* **14**, 170.

Roberts, K. V. and Taylor, J. B.: 1965, *Phys. Fluids* **8**, 315.

Roberts, P. H.: 1967, *An Introduction to Magnetohydrodynamics*, Longmans, London.

Robinson, D. C.: 1971, *Plasma Phys.* **13**, 439.

Rosner, R., Low, B. C., and Holzer, T. E.: 1986, in P. A. Sturrock, T. E. Holzer, D. M. Mihalas, and R. K. Ulrich (eds), *Physics of the Sun*, D. Reidel Publ. Co., Dordrecht, Holland.

Sakanaka, P. H. and Goedbloed, J. P.: 1974, *Phys. Fluids* **17**, 919.

Sakurai, T.: 1976, *Publ. Astron. Soc. Japan* **28**, 177.

Sakurai, T.: 1989, *Solar Phys.* **121**, 347.

Schindler, K., Birn, J., and Janicke, L.: 1983, *Solar Phys.* **87**, 103.

Schmieder, B.: 1989, in E. R. Priest (ed), *Dynamics and Structure of Quiescent Solar Prominences*, Kluwer Academic Publishers, Dordrecht, Holland.

Schnack, D. D., Mikić, Z., Barnes, D. C., and Van Hoven, G.: 1990, *Comp. Phys. Comm.* **59**, 21.

Schwarzschild, K.: 1906, *Göttinger Wiss. Nachr. (Math.-Phys. Klasse)* **1**, 41.

Schwarzschild, M.: 1958, *Structure and Evolution of the Stars*, Princeton University Press, Princeton, New Jersey.

Shafranov, V. D.: 1970, *Soviet Phys.-Tech. Phys.* **15**, 175.

Sneyd, A. D. and Craig, I. J. D.: 1989, *Astrophys. Space Science* **151**, 265.

Solov'ev, L. S.: 1967, in M. A. Leontovich (ed), *Reviews of Plasma Physics*, Consultants Bureau, New York, **3**, 277.

Sparks, L. and Van Hoven, G.: 1988, *Astrophys. J.* **333**, 953.

Sparks, L., Van Hoven, G., and Schnack, D. D.: 1990, *Astrophys. J.* **353**, 297.

Spies, G. O.: 1974, *Phys. Fluids* **17**, 2019.

Spies, G. O.: 1988, *Plasma Phys. Control. Fusion* **30**, 1025.

Strauss, H. R.: 1981, *Phys. Fluids* **24**, 2004.

Strauss, H. R.: 1989, *Geophys. Res. Lett.* **16**, 219.

Su Qing-rui: 1984, *Acta Astron. Sinica* **25**, 376.

Suydam, B. R.: 1958, in *Proc. Second United Nations Internat. Conference on the Peaceful Uses of Atomic Energy*, United Nations, Geneva, **31**, 157.

Tasso, H.: 1975, *Plasma Phys.* **17**, 1131.

Tasso, H.: 1977, *Plasma Phys.* **19**, 177.

Tayler, R. J.: 1957, *Phil. Mag. (Ser. VIII)* **2**, 33.

Tayler, R. J.: 1973, *Monthly Notices Roy. Astron. Soc.* **161**, 365.

Taylor, Sir Geoffrey: 1950, *Proc. Roy. Soc. London* **A201**, 192.

Taylor, J. B.: 1986, *Rev. Mod. Phys.* **58**, 741.

Thomson, Sir William: 1871, *Phil. Mag. (Ser. IV)* **42**, 362.

Tsinganos, K. C.: 1982, *Astrophys. J.* **259**, 820.

Uchida, Y.: 1986, *Astrophys. Space Science* **118**, 127.

Van Assche, W., Tayler, R. J., and Goossens, M.: 1982, *Astron. Astrophys.* **109**, 166.

Van Ballegooijen, A. A. and Martens, P. C. H.: 1989, *Astrophys. J.* **343**, 971.

Van der Linden, R., Goossens, M., and Hood, A. W.: 1988, *Solar Phys.* **115**, 235.

Van der Linden, R. A. M., Goossens, M., and Kerner, W.: 1990, *Comp. Phys. Comm.* **59**, 61.

Van Hoven, G.: 1981, in E. R. Priest (ed), *Solar Flare Magnetohydrodynamics*, Gordon and Breach Science Publishers, New York.

Velli, M., Einaudi, G., and Hood, A. W.: 1990a, *Astrophys. J.* **350**, 419.

Velli, M., Einaudi, G., and Hood, A. W.: 1990b, *Astrophys. J.* **350**, 428.

Velli, M. and Hood, A. W.: 1986, *Solar Phys.* **106**, 353.

Velli, M. and Hood, A. W.: 1987, *Solar Phys.* **109**, 351.

Velli, M. and Hood, A. W.: 1989, *Solar Phys.* **119**, 107.

Velli, M., Hood, A. W., and Einaudi, G.: 1988, in *Proc. Internat. Workshop on Reconnection in Space Plasma*, Potsdam, GDR, ESA SP–285 (Vol II).

Voslamber, D. and Callebaut, D. K.: 1962, *Phys. Rev. (Ser. II)* **128**, 2016.

Vršnak, B.: 1990, *Astrophys. Space Science* , in press.

Vršnak, B., Ruždjak, V., Brajša, R., and Zloch, F.: 1990, *Solar Phys.* **127**, 119.

Webb, G. M. and Ko, C. M.: 1989, *Astrophys. J.* **342**, 1142.

Wesson, J. A.: 1978, *Nuclear Fusion* **18**, 87.

Wolfson, R. L. T.: 1982, *Astrophys. J.* **255**, 774.

Woltjer, L.: 1958a, *Proc. Nat. Acad. Sci. USA* **44**, 489.

Woltjer, L.: 1958b, *Proc. Nat. Acad. Sci. USA* **44**, 833.

Woltjer, L.: 1959, *Proc. Nat. Acad. Sci. USA* **45**, 769.

Woolley, M. L.: 1990, *J. Phys. A.* **23**, 2379.

Wu, F.: 1987, *Astrophys. J.* **320**, 418.

Wu, F. and Low, B. C.: 1987, *Astrophys. J.* **312**, 431.

Yeh, T.: 1973, *Phys. Fluids* **16**, 516.

Zaidman, E. G. and Tajima, T.: 1989, *Astrophys. J.* **338**, 1139.

Zirin, H.: 1988, *Astrophysics of the Sun*, Cambridge University Press, Cambridge.

Zweibel, E. G.: 1981, *Astrophys. J.* **249**, 731.

Zweibel, E. G.: 1982, *Astrophys. J.* **258**, L53.

Zweibel, E. G.: 1985, *Geophys. Astrophys. Fluid Dyn.* **32**, 317.

Zweibel, E. G. and Hundhausen, A. J.: 1982, *Solar Phys.* **76**, 261.

Zweibel, E. G. and Kulsrud, R. M.: 1975, *Astrophys. J.* **201**, 63.

Zwingmann, W.: 1987, *Solar Phys.* **111**, 309.